NOVEL DESIGN AND ENERGY MANAGEMENT APPROACHES FOR SEAMLESS INTEGRATION AND ADOPTION OF PLUG-IN ELECTRIC VEHICLES

ABDULLAH AZHAR ABDULLAH AL-OBAIDI

A DISSERTATION SUBMITTED TO THE FACULTY OF GRADUATE STUDIES
IN PARTIAL FULFILMENT OF THE REQUIREMENTS
FOR THE DEGREE OF
DOCTOR OF PHILOSOPHY

GRADUATE PROGRAM IN ELECTRICAL ENGINEERING AND COMPUTER SCIENCE
YORK UNIVERSITY
TORONTO, ONTARIO

SEPTEMBER 2022

Abstract

Electric vehicles (EVs) are witnessing increased utilization throughout the world as an alternative to fossil–fueled vehicles. However, the adoption of EVs and their integration into the power grid is yet to be fully materialized due to several issues, of which two are the most salient. First, the extensive deployment of EVs can bring challenges to the grid if not properly managed. Second, access to a variety of EV supply equipment (EVSE) in different areas is still lacking.

To that end, the research in this thesis aims to address these issues through the development of adaptive approaches that enhance the management of EV energy and the development of a charging strategy and a design approach that help to expand the proliferation of EV charging infrastructure.

Three approaches that are adaptive to their operator/user preferences are developed to enhance energy management in EVs. The first approach allows adaptive utilization of EV batteries' distributed energy resources in an EV fleet system for concurrent services to the transportation sector and ancillary services market. The second approach is a decentralized quality of service (QoS)-based scheme for peer-peer (P2P) energy trading among EV energy providers and consumers. The proposed mechanism is designed to match energy traders based on consumers' and providers'

QoS requirements and offers, respectively. The third approach is a bidirectional smart charging algorithm for EVs considering P2P energy trade, provision of ancillary services to the grid, and utilization of low electricity prices for battery charging. The algorithm incorporates user preferences into the scheduling process enabling it to adapt to various conditions.

Further, to expand the proliferation of EV charging infrastructure, this thesis introduces (i) a charging control strategy that does not require a communication network, which in turn reduces additional grid upgrades, and (ii) a design approach for EV parking lots that helps private investors to participate in the growth of charging facilities.

The findings of this thesis highlight the efficacy of the proposed approaches in achieving their objectives. This would provide implementable and cost-effective solutions to facilitate EVs deployment and address imminent and timely concerns that limit the wide adoption of EVs into electric distribution infrastructure.

To my beloved father

To my precious mother

To my dear wife

Acknowledgements

All praise is due to Allah almighty, who taught humans what they knew not and whose countless bounties have enabled me to complete this thesis successfully.

Even though this dissertation has my name on it, I believe that this accomplishment would not have been possible without the dedication and support provided by those around me.

I would like to express my deepest gratitude to my advisor, Prof. Hany Farag, for his guidance, care, and patience and for providing me with such a wonderful atmosphere for conducting research. I would particularly like to thank him for inviting me to collaborate on interesting problems, while also encouraging me to pursue my research interests as well. My admiration and respect for him only grew each day I spent under his supervision. Thank you for making my Ph.D. life easier.

I would not have been able to finish my dissertation without the guidance and support of my friends in the Smart Grid Research Lab, Dr. Mohamed Zaki, Dr. Nader El-Taweel, and Dr. Abdullah Sawas.

Special thanks to Dr. Hadi Khani for guiding my research and helping me to develop my background, and to Prof. Moataz Mohamed for all the successful collaborations we had.

I would also like to thank my family for their continued support of my endeavors and helping me with getting motivated at the most challenging times and for always standing by me through both the good times and the bad.

I am honored that this dissertation has been examined by Dr. Andrew Maxwell, Dr. Chadi Assi, Dr. Ping Wang, and Dr. Pirathayini Srikantha. I owe respect and thanks to them for their time and insight.

My PhD thesis studies was in part supported by the Ontario Graduate Scholarship, the Hadi and Ozra Arjomandi Graduate Scholarship, and the Mitacs Accelerate Research Internship.

Table of Contents

List of Tables

List of Figures

Abbreviations

BD bi-directional

CAPEX Capital Expenditure

DG Distributed Generation

DN Distribution Network

DR Demand Response

EC Energy Consumer

EP Energy Provider

EV Electric Vehicle

EVCS Electric Vehicle Charging Station

EVPL Electric Vehicle Parking Lot

EVSE Electric Vehicle Supply Equipment

G2V Grid to Vehicle

GHG Greenhouse Gases

IRR Internal Rate of Return

IMG Islanded/Isolated Microgrid

MCMP Multiple–Consumers to Multiple-Providers

NPV Net Present Value

O&M Operation and Maintenance

OPEX Operation Expenditure

P2P Peer to Peer

PCC Point of Common Coupling

QoS Quality of Service

SCMP Single–Consumer to Multiple-Providers

SOC State of Charge

ToU Time of Use

UD uni-directional

V2G Vehicle to Grid

V2V Vehicle to Vehicle

List of Publications

In This Thesis

Some of the research leading to this thesis has appeared previously in or is currently submitted to the following publications.

Journal Articles

1. **A. Al-Obaidi**, H. Khani, H. E. Farag, and M. Mohamed, “Bidirectional smart charging of electric vehicles considering user preferences, peer to peer energy trade, and provision of grid ancillary services,” *International Journal of Electrical Power & Energy Systems*, vol. 124, p. 106 353, 2021, ISSN: 0142-0615.

2. **A. A. Al-obaidi** and H. E. Z. Farag, "Adaptive Optimal Management of EV Battery Distributed Energy for Concurrent Services to Transportation and Power Grid in a Fleet System Under Dynamic Service Pricing," in *IEEE Transactions on Industrial Informatics*, vol. 18, no. 3, pp. 1618-1628, March 2022, doi: 10.1109/TII.2021.3088420.

3. **A. A. Al-Obaidi** and H. E. Z. Farag, "Decentralized Quality of Service Based

System for Energy Trading Among Electric Vehicles," in *IEEE Transactions on Intelligent Transportation Systems*, doi: 10.1109/TITS.2021.3058514.

4. **A. A. Al-Obaidi**, M. Z. El-Sharafy, H. E. Z. Farag, S. Saifullah, and A. Al-Awami, "Autonomous Control of EV Residential Charging in Droop-controlled Islanded Microgrids," Submitted to *IEEE Access*.

5. **A. A. Al-Obaidi**, and H. E. Z. Farag, "Optimal Design and Operation Management of EV Charging Facilities within Parking Lots," Submitted to *IEEE Transactions on Transportation Electrification*.

Conference Papers

1. **A. A. Al-Obaidi** and H. E. Z. Farag, "Electric Vehicles Optimal Scheduling for Peer-to-Peer Energy Trade and Ancillary Services Provision to the Grid," *2020 IEEE Power & Energy Society General Meeting (PESGM)*, 2020, pp. 1-5, doi: 10.1109/PESGM41954.2020.9281627.

Chapter 1 - Introduction

1.1 Background and Motivation

The current environmental crisis caused by increasing levels of GHG is accelerating the need to substitute fossil fuel-based vehicles with a more environmentally friendly transportation solution [1]. In 2020, the transportation sector was the second-largest contributor of GHG in Canada, accounting for 24% of total emissions, with the majority coming from light-duty vehicles [2]. Since electricity GHG intensity has dropped significantly in recent years due to a switch to lower-carbon energy sources for electricity production, transportation electrification is becoming increasingly important to mitigating climate change [3]. In this context, EVs have attracted significant attention as a sustainable and clean transportation alternative. To that end, more than 90000 EVs were sold in Canada and over 5.6 million in the world in the last decade [4]-[5]. However, several issues impede the wide adoption of electric vehicles and their integration into power grids. The two most salient issues are the EV charging negative effects on the electrical power grid and the the lack of access to EVSE due to the high financial investments required for the proliferation of EVSE and its associated electrical grid infrastructure upgrades [6]-[7].

Despite their environmental benefits, the extended penetration of EVs has been associated with several unwanted effects on local distribution networks [8]. The biggest

impact stems from the uncoordinated charging resulting in a demand peak that can coincide with other traditional load peaks. This would, in turn, cause higher power losses and voltage regulation issues. Further, EVs deployment in large scale would lead to a large shift in the total demand that cannot easily be handled by the existing distribution network infrastructures, which can lead to electrical equipment overloading and a reduction in distribution transformers lifespan [9]. These effects, among others, have obstructed integration of EVs into power grids and called for energy management methods that optimally coordinate EV charging/discharging setpoints, incentivize EV owners to shift their consumption away from the peak periods, and provide ancillary services to the power grid [10].

The management of EV charging is mainly classified into G2V and V2G schemes [10, 11]. G2V methods govern and coordinate EV charging from the grid to achieve goals including lowering EV charging costs, regulating load to meet power system limits, and/or promoting societal welfare and charging fairness. With the recent improvement in communication networks and the advancements in EV charger technology that facilitated bidirectional power flow between EVs and the grid, EVs can now be operated under V2G schemes that take advantage of EVs' energy storage capabilities to provide ancillary services to the grid [12]. In this regard, while the battery of each EV offers small storage, hundreds of EVs collectively can offer large energy storage to serve a power grid in V2G schemes. Since some of the most well-known EV fleet management systems such as UBER have committed to switching to 100% EV utilization by the next decade [13], and in order to promote faster utilization of EVs in fleet systems, their full benefit needs to be exploited [14]. Therefore, new optimal scheduling approaches should be developed to fully coordinate the operation of many EVs in a fleet system for various services to

the transportation sector and ancillary services market.

In contrast to G2V and V2G techniques, P2P energy trading amongst EVs (i.e., V2V charging) has been presented as an energy management method that provides distributed and flexible control of EV energy by balancing supply and demand through local transfers between EVs [15]. EVs could schedule their charging (i) during off-peak periods when electricity prices are low, and/or (ii) from their local renewable energy sources, and then sell their stored energy at competitive rates to other EVs during peak times to generate profits [16]. This would, in turn, provide an economic benefit for both sides of the transaction while helping local distribution systems to shift power demand from peak times. However, although the utilization of EVs for P2P energy trade could bring significant advantages to the grid, it also comes with serious implementation challenges as to how the trading is coordinated and administered among the different participants. Therefore, P2P energy trading coordination schemes should be designed to facilitate resilient and reliable transactions that would encourage EV owners to consider V2V charging as a reliable service.

Furthermore, the research on G2V, V2G, and V2V schemes mainly focuses on the control of EV charging and/or discharging from the perspective of system operators and aggregators. However, given that there is at least one human user per vehicle, it is expected that EV users will have various interactions based on their own preferences, and thus, different options are required to accommodate their preferences. It is also argued that EVs can be scheduled for joint applications concurrently including V2V energy trade and V2G services to the grid. Thus, it is important to consider EV users' input into the scheduling process through self-scheduling (i.e., user-based) algorithms that help each individual EV user determine the optimal charging and discharging setpoints

for their EV batteries.

The aforementioned energy management techniques for EVs require communication links to be connected to individual EVs' chargers to communicate with the grid operator and/or other EVs to coordinate the charger's setpoints [17]. Such a communication network is typically not available in all distribution networks, especially at the secondary distribution level, and requires a costly infrastructure upgrade [18]. Furthermore, access to a variety of EVSE in different areas is critical to popularizing the use of EVs. Therefore, it is significant to introduce implementable and cost-effective solutions that could potentially accelerate the growth of charging facilities, and reduce the anticipated electrical grid upgrades that are required for such adoption.

In this regard, firstly, autonomous and communication-less EV charging techniques should be developed to facilitate the adoption of EVs for many electric distribution systems in residential areas that have limited or no communication infrastructure. The autonomous EV charging can regulate the EV load without the need for a communication network by utilizing local system measurements at the point of charger connection with the grid to decide the charging power that does not disrupt the system stability [19]-[20]. Secondly, while public investments and government incentives are needed for the development of EVSE infrastructure, it is important to benefit from the private sector resources to reduce the government's financial burden and accelerate the growth of charging facilities [21]. In this case, the private sector can invest in the design, construction, and operation of EVSE infrastructure in return for making profit on charging services to EVs and V2G services to the grid [22]. In densely populated areas, charging EVs at home may not be practical or economically feasible. In this context, private investors could be involved in the proliferation of public charging infrastructure

to help accommodate the deployment of EVs. In particular, the deployment of EVPLs with charging capability in commercial and workplace districts has been proposed as a solution for EV owners in these areas to meet their charging needs [23]. Furthermore, the storage capacity of EVs in EVPLs could be used in V2G schemes coordinated by the EVPL owner to provide grid relief during peak hours [24]. Therefore, it is important to introduce new approaches that can help investors to design and assess their investments in EVPL infrastructure used for charging and V2G services in terms of its technical viability and economical feasibility.

1.2 Thesis Objective

The research in this thesis aims to enhance the adoption of EVs and their integration into the power grid through two objectives. The first objective involves the development of adaptive systems that enhance the management of EV energy, while the second objective is concerned with the development of charging strategies and design approaches that help to expand the proliferation of EV charging infrastructure. Therefore, the thesis includes five sub-objectives related to these main objectives as shown in Fig. 1.1 and outlined below.

1.2.1 Objective (1): Enhancing EV Energy Management

This thesis enhances the current research on EV energy management techniques by introducing three novel systems that are adaptive to operator/user preferences.

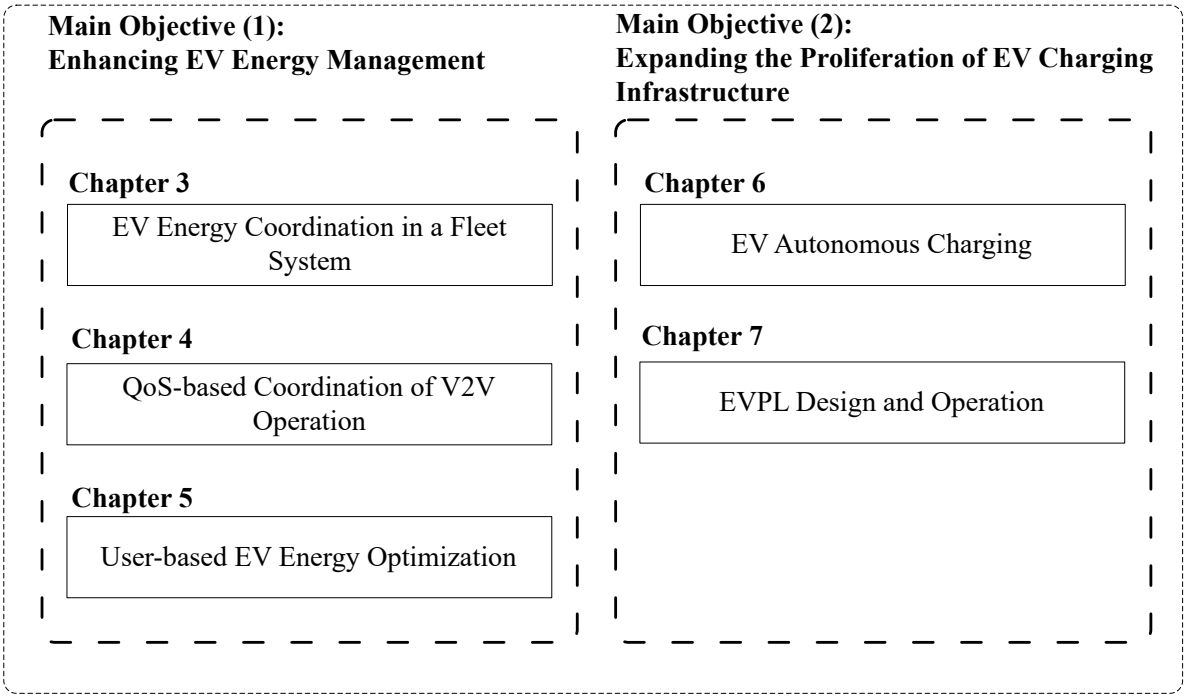

Fig. 1.1. Layout of the thesis research objectives

Sub-objective (1): EV Energy Coordination in a Fleet System

The aim of this objective is to develop an optimization model for a central controller in a fleet system that allows adaptive utilization of EV batteries distributed energy resources for concurrent services to the transportation sector and ancillary services market. The optimization model incorporates various slack variables and control parameters for managing real–time fare prices, adaptive energy, and reserve margin allocation, interaction with the grid operator, and meeting the fleet target revenue. A dynamic pricing mechanism is developed for real–time calculation of fare rates to allow the EV fleet optimization problem to achieve a daily revenue target while limiting fare prices in order to make the fleet more competitive in the market.

Sub-objective (2): QoS-based Coordination of V2V Operation

The aim of this objective is to design a novel decentralized QoS-based system for P2P energy trading among EV energy providers and consumers. Two QoS-based mechanisms are proposed to match trading EVs in this system. The proposed mechanisms are designed to match single-consumer to multiple-providers and multiple-consumers to multiple-providers based on consumers' and providers' QoS requirements and offers, respectively.

Sub-objective (3): User-based EV Energy Optimization

The research in this objective aims to develop a new algorithm for bidirectional smart charging of EVs considering P2P energy trade, provision of ancillary services to the grid and utilization of low electricity prices for battery charging. The algorithm incorporates user preferences into the scheduling process, enabling the algorithm to adapt to various conditions.

1.2.2 Objective (2): Expanding the Proliferation of EV Charging Infrastructure

To expand the proliferation of EV charging infrastructure, this thesis introduces (i) a charging control strategy that does not require communication network, which in turn reduces additional grid upgrades, and (ii) a design approach for EVPL that helps private investors to participate in the growth of charging facilities.

Sub-objective (4): EV Autonomous Charging

This objective involves the development of a communication-less control strategy for EV residential charging. The strategy considers social charging fairness and can work in droop-controlled IMGs. A charging fairness system that assigns priority levels to EVs based on their past charging power allocation is developed. The priority level is utilized to adjust the Sigmoid-based controller to provide more system capacity to the EVs with higher priority levels. Further, the strategy includes a novel EV load shedding scheme that gets triggered when an under-voltage or under-frequency event occurs in the IMG when the generation does not meet the required demand.

Sub-objective (5): EVPL Design

This objective aims to develop an optimal design approach for EVPLs that can provide services to the electrical power grid. The approach allows multi-objective planning for the maximization of operator profit or user comfort. Further, the approach enables the design of an EVPL with the optimal combination of uni-directional and bi-directional chargers, considering the financial aspects of the provision of V2G services and the incentive-participation modeling of EV users. Moreover, the approach decouples the intertwined economic dynamics of EV charging and discharging services in the EVPL through revenue models that target each service separately.

1.3 Thesis Layout

The remainder of this thesis is organized as follows:

- **Chapter 2:** Presents a critical literature survey on topics relevant to the thesis

research objectives.

- **Chapter 3:** Presents a new optimization model for a central controller in a fleet system that allows adaptive utilization of EV batteries distributed energy for concurrent services to the transportation sector and ancillary services market.
- **Chapter 4:** Presents a new bidirectional smart charging algorithm of EVs for P2P energy trade and ancillary services provision to the grid.
- **Chapter 5:** Introduces a novel QoS-based coordination approach for P2P energy trading systems among EV energy providers and consumers.
- **Chapter 6:** Introduces a novel autonomous control strategy for EV charging in residential droop-controlled IMGs.
- **Chapter 7:** Presents a design approach for an EVPL that can provide services to the electrical power grid.
- **Chapter 8:** Presents the conclusion and contributions of this dissertation, and offer possible directions for future work.

Chapter 2 - Literature Survey

2.1 Introduction

This chapter provides a literature review on the state-of-the-art of EV energy management approaches, as well as autonomous EV charging and EVPL design and operation management. Then, the gaps and shortcomings of the works addressed in the literature are summarized at the end of the chapter.

2.2 EV Energy Management

2.2.1 G2V and V2G Management

Traditionally, researchers have focused on developing EV energy management methods that involve coordinated G2V charging management. The authors in [11] propose distributed online and offline EV scheduling algorithms where aggregators aim to generate revenue by optimizing the charging schedule of EVs. In [25], a heuristic method is presented which determines the most suitable charging/discharging instances for an EV battery in a day-long period for reducing the energy cost. The method requires some basic input parameters, such as real-time market prices, household demand, and parameters of the EV. Similarly, in [26], an optimal EV charging coordination approach is presented with the objectives of minimizing the charging cost and energy losses in

an unbalanced residential distribution network. A decentralized charging scheduling algorithm is proposed in [27] based on the augmented Lagrangian method. A scheduling algorithm for large residential EV populations is implemented in [28] using a two-stage hierarchical optimization approach. A real–time energy management system is proposed in [29] for optimal scheduling of EVs to reduce the energy cost associated with EV charging. Similarly, charging scheduling is implemented in [30] using a collaborative multi–aggregator approach with variable energy purchase charges. The study in [31] investigates a game-theoretical approach that considers social incentives to help reduce charging costs of EVs while satisfying individual EV charging requirements and charging stations constraints. The authors in [32] develop a method based on the multi-modal approximate dynamic programming to manage charging/discharging of EVs in a grid-connected charging station.

Electricity prices have been considered for optimal management of EV charging patterns in several studies. For example, a method is presented in [33] to reduce the peak load of EV charging stations by utilizing dynamic prices for different charging schedules and deadlines. The authors in [34] utilize a game theory model based on Nash equilibrium to develop a day-ahead charging scheduling algorithm that considers the interplay between EV demands and electricity prices. A robust optimization technique is utilized in [35] for scheduling of EV aggregators considering uncertainties associated with electricity prices.

While the aforementioned G2V schemes help coordinate EVs charging, it is important to take advantage of EVs' energy storage capabilities to improve the grid's resiliency through V2G energy management approaches. In [36], a hierarchical management system is proposed for integration of EVs into a distribution grid aiming to prevent grid's

congestion. Numerical studies indicate that the grid's congestion can be prevented via proper controlling of the EV charging. Authors in [37] formulate a binary optimization problem for real-time charging of EVs in a parking lot. The scheme coordinates EV loads based on dynamic electricity pricing and demand response signals issued by the grid operator. Primary frequency regulation and dynamic grid support with EVs participation are implemented in [38]. The authors in [39] propose a scheduling strategy that utilizes the droop control in response to frequency uncertainties while satisfying EVs charging loads. In [40], a two-phase hierarchical V2G scheduling process is devised to schedule EVs for providing frequency regulation service to the grid. The authors in [41] present an optimal charging strategy that utilizes reactive power injection capability of the EVs to support the grid. The work in [42] develops an aggregate EV model to estimate V2G capacity for use in applications such as participating in frequency regulation and providing operating reserve to the grid. The model shows a high accuracy level in reducing real-time reserve shortages. The authors in [43] present a dynamic demand response-based V2G capacity model that accounts for EVs' movement across the energy network. The study in [44] proposes a strategy to manage and utilize V2G capacities to control voltage rises and reverse power flow that result from PV system integration into the grid. The study in [45] proposes to incorporate a demand response and inter-EV sharing frameworks into the scheduling strategy of EVs in residential networks.

2.2.2 V2V Charging Management

Recent initiatives towards distributed solutions as well as advancement in P2P communication networks have extended EV charging schemes to involve V2V charging. In this context, the authors in [46] incorporate V2V charging into a scheduling algorithm

of EVs charging inside a station to reduce the charging cost and increase renewable energy utilization. The study in [47] optimizes the trading prices between energy trading EVs considering charging scheduling of individual EVs. In [48], an optimal charging scheduling model is developed considering a scenario where EVs could charge from the grid, other EVs, or mobile charging vehicles. However, V2V schemes proposed in [46],[47]–[48] are dependent on G2V scheduling models and do not introduce separate P2P energy market schemes for EVs.

An independent energy trading market managed by a fog computing-based coordinator is proposed in [49]. The coordinator sets trading prices based on non-profit-oriented or profit-oriented behaviors. In [50], the authors develop an auction-based energy market between EVs. The market is coordinated by a central auctioneer that runs a naive auction process iteratively to determine energy prices. Similarly, the study in [51] proposes an online double auction mechanism for P2P energy trading among EVs that includes anonymity schemes to tackle the issue of trading participants' identity and location leakage. A matching scheme is implemented for cooperative P2P energy trading among EVs in [15] where a Pareto optimal matching algorithm is utilized to assign discharging and charging EVs based on their utility preferences. Another V2V charging management scheme is proposed in [52], where matching algorithms are utilized to maximize the social welfare of trading participants considering cost and profit preferences. The study in [53] designs an integer linear program to optimize the routes and the schedules of charging trucks to maximize the served number of EVs through V2V energy transfer. Nevertheless, studies conducted in [15], [46]–[52] have relied on the existence of a central third party to coordinate between the market participants, which makes them prone to single-point failures, as well as privacy and security issues. To address such a drawback,

blockchain technology has been proposed as a platform that allows decentralized EV energy trading without the presence of a third party [54].

Blockchain is essentially a distributed ledger that contains a record of system states and digital transactions and is controlled by a group of nodes instead of one central entity. These nodes share the tasks of verifying the integrity of the distributed ledger and preserving its data in their data storage devices, which makes transactions in these systems more transparent [55]. Further, blockchain eliminates the costs required to be paid to third parties to manage central systems [56]. Researchers in the literature have recently investigated the application of blockchain in P2P energy trading among EVs. In order to reduce the power fluctuation level in the grid, the work in [57] develops a blockchain-based EV participation scheme to facilitate and match large volumes of EV charging and discharging demands. In [58], the authors propose a blockchain-based energy trading model between EVs inside local parking lots. An iterative double auction audited by authorized local aggregators is introduced to maximize total participants' utility. A framework for P2P energy trading between EVs is studied in [59] considering the use of blockchain, contract theory, and computational intelligence.

2.2.3 Energy Management of Electrified Private Transportation Fleets

Private transportation fleets are among the major transportation sectors that are expected to be converted to EVs [60]. In this context, the authors in [61] introduce an optimal deployment framework for public charging stations considering EV fleet drivers and passengers' demands as well as power distribution network constraints.

Similarly, the work in [62] studies the optimal location of public charging stations using a multi-agent system and evidential reasoning approach. The multi-agent system is utilized to simulate and quantify EV taxi fleets charging demand, while evidential reasoning optimizes stations' locations based on the total charging cost, power losses, and voltage deviations. The study in [63] considers the dynamic distribution and charging requirements of electric taxis to develop a model for locating charging stations that can meet the requirements of EV taxi fleets. The authors in [64] design a charging system for electric taxis considering the historical charging patterns and real-time global positioning system data mining. Nonetheless, the studies in [60]-[64] are limited to the optimal design and integration of charging stations for EV fleets without considering the development of energy management systems for their EV batteries.

Various energy management strategies have been proposed in the literature to effectively integrate EV-based fleets into the electric grid. The study in [65] utilizes a real-time pricing method to regulate the charging loads of electric private transportation fleets. The method introduces a special real-time electricity market for EV fleets to follow the desired load profile while giving autonomous charging decisions for drivers. The authors in [66] propose a distributed two-stage charging decision process for electric taxis. The process aims to reduce the charging cost for each taxi by choosing the best charging time slot and charging station using a thresholding method and a game-theoretical approach. The work in [67] models electric taxi charging loads in temporal and spatial dimensions. Accordingly, the operation of the electric taxis fleet is modeled using a Java-based multi-agent framework, and a reinforcement learning algorithm is utilized to make decisions that maximize the taxis' revenue by charging at the lowest costs. The authors in [68] use the Markov decision process in modeling and optimization of electric

taxi services strategy. The strategy aims to assist drivers in improving their revenue considering different EV related constraints, such as constrained battery capacity and limited charging stations. The work in [69] presents a stochastic game model based charging scheme for electric taxis. The objective is to reduce taxi charging costs while considering distribution network transformer aging risks. The authors in [70] formulate and solve a constrained binary programming problem for charging of electric taxis. The problem considers EV battery constraints aiming to maximize the long-term profit for drivers. The study in [71] integrates the scheduling of private and taxi EVs in a two-stage distributed model that can obtain optimally feasible charging profiles for both types.

Centralized and decentralized approaches are considered in the charging control of EV fleets. In centralized approaches, the authors in [72] propose a mixed-integer linear programming-based algorithm for management of EV fleet charging from PV units. The algorithm integrates several applications including ancillary services support to the grid, but it is limited to EV charging in workplace parking lots. The authors in [73] employ a four-quadrant control system for EV chargers in order to inject or absorb reactive power, depending on the voltage profile of the grid.

In decentralized approaches, the study in [74] proposes a strategy for EV fleets charging coordination. The strategy is formulated as a large population game, with EV players coupled by the same electricity price signal aiming to minimize the operating cost of individual EVs. The work in [75] develops a decentralized EV charging management scheme based on evolutionary game dynamics, where EVs can also provide ancillary services to the grid. Nevertheless, game-theoretical approaches assume that participants are rational and that complete information is available to strategy players which may not be feasible in practical applications. The authors in [76] develop a decentralized

optimal charging algorithm that involves an operator broadcasting a control signal to EVs. Based on this signal, EVs update their charging profiles in order to shift the charging load away from peak periods. Similarly, the work in [77] designs a decentralized charging algorithm to reduce overloading in power distribution feeders. A hierarchical framework is developed by the authors in [78] to concurrently optimize power flow routing and frequency regulation service scheduling. Despite their strong mathematical basis, the decentralized charging methods proposed in [76]- [78] are designed from the grid operator's perspective, which may not be efficient to EV fleet operators that need to be in control of their own scheduling operations with a high degree of certainty. Centralized approaches are more effective and offer better performance in coordinating EV operations in a fleet system for various services to the transportation sector and ancillary services market. Due to complete information being available to the main controller, centralized controllers are able to obtain optimal solutions to EV charging control problems. Further, in the case where EVs are owned by a single entity like a private transportation company company, centralized approaches enable complete control of EV operations, as well as enhanced ability to forecast electricity prices and EVs driving patterns. Moreover, management of business models that involve EV fleets can be more thoroughly performed with centralized approaches [79].

2.3 Autonomous EV Charging

In contrast to the EV energy management systems described in the previous works reviewed so far in this chapter, autonomous EV charging techniques can regulate the EV load without the need for a communication network [19]. The basic concept of autonomous charging is to utilize local system measurements at the point of charger

connection with the grid to decide the charging level that does not disrupt the system stability [20]. These techniques help to facilitate the adoption of EVs for many electric distribution systems that have limited or no communication infrastructure and reduce the computational burden on system operators. There have been numerous studies in the literature that have proposed autonomous EV charging control schemes. A charging technique based on duty cycles and EV departure time is proposed in [80]. The departure time input by the user is used to calculate a unique duty cycle that switches on and off the charger at a different rate from other chargers in the system to prevent simultaneous power consumption. The work in [81] also proposes to use the user departure time in order to decide whether to charge EV once it is plugged in or delay it to avoid peak loading times. The methods introduced in [80] and [81] assume that EV users will input their departure time accurately. Nevertheless, this assumption is not always valid and users can “game" these methods by inputting false early departure times to charge their EVs faster. The study in [82] presents an autonomous algorithm based on historical records of system conditions at the EV charger point. This algorithm is not reliable because it does not account for future changes in the system's configuration and loading.

Several studies have considered the use of measured voltage at the PCC as a direct input to control the EV charging load. The study in [83] introduces a voltage-based EV charging controller that adjusts the charging load through a voltage-droop function. The work in [84] proposes a non-linear voltage-based autonomous controller with an exponential function that compares the PCC voltage with a reference voltage to decide the charging rate. A fuzzy-based charging scheme that is sensitive to voltage levels at the PCC is proposed in [85]. Other studies have investigated the control of EV charging based on the system frequency. In this regard, the operation of IMGs is

more constrained than grid-connected systems, where the low short circuit capacity of IMGs could result in frequency deviations as a result of any configuration change [86]. Further, droop-controlled IMGs require the drooping of frequency and voltage in order to achieve active and reactive power-sharing. Therefore, it is important to consider system frequency in autonomous EV charging control logic in IMGs. A frequency-based controller is introduced in [87], where EV charging load is controlled based on the microgrid's frequency deviation. Similarly, the authors in [88] propose to use the system frequency to regulate the EV charging load, while the bus voltage is used to control the level of EV's reactive power support to the grid.

2.4 Design and Operation Management of EVPL

Several studies have proposed models for the design of EVPLs in electric DNs. An economic design model for EVPL sizing and location siting is introduced in [89]. The model maximizes the investor NPV considering the traffic flow, as well as electric power grid and EV charging constraints. The authors in [90] present a design and operation management model for EVPLs considering the driving and behavioral patterns of EV users. The work in [91] proposes a planning method that considers different power charging capacities. The model minimizes the annualized cost of the EV charging system including the costs related to investment, grid reinforcement, and O&M. The study in [92] proposes a method for minimizing the capital and operational cost of EVPLs using a battery energy storage system. A planning framework for residential, commercial, and industrial EVPLs is introduced in [93]. The framework is formulated from the perspective of a social planner and aims to minimize the total social costs of all planned charging systems. Nevertheless, the studies in [89]-[93] do not consider the provision of

V2G services to the grid by the EVPL. Utilizing the power injection capacity of EVPLs can enhance the DN operation and provide economic benefits to the EVPL owners and EVs that participate to V2G services [94].

An EVPL planning model that maximizes the operator profit through the provision of V2G services to the energy and reserve markets is proposed in [95]. The model also considers the minimization of operating DN costs resulting from power losses and voltage deviations. The study in [96] presents a model to determine the optimal location and capacity of EVPLs considering optimal scheduling of EV charging and discharging, minimization of EVPL distance to EV users, and maximization of DN operator profit. The work in [97] utilizes a probabilistic approach to model the uncertain parameters in driving patterns of EVs and optimize EVPL power exchange with the grid. The authors in [94] propose a stochastic model for optimal placement of EVPLs in DNs in view of EV owners' payoffs from subscribing to EVPL services. The study in [98] formulates a multi-objective bi-level model for dynamic planning of DN that involves the sizing of new EVPLs. The model considers the conflicting objectives of DN and EVPL operators and aims to enhance DN flexibility through the use of EVPLs as a backup power supply during faults. Another bi-level model is introduced in [99] where the distributed storage of EV batteries in EVPLs is utilized to defer investment in DN. A planning model is proposed to design and site EVPLs given the improvement of renewable energy integration into DNs [100]. The authors in [101] propose a collaborative multi-objective DN and EVPL expansion planning model. The model aims to find the optimal location and size of EVPL that would maximize the profit of DN and EVPL operators and provide reinforcement to the DN. The study in [102] models the EVPL as a DG in the DN and presents a multi-objective approach to determine their optimal

location and size. The authors in [103] investigate the sizing and siting of EVPL in the reconfigurable DNs, taking into account the minimization of power losses and reliability issues through the G2V and V2G programs. The work in [104] presents an approach for planning and siting of EVPLs in a DN considering uncertainties in cost of investment and availability of budget. The study in [105] proposes an optimal mixed-integer nonlinear model to decide the number of EV chargers and size of photovoltaic (PV) panels in an EVPL. The uncertainty in EV owners' behavior is considered in parking lot planning and investment decision in the model proposed by the work in [106]. The model aims to maximize the revenue of parking lot operators through optimization of parking lot allocation and operation management. EVPLs are planned to act as backup generators during outages and help in the service restoration process of faulted zones as examined by the study in [107].

Chapter 3 - Adaptive Optimal Management of EV Battery Distributed Energy in a Fleet System

3.1 Introduction

Deployment of EVs in a fleet system to deal with environmental issues has been at the center of attention over the past several years [108]. In regards to EV fleet energy management, what is missing from the literature is a multiobjective optimization model that can fully coordinate the operation of several EVs in a private transportation fleet system for various services to the transportation sector and ancillary services market. In prior studies, the full benefit of the huge distributed energy in EV batteries within a fleet system is not exploited. As such, a new model is needed for full integration of hundreds of EVs into a fleet with consideration of various parameters including real-time dynamic fare prices, energy and reserve margin allocation, full interaction with the grid operator, and the target revenue of the fleet system. Therefore, this research unveils a new optimization model to fill the gap between the existing works and one that can optimally integrate and manage several EVs within a fleet system for various services while enhancing the financial profile of the fleet system. In particular, this research contributes to the existing works via the following avenues:

1) Development of a model for a central controller in a private transportation fleet system that allows adaptive utilization of EV batteries distributed energy for concurrent services to the transportation sector and ancillary services market.

2) Proposing a cooperative–based model to coordinate and manage the operation of each EV in order to provide a large operating reserve to the grid while maintaining services to the transportation sector.

3) The optimization model incorporates various slack variables and control parameters for managing real–time fare prices, adaptive energy, and reserve margin allocation, interaction with the grid operator, and meeting the fleet target revenue. Integration of slack variables also allows the optimization problem to converge in case it is not feasible for an EV to participate in a service request.

4) The model incorporates the EV driver's preferences into the scheduling process in order to allow the driver to adjust the minimum and maximum limits of the EV battery prior to data sharing with the central controller. This allows EV drivers to flexibly manage their battery capacities based on their availability and assessment of the transportation services demand when needed.

5) A dynamic pricing mechanism is developed for real–time calculation of fare rates to allow the EV fleet optimization problem to achieve a daily revenue target while limiting fare prices in order to make the fleet more competitive in the market.

Numerical studies are utilized to demonstrate the efficacy and feasibility of the proposed model under various scenarios. It is indicated that the new model in this research reinforces the fleet financial parameters while lowering the fare prices for the customers who use the fleet EVs in order to stay competitive in the market.

Table 3.1 compares the proposed model in this work with previous studies in the

literature. The table indicates how the proposed model has contributed to the existing studies. As reported in the table, in the proposed model, various objectives are concurrently included and integrated. It is worth noting that the results in Table 3.1 do not indicate that the proposed model is simply including more objectives than prior studies. It expresses how various services are integrated into the model and the EV fleet is scheduled for various services concurrently.

Table 3.1: Comparison of the Proposed Model with Prior Studies in Literature.

Model Objectives / Reference	[45]–[78]	[65]–[71]	Proposed
Management of Distributed EVs	✓	✓	✓
Transportation Operation Services		✓	✓
Dynamic Fare Prices Mechanism			✓
Return on Investment Optimization			✓
Ancillary Service Provision	✓		✓
User-based Battery Management			✓

Table 3.2: Chapter 3 Nomenclature

Indices

s	Index of EVs in the fleet.
t	Index of time steps.

Sets

$\mathcal{S}$	Set of fleet EVs in optimization problem.
$\boldsymbol{\mathcal{T}}$	Set of optimization problem time steps.

Constants

ΔT	Optimization problem time interval (h).
$\alpha_s^{LB,Res}$	User adjustable lower bound reserve SOC factor.
$\alpha_s^{UB,Res}$	User adjustable upper bound reserve SOC factor.
B_s	Battery capacity (kWh).
κ^{Dsp}	Energy dissipation factor (%).
N^{Con}	Rate of energy consumption (kWh/km).
OC^{Chg}	Battery charging operating cost (\$/kWh).
OC^{Dhg}	Battery discharging operating cost (\$/kWh).
$P_{s,min}^{Chg}$	EV minimum charging power (kW).
$P_{s,max}^{Chg}$	EV maximum charging power (kW).
$P_{s,min}^{Dhg}$	EV minimum discharging power (kW).
$P_{s,max}^{Dhg}$	EV maximum discharging power (kW).
R^{Exp}	EV fleet revenue target. (\$).
$SOC_{s,min}^{H}$	Minimum physical level of EV battery (kWh).
$SOC_{s,min}^{H}$	Maximum physical level of EV battery (kWh).

Time–Dependent Parameters

$\sigma_t^{Res,LB}$	Penalty factor for management of lower reserve SOC limit (\$/kWh^2).
$\sigma_t^{Res,UB}$	Penalty factor for management of upper reserve SOC limit (\$/kWh^2).
$\sigma_t^{Trp,Adj}$	Penalty factor for management of passenger trip price.
$\sigma_t^{Exp,Adj}$	Penalty factor for management of EV fleet daily revenue.
$\sigma_{s,t}^{Flt}$	Ancillary services penalty factor (\$/kWh).
C_t^{ToU}	ToU electricity prices (\$/kWh).
C_t^{Flt}	Ancillary services price (\$/kWh).
D_t	EV transportation distance at time t (km).
J_t	EV charger plug–in status, $J = 1$ when plugged–in.
$M_t^{Trp,Min}$	Minimum passenger trip price (\$).
P_t^{Anc}	Ancillary services signal (kW).
$SOC_t^{Flt,LB}$	Collective SOC level lower limit of EV fleet (kWh).
$SOC_t^{Flt,UB}$	Collective SOC level upper limit of EV fleet (kWh).

Table 3.2: Chapter 3 Nomenclature ... continued.

Variables	
E_t^{Drv}	EV driving energy consumption (kWh).
$M_t^{Trp,Adj}$	Slack variable for passenger trip price adjustment ($).
P_t^{Drv}	EV driving power consumption (kW).
$P_{s,t}^{Chg}$	EV charging power (kW).
$P_{s,t}^{Dhg}$	EV discharging power (kW).
$P_{s,t}^{Utl}$	EV power charge from the grid (kW).
$P_{s,t}^{Flt}$	Ancillary services power provided by EV fleet (kW).
$P_t^{Flt,Chg}$	Slack variable for charging ancillary services contribution (kW).
$P_t^{Flt,Dhg}$	Slack variable for discharging ancillary services contribution (kW).
$R_t^{Exp,Adj}$	Slack variable for EV fleet daily revenue adjustment ($).
$SOC_t^{Dod,S}$	Slack variable for depth of discharge management (kWh).
$SOC_{s,t}^{H}$	SOC level of EV s (kWh).
$SOC_{s,t}^{Res,LB}$	Slack variable for lower bound reserve SOC level (kWh).
$SOC_{s,t}^{Res,UB}$	Slack variable for upper bound reserve SOC level (kWh).

3.2 Optimal Scheduling Model

The proposed scheduling model for the EV fleet system is described in this section. It is assumed that the fleet is utilized by a privately owned chauffeured EV transportation company. It is also assumed that the trip fares do not follow any city regulations. The communication scheme between the central controller, EVs, and utility operator is shown in Fig. 3.1. In this scheme, the central fleet operator receives EV operators' preferences as well as their EV status. The EV user preferences information includes how much reserve each EV is willing to maintain for the provision of ancillary services to the grid. The controller also receives ancillary service signals from the utility operator, including operating reserve signals that require either injecting or absorbing power to/from the grid. Based on these signals, the central controller sends a provision request to each EV user in the fleet and based on their responses, it decides the amount of accumulated

power that will be serviced to the grid.

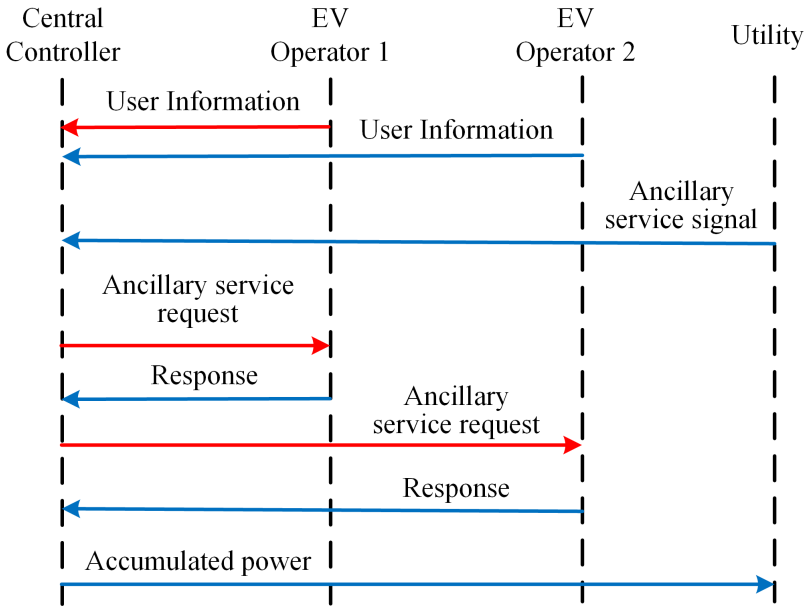

Fig. 3.1. Communication scheme among EVs, central controller, and utility.

It is important to emphasize here that the proposed model does not have to rely on private communication networks, but can be implemented using the existing communication platforms, i.e., the internet. The internet is proven to be fairly solid and reliable, and therefore, it is possible to implement a centralized architecture with a high degree of success. This has been proven by major internet-based ride-sharing/hailing companies such as Uber, which rely on the internet for all of their communication needs.

3.2.1 Mathematical Formulation

Table 3.2 presents the nomenclature of the proposed model. The developed model in this research is based on a real-time scheduling model that is run using the approach referred to as the rolling time horizon or model predictive control [109], [110]. In this approach,

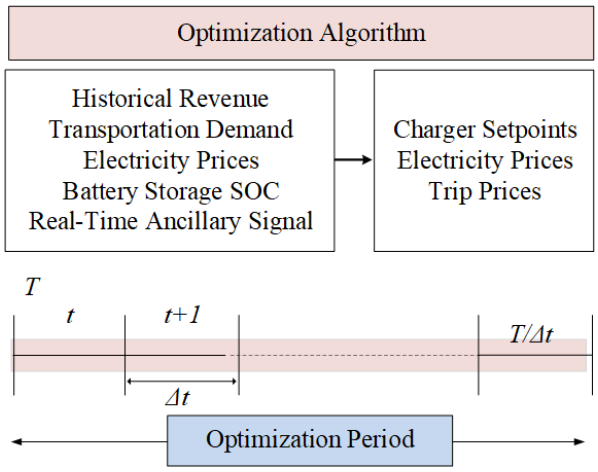

Fig. 3.2. Real-time optimization problem.

the optimal scheduling model is converted into a multi-interval optimization problem, where optimal setpoints are issued for the current and look ahead time steps as shown in Fig. 3.2. Therefore, the optimization problem is re-run at every time step, and the optimal setpoints are updated recursively, which alleviates the uncertainty associated with the time-varying nature of the optimization parameters. Without loss of generality, the optimization horizon in this work is set to look at the next six time steps ahead, with each step equal to one-hour interval. It should be noted that the problem is modeled as a deterministic optimization model because it is assumed that the trips requested by passengers are booked in advance. Stochastic models including Markov decision process (MDP) could be utilized in case the model is applied to a transportation service where the trips are requested randomly [111].

The mathematical formulation of the proposed optimal EV fleet scheduling model is given below.

Objective Function

The objective function of the EV fleet central controller is given by (3.1):

$$\text{Maximize}: \sum_{t\in\boldsymbol{\mathcal{T}}}\sum_{s\in\boldsymbol{\mathcal{S}}}\left\{\begin{array}{l} |P_{s,t}^{Flt}|\,.\,C_t^{Flt} - P_{s,t}^{Utl}\,.\,C_t^{ToU} \\ -OC_s^{Dhg}\,.\,P_{s,t}^{Dhg} - OC_s^{Chg}\,.\,P_{s,t}^{Chg} - \sigma_t^{Trp,Adj}\,.\,M_t^{Trp,Adj} \\ -\sigma_t^{Exp,Adj}\,.\,R_t^{Exp,Adj} - \sigma_{s,t}^{Anc}\,.\,(P_t^{Flt,Chg} + P_t^{Flt,Dhg}) \\ -\sigma_{s,t}^{Res,LB}\,.\,SOC_{s,t}^{Res,LB} - \sigma_{s,t}^{Res,UB}\,.\,SOC_{s,t}^{Res,UB} \end{array}\right\}.\Delta T. \tag{3.1}$$

The objective function in (3.1) aims to optimally manage the EV fleet to maximize the system profit which is achieved via:

- Participation of fleet EVs to grid's ancillary services: $\sum_{s\in\boldsymbol{\mathcal{S}}} |P_{s,t}^{Flt}|\,.\,C_t^{Flt}$
- Minimization of EV fleet charging costs: $-\sum_{s\in\boldsymbol{\mathcal{S}}} P_{s,t}^{Utl}\,.\,C_t^{ToU}$
- Management of passenger trips and fleet revenue:

  $-\sigma_{s,t}^{Trp,Adj}\,.\,M_{s,t}^{Trp,Adj} - \sigma_{s,t}^{Exp,Adj}\,.\,R_{s,t}^{Exp,Adj}$
- Limiting fleet charging/discharging operating cost:

  $-OC_s^{Dhg}\,.\,P_{s,t}^{Dhg} - OC_s^{Chg}\,.\,P_{s,t}^{Chg}$
- Controlling ancillary services participation levels:

  $-\sigma_{s,t}^{Anc}\,.\,(P_t^{Flt,Chg} + P_t^{Flt,Dhg})$
- Controlling the SOC reserve of individual EVs in the fleet:

  $-\sigma_{s,t}^{Res,LB}\,.\,SOC_{s,t}^{Res,LB} - \sigma_{s,t}^{Res,UB}\,.\,SOC_{s,t}^{Res,UB}$

EV Fleet Operation Constraints

The operation of fleet EVs are subject to the following operational constraints:

$$J_{s,t} \,.P^{Chg}_{s,min} \leq P^{Chg}_{s,t} \leq J_{s,t} \,.P^{Chg}_{s,max} \quad \forall s \in \mathcal{S} \wedge \; t \in \boldsymbol{\mathcal{T}} \tag{3.2}$$

$$J_{s,t} \,.P^{Dgh}_{s,min} \leq P^{Dhg}_{s,t} \leq J_{s,t} \,.P^{Dhg}_{s,max} \quad \forall s \in \mathcal{S} \wedge \; t \in \boldsymbol{\mathcal{T}}, \tag{3.3}$$

where (3.2) and (3.3) represent the charging and discharging limits for EV s, respectively. The charger connection time parameter $J_{s,t}$ indicates that charging and discharging operations are only possible when the EV is plugged-in. The constraints in (3.4) and (3.5) restrict charging/discharging to G2V and V2G operations and required power for meeting the trip requirements:

$$P^{Chg}_{s,t} = P^{Flt}_{s,t} \;\vee\; P^{Utl}_{s,t} \qquad \forall \; P^{Dhg}_{s,t} = 0 \wedge \; s \in \mathcal{S} \wedge \; t \in \boldsymbol{\mathcal{T}}, \tag{3.4}$$

$$P^{Dhg}_{s,t} = P^{Flt}_{s,t} \quad \forall \; P^{Chg}_{s,t} = 0 \wedge \; s \in \mathcal{S} \wedge \; t \in \boldsymbol{\mathcal{T}}. \tag{3.5}$$

The energy consumed by the EV during driving is represented by the following equation [112]:

$$E^{Drv}_{s,t} = (1 - J_{s,t}) \;.\; D_{s,t} \;.\; N^{Drv}_{s} \qquad \forall t \in \mathbb{T}, \tag{3.6}$$

where the term $(1 - J_{s,t})$ prevents the model from consuming energy for driving when the EV charger is plugged in.

EV Storage Constraints

The battery storage of EVs in the fleet is managed by the central controller according to the energy demand from the transportation sector as well as the G2V and V2G services. Therefore, battery storage of EV s is subject to the following physical and operational constraints:

$$SOC^{H}_{s,t} = SOC^{H}_{s,t-1} + \Big(J_{s,t}.\, P^{Flt}_{s,t}/B_s + J_{s,t}.\, P^{Utl}_{s,t}/B_s\Big).\, \Delta t - E^{Drv}_{s,t}/B_s - \kappa^{Dsp}.\, SOC^{H}_{s,t}$$
$$\forall s \in \boldsymbol{\mathcal{S}} \wedge\ t \in \boldsymbol{\mathcal{T}}, (3.7)$$

where (3.7) represents the SOC balance taking into consideration the previous state, and all charging and discharging operations as well as the energy dissipation of the battery. It is worth noting here that for the smart charging models, detailed battery behavior models including data-driven models [113, 114] are important to effectively use the charging infrastructures. However, this research is focused on development of a scheduling model for EV fleets that use the existing charging infrastructures and may include different types of EVs with different battery charging behaviors. Therefore, the proposed model does not aim to discuss the details of charging behaviors for each EV in the fleet system, and assumes that the EV charger operates to reach the target battery SOC setpoints.

The minimum and maximum limits of the battery in the s^{th} EV are adjusted according to the user preferences shared with the central controller. This allows the EV drivers to flexibly manage their battery capacities based on their availability and assessment of the transportation services demand. The $SOC_{s,t}$ of each EV is subject to

the following equations:

$$SOC^{H}_{s,t} \geq \alpha^{LB,Res}_{s,t} \,.\, SOC^{H}_{s,min} - SOC^{Res,LB}_{s,t} \quad \forall t \in \mathcal{T} \wedge \forall s \in \boldsymbol{\mathcal{S}} \wedge S^{Flt}_{t} = 0 \tag{3.8}$$

$$SOC^{H}_{s,t} \leq \alpha^{UB,Res}_{s,t} .SOC^{H}_{s,max} + SOC^{Res,UB}_{s,t} \quad \forall t \in \mathcal{T} \wedge \forall s \in \boldsymbol{\mathcal{S}} \wedge S^{Flt}_{t} = 0, \tag{3.9}$$

where (3.8) and (3.9) represent the upper and lower bound reserve limits of the SoC, respectively. Both limits are adjusted and controlled by the ancillary services contribution factors for each EV s ($\alpha^{LB,Res}_{s,t}$, $\alpha^{UB,Res}_{s,t}$), as well as slack variables ($SOC^{Res,LB}_{s,t}$, $SOC^{Res,UB}_{s,t}$). The slack variables allow the optimization program to converge in case it is not feasible for an EV to participate in ancillary services. When the value of a slack variable is zero, it means that the EV is able to contribute to the ancillary service signal in full. The slack variables are limited by the following:

$$0 \leq SOC^{Res,LB}_{s,t} \leq (\alpha^{LB,Res}_{s,t} - 1) \,.\, SOC^{H}_{s,min} \quad \forall t \in \mathcal{T} \wedge \forall s \in \boldsymbol{\mathcal{S}} \wedge S^{Flt}_{t} = 0, \tag{3.10}$$

$$0 \leq SOC^{Res,UB}_{s,t} \leq (1 - \alpha^{UB,Res}_{s,t}) \,.\, SOC^{H}_{s,max} \quad \forall t \in \mathcal{T} \wedge \forall s \in \boldsymbol{\mathcal{S}} \wedge S^{Flt}_{t} = 0, \tag{3.11}$$

where (3.10) and (3.11) represent the limit for battery reserve management slack variables.

Fleet Storage Constraints

The collective storage capacity controlled by the EV fleet operator is represented as follows:

$$\sum_{s \in \boldsymbol{\mathcal{S}}} SOC^{H}_{s,min} + SOC^{Flt,LB}_{t} \leq \sum_{s \in \boldsymbol{\mathcal{S}}} SOC^{H}_{s,t} \leq \sum_{s \in \boldsymbol{\mathcal{S}}} SOC^{H}_{s,max} - SOC^{Flt,UB}_{t} \quad \forall t \in \mathcal{T} \wedge S^{Flt}_{t} = 0, \tag{3.12}$$

where $SOC_t^{Flt,LB}$ and $SOC_t^{Flt,UB}$ in (3.12) are adjustment parameters decided depending on the reserve contribution factor of each individual EV, as follows:

$$SOC^{Flt,LB} = \sum_{s \in \boldsymbol{\mathcal{S}}} (\alpha_{s,t}^{LB,Res} - 1) \,.\, SOC_{s,min}^{H} \quad \forall t \in \mathcal{T} \wedge S_t^{Flt} = 0 \tag{3.13}$$

$$SOC^{Flt,UB} = \sum_{s \in \boldsymbol{\mathcal{S}}} (1 - \alpha_{s,t}^{UB,Res}) \,.\, SOC_{s,max}^{H} \quad \forall t \in \mathcal{T} \wedge S_t^{Flt} = 0. \tag{3.14}$$

Ancillary Service Constraints

The collective EV fleet response to an ancillary service signal by the grid is modeled as below:

$$P_{s,t}^{Flt} = P_t^{Anc} + P_t^{Flt,Dhg} - P_t^{Flt,Chg} \quad \forall t \in \mathcal{T} \wedge S_t^{Flt} = 1 \tag{3.15}$$

$$SOC_{s,min}^{H} \leq SOC_{s,t}^{H} \leq SOC_{s,max}^{H} \quad \forall t \in \mathcal{T} \wedge \forall s \in \boldsymbol{\mathcal{S}} \wedge S_t^{Flt} = 1, \tag{3.16}$$

where $P_t^{Flt,Dhg}$ and $P_t^{Flt,Chg}$ in (3.15) control the ancillary service contribution for the entire fleet and ensure that the optimization model converges in case it is not profitable or it is infeasible to participate. Equation (3.16) indicates that the reserved energy can be released when an ancillary service signal is received. The slack variables in (3.15) are limited by:

$$P_t^{Flt,Chg},\ P_t^{Flt,Dhg} \geq 0 \quad \forall t \in \mathcal{T}. \tag{3.17}$$

Profit Target Constraints

The EV fleet optimization problem aims to achieve a daily revenue target, while limiting fare prices in order to make the fleet more competitive in the market. This is achieved

through the following price control model:

$$M_t^{Trp} = M_t^{Trp,Min} + M_t^{Trp,Adj} \quad \forall\, t \in \boldsymbol{\mathcal{T}} \tag{3.18}$$

$$0 \leq M_t^{Trp,Adj} \leq \gamma_t^{Trp} \cdot M_t^{Trp,Min} \quad \forall\, t \in \boldsymbol{\mathcal{T}}, \tag{3.19}$$

where (3.18) controls the price through adjustable slack variable limited by (3.19). The control model ensures a minimum price adjusted according to a target daily revenue. The target revenue model is given by the following:

$$R^{Exp} - R_t^{Exp,Adj} \leq \sum_{t \in \boldsymbol{\mathcal{T}}^*} \sum_{s \in \boldsymbol{\mathcal{S}}} \Big\{ P_{s,t}^{Flt}.C^{Flt} - P_{s,t}^{Utl}\,.\,C_t^{ToU} + M_t^{Trp,Min}.\, D_{s,t} + M_t^{Trp,Adj}.\, D_{s,t} \Big\} \forall t \in \boldsymbol{\mathcal{T}}^*, \tag{3.20}$$

where T^* is a set of historical and look-ahead time steps as shown in Fig. 3.3. The figure shows that the scheduling model stores and utilizes the historical revenue data that are added to the future revenue values. The fare is computed based on the expected revenue over a given time period (i.e., T^*). The calculated profit is resulted from the sum of the historical revenue data over the past several hours and the look–ahead revenue values. This would ensure that unexpected and sudden changes in the market does not cause abrupt changes in the fare prices. In such a case, the price follows a smoother trend to ensure that the longer–term revenue quantities meet the expected value rather than very short–term targets. The target revenue model in (3.20) indicates that revenue achieved at time step t should be at least equal to the summation of historical and expected revenue in the next several time steps that are pre-defined in the model. Since transportation and ancillary services as well as charging operations are unpredictable,

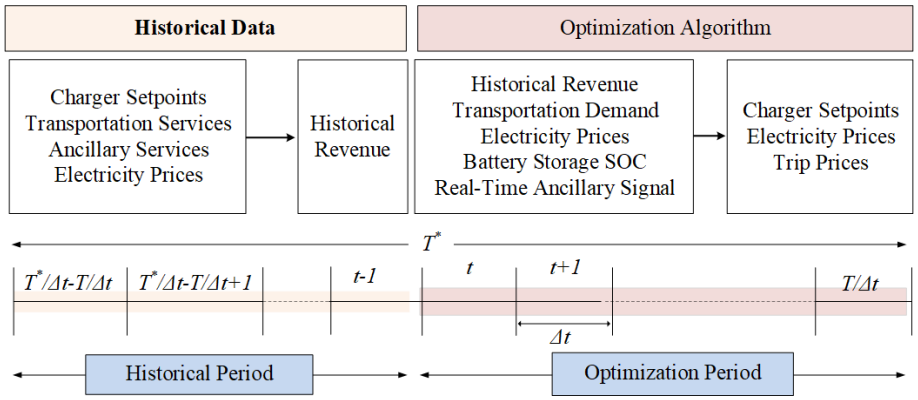

Fig. 3.3. Revenue calculation during historical and look-ahead time period.

a slack variable $R_t^{Exp,Adj}$ is utilized to ensure that the model converges in case it did not achieve the target revenue. The revenue adjustment slack variable is limited by the following:

$$0 \leq R_t^{Exp,Adj} \leq \gamma^{Exp}.R^{Exp} \quad \forall\, t \in \boldsymbol{\mathcal{T}}. \tag{3.21}$$

Since the price and revenue adjustment slack variables are conflicting, the penalty terms are set to assign priority to price adjustment rather than the revenue as follows:

$$\sigma_t^{Trp,Adj} \leq \sigma_t^{Exp,Adj} \quad \forall\, t \in \boldsymbol{\mathcal{T}}. \tag{3.22}$$

3.3 Numerical Studies

The proposed model in Section 3.2 is simulated to evaluate its effectiveness. Practically, a fleet can consist of any number of vehicles [115]. Without loss of generality, simulations are carried out on a fleet of 10 EVs because it is difficult to show detailed simulations results for higher numbers, but the model can be extended to thousands of EVs. The EVs considered in the simulation platform are considered as being the same type of Tesla

Model S. This type of EV has a battery capacity (i.e., SOC^{H}_{max}) of 75 kWh and an average energy consumption rate N^{Drv} of 22kWh/100km [116]. The onboard charger available for this EV is rated at 11.5 kW [117]. Figs. 3.4 (a) and (b) show the electricity prices and the expected travel plan for a typical day used for simulation studies, respectively. The price for electricity purchase by EVs is based on Ontario ToU rates [118] consisting of:

- Off-peak rate from 7 p.m. to 7 a.m.: 6.5 cents/kWh.
- Mid-peak rate from 7:00 a.m. to 11:00 a.m. and from 5:00 p.m. to 7:00 p.m.: 9.4 cents/kWh.
- On-peak rate from 11:00 a.m. to 5:00 p.m.: 13.2 cents/kWh.

Further, different trip profiles are considered for each EV in the fleet as illustrated by Fig. 3.4 (b). The EV fleet is simulated for two cases, the first case considers only normal fleet management and does not include a provision of ancillary services to the grid. In the second case, a provision of ancillary services to the grid with different hours of support per day is considered in the simulations. It is worth noting that the operating reserve is considered as the ancillary services to the grid for simulation purposes.

3.3.1 Case 1: No Ancillary Services Support to Power Grid

Fig. 3.5 shows the simulation results when EV fleet is operating for transportation services only. In particular, Fig. 3.5 (a) shows the charger power of each EV in the fleet, while Figs. 3.5 (b) and (c) demonstrates the SOC of each EV and the total fleet SOC, respectively. Figs. 3.5 (a) and (b) show that each EV has its own charging profile

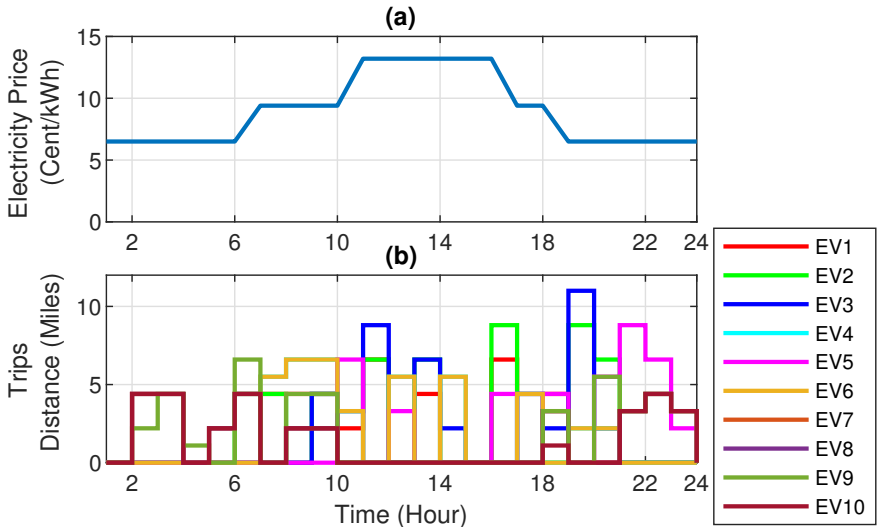

Fig. 3.4. Simulation parameters for Cases 1 and 2, (a) Electricity prices as per Ontario ToU rates, and (b) Simulated trips profiles for fleet EVs considered for simulation.

that is optimized to reduce charging costs and manage the battery level to be ready for all trips. For example, EV no. 6 starts at an SOC equal to 29% and charges at rated power when the electricity price is lower in order to reach an SOC level of 50%. During peak electricity rates, it charges only at half of the rated charger power to reduce the cost while maintaining the energy in the battery to satisfy the planned trip as shown in Figs. 3.5 (a) and (b). The total SOC of all EVs in the fleet starts at around 37% and end up with 31% at the end of the simulation time. This small decrease is due to all the charging signals that the central controller sends in order to keep enough battery level required for the operation of EVs. It is worth noting that the EV fleet does not keep a reserve margin in this case since it only operates for transportation services. Therefore, the charging setpoints are optimized to keep the collective SOC within the fleet above the minimum value (i.e. 10%) and charge only when it is required to satisfy the expected travel plan. Figs. 3.5 (d) and (e) demonstrate the fleet revenue and trip

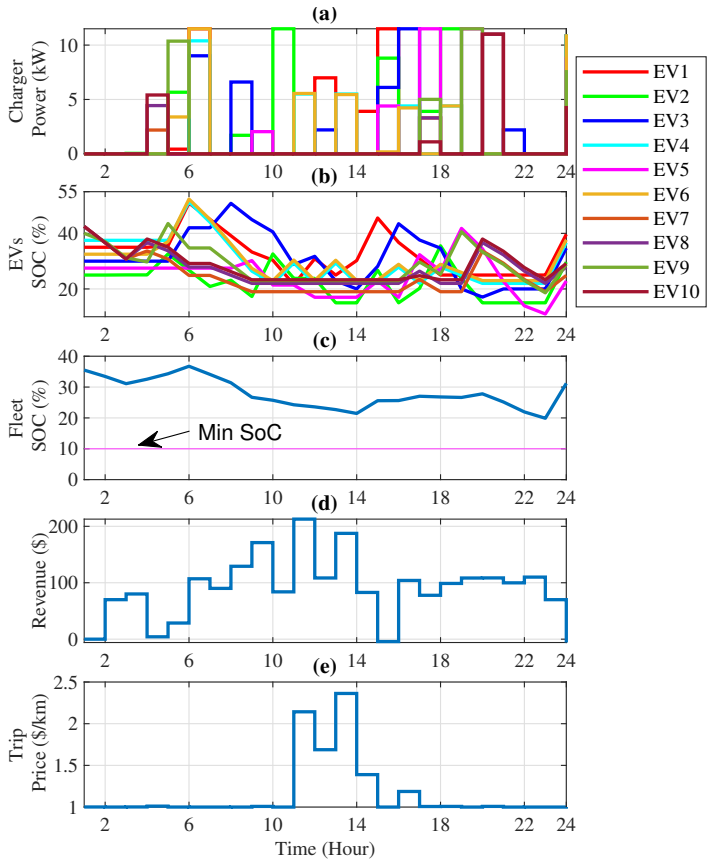

Fig. 3.5. Simulation results when EV fleet is operated for transportation services only, (a) EV chargers' power, (b) EVs SOC, (c) EV fleet total SOC, (d) Fleet operator revenue, and (e) Passenger trip price.

price for each hour of the scheduling time, respectively. It can be seen from Fig. 3.5 (e) that the trip price increases during peak time in order to achieve the daily target revenue. The average price over the simulation period is $1.158.

3.3.2 Case 2: With Ancillary Services Support to Power Grid

In this case, the EV fleet operates to provide concurrent services to the transportation system and the ancillary services market. Figs. 3.6, 3.7, and 3.8 show the simulated

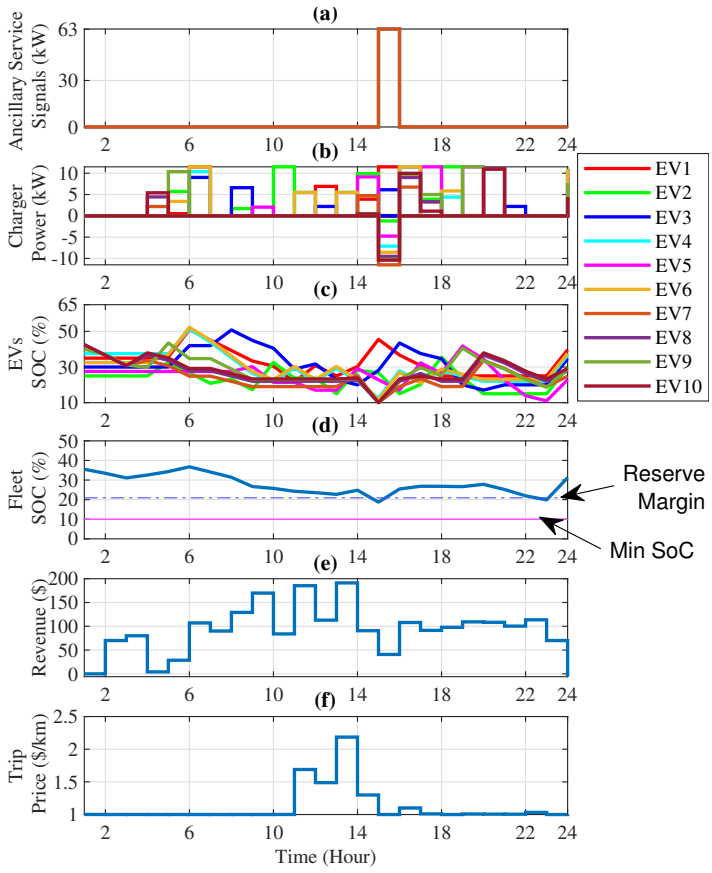

Fig. 3.6. Simulation results when EV fleet is operated for transportation services and *one hour* of ancillary service per day, (a) Ancillary service signals, (b) EV chargers' power, (c) EVs SOC, (d) EV fleet total SOC, (e) Fleet operator revenue, and (f) Passenger trip price.

operating parameters when the fleet is operated for one, two, and four hours of ancillary services, respectively. Fig. 3.6 (a) shows the ancillary service signals sent by the grid to the fleet operator. The charger power of each EV in the fleet is shown in Fig. 3.6 (b), while Figs. 3.6 (c) and (d) demonstrate the SOC of each EV and the total fleet SOC, respectively. Figs. 3.6 (e) and (f) demonstrate the fleet revenue and trips price for each hour of the scheduling time, respectively. In this case, the ancillary service signals are issued at 3 p.m for Case 1, at 11 a.m and 3 p.m for Case 2 (two hours contribution),

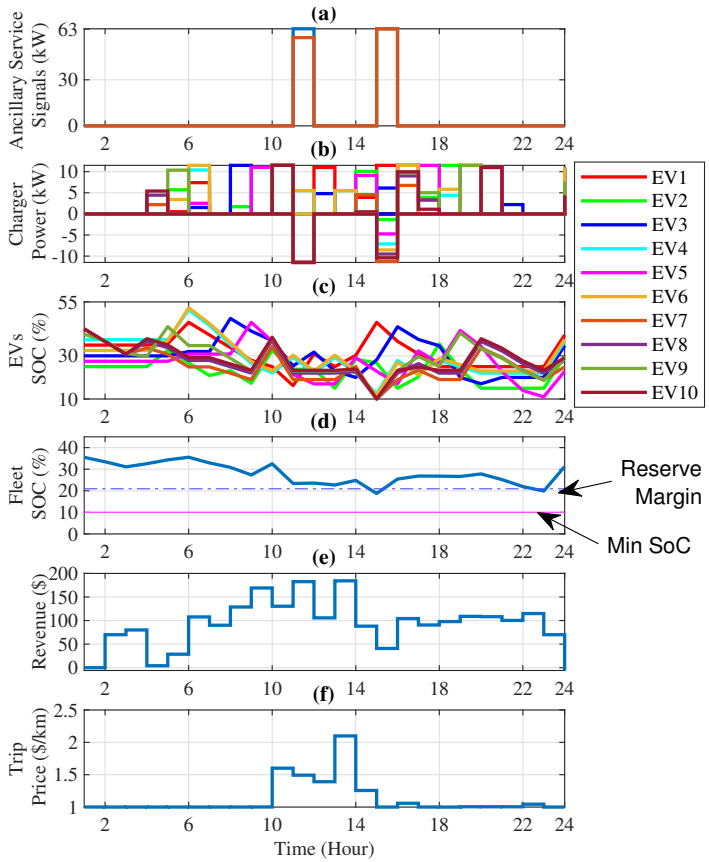

Fig. 3.7. Simulation results when EV fleet is operated for transportation services and *two hours* of ancillary service per day, (a) Ancillary service signals, (b) EV chargers' power, (c) EVs SOC, (d) EV fleet total SOC, (e) Fleet operator revenue, and (f) Passenger trip price.

and at 3 a.m, 4 a.m, 11 a.m, and 3 p.m for Case 4 (four hours contribution). Such signals are sent during the day including discharging requests in order to assist the grid during the peak load demand. Charging signals are sent when there is surplus generation from renewables at night, as studied in Case 2. It can be noticed from Figs. 3.6, 3.7, and 3.8 that the model always maintain the EV fleet SOC above the reserve margin level which is set at 22%, calculated based on the required energy in the fleet. However, when an ancillary service request is received, the model releases this reserve if

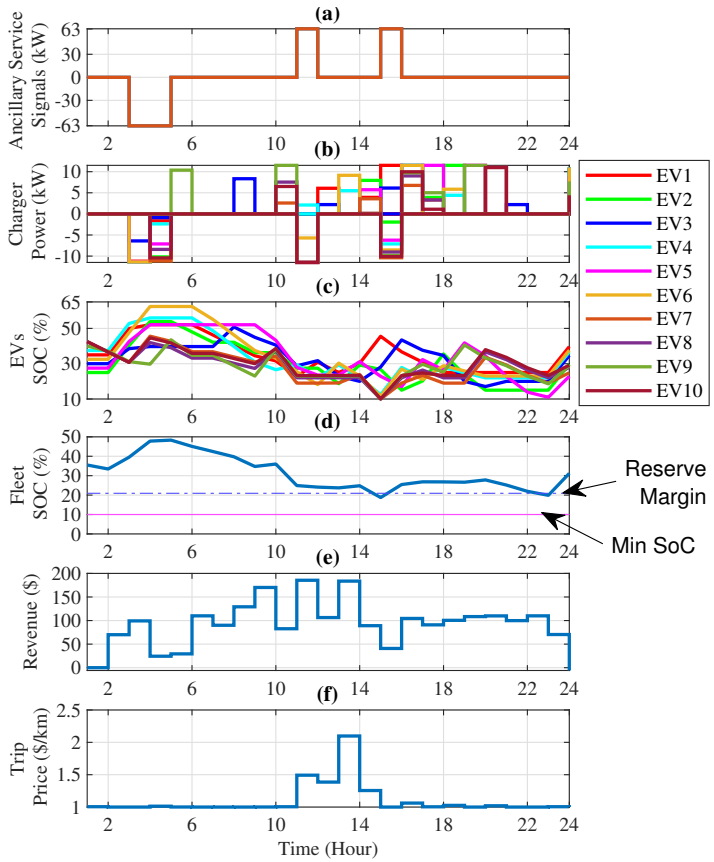

Fig. 3.8. Simulation results when EV fleet is operated for transportation services and *four hours* of ancillary service per day, (a) Ancillary service signals, (b) EV chargers' power, (c) EVs SOC, (d) EV fleet total SOC, (e) Fleet operator revenue, and (f) Passenger trip price.

necessary to provide the required service to the grid. For example, Fig 3.6 (d) shows that during the peak time when EVs SOC is depleted for EV transportation, the model releases 3.5% of the EV fleet SOC reserve (equal to 26 kWh) in order to respond to the signal received at 3 p.m. Once the signal comes to an end, the model immediately starts raising the EV fleet SOC above the reserve level. Nevertheless, the availability of reserve SOC is not the only factor that affects the response to the ancillary signals. Since the model utilizes the distributed SOC of individual EVs to respond to such ancillary service

signals, the availability of the EVs might limit the capability of the fleet to respond. This is shown in Fig. 3.7 (a), where the EV fleet only provides 57 kWh in response to a 64 kWh discharging signal (compare blue vs. red curves at hour 11:00 a.m). This limited response occurs due to the fact that most EVs serving trips at the issue time of the signal . Therefore, the model manages such a situation by partial cancellation of the signal in order to converge. This demonstrates the distributed management capability of the model in managing concurrent services to the grid and transportation sector. Further, the average trip prices are calculated for each ancillary service participation level and found to be $1.123 for one hour, $1.117 for two hours, and $1.098 for four hours. This indicates that the more the fleet participates in the ancillary services, the lower the trip price becomes. This allows the fleet to stay competitive in the market, which translates into higher revenue in long term.

3.3.3 Financial Analysis of Case Studies 1 and 2

Several financial parameters are computed under various ancillary service provisions, and the results are listed in Table 3.3. The parameters are defined as follows [119, 120]:

- Gross income: indicates the fleet total revenue from services less the operating costs.
- Net income: represents the fleet's profit after considering all expenses, including capital and operating costs.
- NPV: represents the difference between the present and future cash inflows, considering the discount rate throughout the years.

- Break even time: the time required for the discounted cash inflows in the fleet to match the initial capital costs.
- IRR: shows the percentage of profit from the fleet throughout its lifetime. An iterative trial and error method is used to calculate this value based on cash inflows and outflows during the yearly intervals.
- Profitability: the system profitability considering the initial cost and expected return of investment.

As reported in the table, the level of contribution to ancillary services affects the financial parameters of the EV fleet. In general, the gross income, net income, NPV, IRR, and profitability levels all increase with an increase in ancillary services contribution. In particular, the gross and net incomes of the EV fleet are enhanced from \$0.770 M and \$0.172 M (under no participating to ancillary services) to \$0.795 M and \$0.196 M under four hours of services per day. In such a case, the NPV is increased from \$0.765 M to \$0.969 M, while the IRR and the profitability are improved by 0.66% and 1.75%, respectively. The increase is due to compensation paid by the grid to the fleet operator for the serviced energy, as well as payment for the availability to provide the services. It is worth noting that despite the decrease in average trip prices for the passengers at higher levels of ancillary services provision, the profitability of the EV fleet system increases by 1.85%.

3.3.4 Model Solution and Convergence Analysis

This section serves to analyze the convergence and optimality of the optimization problem. The model is linear when no ancillary service provision to the grid is considered. In this

Table 3.3: Annual Financial Parameters of EV Fleet under Various Scenarios.

Ancillary Services	Gross Income	Net Income	Net Present Value	Break Even Time	Internal Rate of Return	Profitability
None	\$0.770 M	\$0.172 M	\$0.765 M	7.77 Year	4.87%	55.95%
One Hour/Day	\$0.786 M	\$0.187 M	\$0.890 M	7.6 Year	5.27%	57.1%
Two Hours/Day	\$0.789 M	\$0.191 M	\$0.920 M	7.58 Year	5.38%	57.3%
Three Hours/Day	\$0.791 M	\$0.192 M	\$0.936 M	7.57 Year	5.41%	57.4%
Four Hours/Day	\$0.795 M	\$0.196 M	\$0.969 M	7.53 Year	5.53%	57.7%

case, the dual simplex method is utilized to obtain optimal solutions to the proposed optimization problem [121]. When an ancillary service participation is considered, the model activates the constraints (3.4) and (3.5), which are needed to force the EV battery to operate in either charging or discharging mode.

With the ancillary service provision taken into consideration, the model becomes a non-convex bi-linear optimization problem. For this problem type, the Gurobi non-convex quadratic-constrained program solver has been used in this research to obtain optimal solutions [122]. Gurobi searches for and guarantees globally optimal solutions to bi-linear QCPs by applying spatial branch-and-bound method to solve the problem. The quality of the solution for this type of optimization has been evaluated and depicted in Fig. 3.9. Fig. 3.9 (a) shows tracking the relative optimality gap percentage between the primal objective bound and the dual objective bound, and (b) depicts tracking the current objective bound for a feasible solution. The relative optimality gap is calculated as follows:

$$Gap\% = \frac{|z_P - z_D| \times, 100}{|z_P|} \tag{3.23}$$

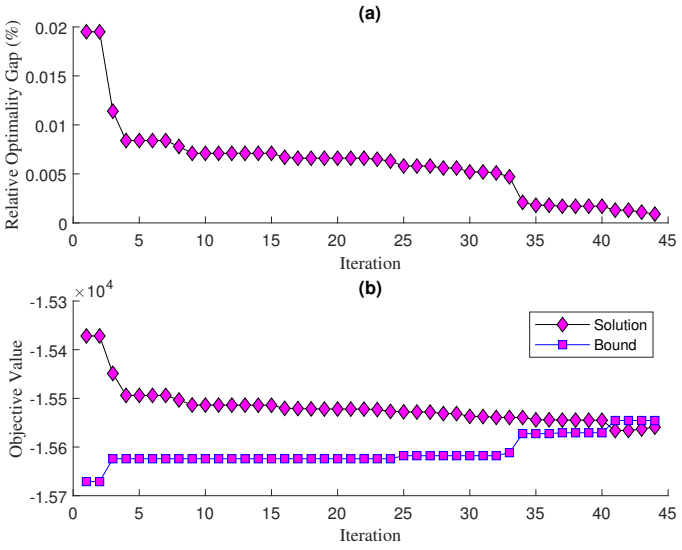

Fig. 3.9. Model convergence analysis.

where z_P and z_D represent the primal and dual objective bounds, respectively. As shown in the figure, the model terminates at the optimal solution after 44 iterations when the relative optimality gap is less then 10^{-6} times the absolute value of the objective solution [122].

3.3.5 Computational Analysis

The model complexity is analyzed is order to study the effect of increasing the fleet size on real-time optimization of the fleet operation. All simulations are run on a desktop PC with a 64-bit Intel Core i7-8700T CPU running at 3.50 GHz with 16 GB RAM. The processing time of the proposed optimization problem includes two stages, pre-optimization and optimization. The pre-optimization stage involves model formation which includes building the objective function and constraints, assigning constant coefficients, and determining problem variables. This stage does not affect the

real-time operation and can be performed offline. The second stage includes operations that need to be handled in real time in order to obtain the optimal solution of the model. This includes assigning time-varying coefficients and algorithm solving. Table 3.3 lists the computational time required for the algorithm formation and optimization.

Table 3.3: Computational Time of the Proposed Model per Number of EVs.

No. of EVs	Model Formation (s)	Model Optimization (s)
10	0.02915	0.316
20	0.04450	0.278
50	0.20695	0.279
75	0.4494	0.282
100	0.7922	0.416
200	3.7107	0.746
500	40.856	1.102
750	132.547	1.382
1000	662.435	1.751

It can be observed from Table 3.3 that the total computational time of the proposed model grows exponentially with the number of EVs. Therefore, the regular PC utilized to run the simulations in this research can only handle few thousands of EVs. In this regard, a super computer with enhanced computational power or a high performance distributed grid computing system is required to handle higher number of EVs. Using a super computer to handle operation optimization and scheduling of more than few thousands of EVs in large fleet systems is expected.

3.4 Discussion and Summary

This chapter develops a model for a central controller in a fleet system that allows adaptive utilization of EV batteries distributed energy for concurrent services to the transportation

sector and ancillary services market. The optimization model incorporates various slack variables and control parameters for managing real–time fare prices, adaptive energy and reserve margin allocation, spotting EV locations, interaction with the grid operator, and meeting the fleet target revenue. The model allows EV drivers to flexibly manage their battery capacities based on their availability and assessment of the transportation services demand when needed. The numerical results for various cases including no contribution, low contribution, and high contribution levels to the ancillary services market are presented. The results demonstrate how distributed energy stored in several EV batteries within the fleet can be used as a whole to support the grid without negative impacts on the regular trip schedule. The effectiveness of the proposed model for creating the reserve margin is evident from the results. The reserve margin is optimally utilized to meet the grid's demand when needed. The success of the proposed dynamic pricing mechanism for real–time calculation of fare rates for achieving daily revenue target in a competitive market is indicated. The results demonstrate that the extra revenue stream from contribution to the ancillary services market on top of the one from regular passenger transport enhances the system profit. It is indicated that the more the EV fleet participates in the ancillary services, the lower the trip prices become, and the more the system profit is enhanced. As such, the proposed model can increase the profitability of an EV fleet management system, thereby promoting investment and success in this area in the near future.

Chapter 4 - Decentralized Quality of Service Based System for Energy Trading Among Electric Vehicles

4.1 Introduction

In recent years, P2P energy trading among EVs (i.e. V2V) has been proposed as an energy management scheme that helps to regulate EV charging process as well as provide economic benefit to its participants [50]. V2V schemes allow distributed and flexible control of EV energy by balancing supply and demand through local transfer between EVs [123]. However, P2P EV energy trading models in the literature are limited to utilizing blockchain as a distributed database without proposing a specific governance mechanism that allows decentralized and autonomous matching and administration of the process. To address such shortfalls, there is a need to integrate EV energy trading within a decentralized platform that can match, monitor, and govern the P2P transactions between EV users. Another common shortfall in previous works of P2P energy trading among EVs is the lack of QoS control metrics that consider user preference and help trading participants achieve reliable and flexible transactions. Despite incorporating user preferences in the P2P energy trading process, the studies in [15] and [52] are only concerned with preferences related to the amount of energy traded and profit/cost

of trade, while the study in [53] only considers the predefined deadlines of EV energy consumers, which may not be sufficient to provide satisfactory services to the participants. For instance, these studies do not consider aspects related to unexpected changes to schedule of EV users in their developed energy trading models, which could pose a risk to P2P trading and cause sudden disruptions/disconnections. For this reason, participants would be discouraged to consider P2P charging as a reliable service and thus careful consideration should be given for the incorporation of QoS management in P2P energy trading among EVs. In this context, this research contributes to the existing literature by proposing a novel QoS-based scheme for P2P energy trading systems among EV energy providers and consumers. Without loss of generality, six QoS attributes have been selected and modeled in this work. These attributes are: requested energy, power transfer rate, risk of disconnection/unavailability, time flexibility, budget, and credibility. Such attributes have been selected considering the goals of achieving user satisfaction with transaction reliability and flexibility. The proposed P2P energy trading scheme includes weight values that are assigned to QoS requirements to reflect their relative importance to energy consumers. In this regard, a fuzzy-based approach with minimum and intelligible input is introduced to determine the weight values of QoS requirements. Also, two QoS-based matching mechanisms that work like reverse auctions are proposed to match energy trading EVs. These include SCMP and MCMP matching mechanism. In order to discourage dishonest requests/offers and ensure that trading parties stick to their contractual obligations, a penalty mechanism is developed and incorporated in the proposed scheme. The proposed QoS–based scheme utilizes a smart contracts platform to carry out (i) the matching between EV energy providers and consumers, and (ii) monitor the delivery of contracts without the presence of a third party. A smart contract

is an autonomous executable software on the blockchain network that enforces specific terms and conditions between transaction parties without the requirement of third-party interference. Smart contracts make the trading process more transparent because its contents can be seen by all nodes and the contract's code logic is more straightforward when compared to the complex language used in traditional contracts [54].

Table 4.1 presents the nomenclature of the proposed system model.

Table 4.1: Chapter 4 Nomenclature

Indices		F	Utility function.
h	Index of QoS attributes.	k	Number of QoS attributes.
j	Index of energy provider EVs.	L	Preference vector.
i	Index of energy consumer EVs.	m	Number of energy provider EVs.
		n	Number of energy consumer EVs.
Sets		O	Energy provider offer.
$\mathcal{C}$	Set of energy consumer EVs.	P	Power transfer rate.
$\boldsymbol{\mathcal{D}}$	Set of energy provider EVs.	R	Energy consumer request.
		RD	Risk of disconnection.
Parameters		T	Time flexibility.
B	Budget.	y	QoS attribute value.
CR	Credibility.		
e	Links (edges) between vertices.		
E	Requested energy.		

4.2 System Model

Fig. 4.1 depicts a schematic diagram of the P2P energy trading system considered in this work. As shown in the figure, the system consists of physical and cyber layers. Transactions in the form of P2P energy transfer occur in the physical layer, which constitutes the parking lot that is agreed upon beforehand between the trading participants. It is assumed that these transactions are carried out in local areas, where designated

parking lots are not more than 10 km far from participants. This restriction can be enforced through smart contracts that only matches between participants located within this distance. The energy consumed to reach the designated parking lots is small and participants are assumed to have taken this cost into their price consideration.As illustrated by Fig. 4.1, the designated parking lots are equipped with connection points that allow bidirectional power transfer using short underground connections with minimum losses. Such a setup has been proposed by many studies, e.g. in [58] and [51]. The main asset traded is energy, which is measured through smart meters/chargers that are connected to the communication layer represented by the blockchain network. This allows the smart contract to monitor the QoS delivery and compliance at runtime. For example, the energy transferred can be measured at the smart charger terminal whereas the time of connection and disconnection to the smart meter is enough to measure any time-related QoS requirements. Moreover, all P2P energy trading transactions between EVs are recorded in a distributed ledger shared by all peers in the network. This feature allows smart contracts to review the transactions they participated in, which could be used to assign a credibility score to each participant. Also, the smart contract has access to e-wallets of trading participants, which are used in transactions settlement.

In this model, an EV that requires energy is represented as an EC, whereas an EV with excess energy to sell is defined as an EP. EPs compete to win energy transfer contracts from ECs by offering better QoS values than competitors. The smart contract receives from ECs their energy requests that include specific QoS requirements. Based on these requirements, the smart contract generates an energy request on the blockchain network that can be read by all other nodes that have access to the distributed ledger. EPs respond by submitting offers based on their capabilities to satisfy the QoS requirements.

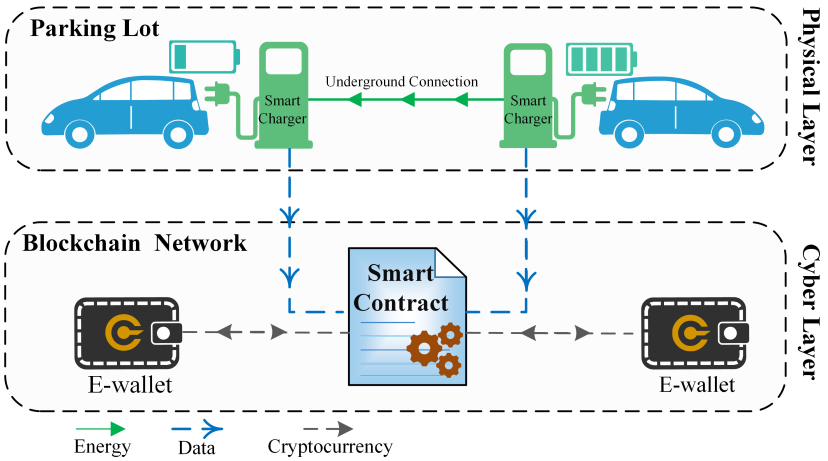

Fig. 4.1. Schematic diagram of a blockchain–based P2P energy trading system between EVs.

The smart contract creates a matching and agreement between the trading parties and administers the trading process to ensure adherence to the terms agreed upon in the contract. The mathematical representation of the system model is given by the following:

Let C and D be the respective sets of ECs and EPs as listed below:

$$i \in C \ \wedge \ C = \{1, 2, .., n\}, \tag{4.1}$$

$$j \in D \ \wedge \ D = \{1, 2, .., m\}, \tag{4.2}$$

where n and m are the number of ECs and EPs, respectively. An EC demands energy in the form of a tuple set R that includes all QoS requirements as follows:

$$R_i = ([R_{1,i}^{min}, R_{1,i}^{max}], ..., [R_{h,i}^{min}, R_{h,i}^{max}], [R_{k,i}^{min}, R_{k,i}^{max}]), \quad \forall i \in C \tag{4.3}$$

where $[R_{i,h}^{min}, R_{i,h}^{max}]$ represents the range of acceptable values of the h^{th} QoS requirement belonging to the i^{th} EC. k is the number of QoS requirements in the request. Similarly,

an EP presents an energy offer in the following tuple form:

$$O^j = (O^j_1, O^j_2, .., O^j_h, O^j_k), \tag{4.4}$$

where O^j_h is the h^{th} QoS attribute value given by the j^{th} EP. O^j must be within the range required by R_i in order to satisfy the EC's QoS requirements and qualify for matching. Given the decision matrix $Q = y_{jh}$ with alternative offers, $j = \{1, 2.., m\}$ and QoS attributes, $h = \{1, 2.., k\}$:

$$Q = \begin{bmatrix} y_{11} & y_{12} & \cdots & y_{1h} \\ y_{21} & y_{22} & \cdots & y_{2h} \\ \vdots & \vdots & \ddots & \vdots \\ y_{j1} & y_{j2} & \cdots & y_{jh} \end{bmatrix}, \tag{4.5}$$

the objective function of the system could be defined as follows:

$$\text{Max}: \quad \sum_i F_i(O^j), \quad \forall j \in D, \tag{4.6}$$

where $F_i(O^j)$ is the utility function of an EC i that indicates the EC satisfaction with the j^{th} EP offer. The utility function in (4.6) is subject to:

$$R^{min}_{h,i} \leq O^j_h \leq R^{max}_{h,i}, \quad \forall i \in C \ \wedge \ \forall j \in D, \tag{4.7}$$

where (4.7) indicates that every EP offer must be within the QoS limits that are pre-specified by the EC.

Based on the above discussions and without loss of generality, six QoS requirements

are modeled in this work as follows:

Requested energy: ECs submit a minimum E_{EC}^{min} and maximum E_{EC}^{max} energy demand limits to engage in P2P energy trade. This opens up the opportunity for more energy providers to submit bids by allowing flexible energy offers.

$$E_{EC}^{min} \leq E_{EP} \leq E_{EC}^{max} \tag{4.8}$$

Power transfer rate: ECs can specify how fast P2P trading is conducted by demanding a minimum discharging power P_{EC}^{min}. The power transfer rate is limited by the physical attribute of EC's charger P_{EC}^{max}.

$$P_{EC}^{min} \leq P_{EP}^{Dhg} \leq P_{EC}^{max} \tag{4.9}$$

Risk of Disconnection/Unavailability: due to the mobility of EVs and the uncertain schedule of EV users, there is a risk that an EV provider does not show up or disconnect during the trade. This requirement specifies how important this energy request to the EC. Risk value mainly affects the penalty imposed for not completing the trade. This deters EPs from engaging in trades that they are not sure to complete.

$$RD_{EP} \leq RD_{EC}^{Max} \tag{4.10}$$

Time flexibility: this requirement indicates how long an EC can wait from the designated time of trade for EP to arrive at the required parking lot and plug in their EV to the smart charger.

$$T_{EP} \leq T_{EC}^{max} \tag{4.11}$$

Budget: expresses the maximum cost EC is willing to pay for a unit of energy.

$$B_{EP} \leq B_{EC}^{max} \tag{4.12}$$

Credibility: given that an EC is looking to charge from another EV instead of the grid, it is reasonable that they prefer to trade with providers who have credibility. Credibility is affected by the number of withdrawals after winning the P2P energy trading contract, as well as the number of times EC's QoS requirements were not satisfied after winning the contract.

$$CR_{EC}^{min} \leq CR_{EP} \tag{4.13}$$

4.3 Decentralized QoS-based Matching System for Energy Trading EVs

This section describes the proposed decentralized QoS-based system for matching and administration of P2P energy trading among EVs. Fig. 4.2 demonstrates the self-enforcing smart contract scheme for matching and administration of P2P energy trading among EVs. As shown in the figure, the system consists of four main stages. In **stage one**, an EC specifies QoS requirements and invokes weight generation function *WeightGen()* to generate weights for these requirements. In this regard, it is required that all QoS requirements are assigned weight values that reflect their relative importance to the EC. These weight values allow ECs to customize their preferences and to differentiate between alternative offers. Further, when there are multiple matching mechanism available, the EC must select the one to be run inside the smart contract. In this work, two types of matching mechanisms are considered, which are SCMP and MCMP. In

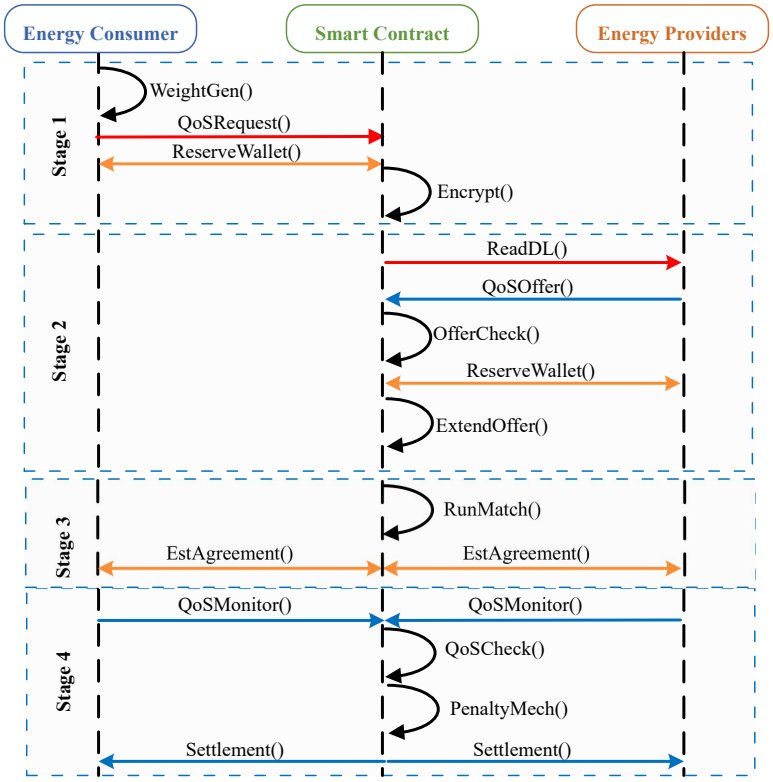

Fig. 4.2. Smart contract process flow diagram for P2P energy trading of EVs.

SCMP, multiple EPs submit energy offers based on the QoS request of a single EC (i.e. $|C| = 1, |D| \geq 1$), whereas multiple energy requests and offers are matched in the MCMP mechanism (i.e. $|C| \geq 1, |D| \geq 1$). These mechanisms work similar to reverse auctions, where the sellers bid to provide services to buyers. The SCMP is tailored to find the offer that provides the best utility to the EC considering their individual QoS requirements. The MCMP mechanism, however, aims to (i) satisfy QoS requirements of ECs, (ii) maximize matching of ECs and EPs, and (iii) maximize the sum of utilities for all matched ECs. Therefore, the two mechanisms have a trade-off in terms of utility and matching maximization. Accordingly, the EC uploads QoS requirements and their weight values, as well as the requested matching mechanism into the smart contract by

invoking *QoSrequest()*. When the smart contract receives *QoSrequest()*, it reserves an amount of B_{EC} from the e-wallet of EC to be used for payments and/or penalties. The matching mechanism and preferences of EC are then encrypted in order to prevent EPs from submitting dishonest offers that are tailored to win the energy contract.

In **stage 2**, an energy request is created on the blockchain network that can be read by all other nodes that have access to the distributed ledger. In response, EPs invoke *QoSOffer()* to upload their offers to the smart contract. The function *OfferCheck()* is then run to discard all offers that violate QoS requirement constraints presented in (4.8)–(4.13). Further, all offers are extended using *ExtendOffer()* to include the credibility attribute value obtained from the distributed ledger.

In **stage 3**, the smart contract runs the matching mechanism selected by the EC to determine the best offers, and then an agreement for P2P trade is established between the ECs and EPs according to the approved QoS attributes.

In **stage 4**, transaction parties carry out the energy trade at the agreed location and the smart contract monitors the energy meters of the transaction parties in order to measure the QoS of the trade. Based on the measured QoS, the function PenaltyMech(), which includes the payment and penalty process, is called to settle the trade with both parties.

4.3.1 Fuzzy-based QoS Attributes Weight Calculation Approach

ECs might not be able to manually determine the proper weight values that reflect the true importance of their QoS requirements because of the conflict of thoughts and priorities, as well as difficulty in expressing number ranking [124]. Several methods have been proposed in the literature to determine weight values based on preference input from

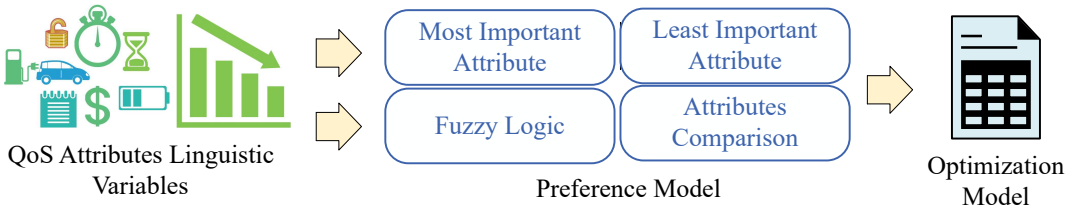

Fig. 4.3. Fuzzy-based approach to determine weight values of QoS requirements.

users but these methods require complicated inputs and suffer from inconsistency, as well as uncertainty [125]. Therefore, a fuzzy-based approach with minimum and intelligible input is proposed in this work to determine the weight values of QoS requirements. In this approach, the simplicity and intelligibility of the inputs help to reduce the inconsistency, whereas the uncertainty is tackled through fuzzy logic.

The proposed approach is illustrated in Fig. 4.3. As shown in the figure, an EC inputs the linguistic importance variables of QoS attributes to a preference generation model, which is used to determine EC's fuzzy preference ranking of the attributes. These preferences are inputted to an optimization model based on the Best Worst Method (BWM) [126], which generates optimal fuzzy weights for each QoS attribute.

Table 4.2: QoS Attributes Preferences Fuzzy Conversion.

Linguistic Terms	Relative Importance	Triangular Fuzzy Importance
Extremely High (EH)	1	(1, 1, 1)
Very High (VH)	2	(1.5, 2, 2.5)
High (H)	3	(2.5, 3, 3.5)
Medium High (MH)	4	(3.5, 4, 4.5)
Medium (M)	5	(4.5, 5, 5.5)
Medium Low (ML)	6	(5.5, 6, 6.5)
Low (L)	7	(6.5, 7, 7.5)
Very Low (VL)	8	(7.5, 8, 8.5)
Extremely Low (EL)	9	(8.5, 9, 9.5)

Algorithm 4.1: Preference Generation Model

Input: Linguistic terms set for QoS attributes
Output: Fuzzy preference vectors L_B^f and L_W^f
Generate relative importance set V from Table 4.2
$L_{bb} \leftarrow min(V_h)$
$L_{ww} \leftarrow max(V_h)$
$L_B \cup L_{bb}$
$L_W \cup L_{ww}$
for *each* $V_h \in V \setminus \{L_{bb}, L_{ww}\}$ **do**
    $L_{bh} = (V_h - L_{bb})$
    $L_{hw} = (L_{ww} - V_h)$
    $L_B \cup L_{bh}$
    $L_W \cup L_{hw}$
end

The linguistic importance terms are listed in Table 4.2. Nine importance levels are considered in this table because they allow a reasonable comparison for most individuals [127]. The linguistic terms are input to the preference generation model, which is shown in Algorithm 4.1. As depicted in the algorithm, the model converts linguistic terms to relative importance numbers V based on Table 4.2. For example, if the EC assigns a Very High (VH) term to a QoS attribute, then the model will convert it to the relative importance of $V = 2$. It is worth noting that the model is designed to interpret a higher V as of lower importance. Therefore, the model designates the attributes with minimum and maximum values of V as the most important and least important, respectively. Based on the relative importance values, the model generates two pairwise comparison vectors between the attributes, which are best-to-others vector L_B and worst-to-others vector L_W. In the L_B vector, the most important QoS attribute takes the rank of 1 (i.e. $L_{bb} = 1$) and the rest of the attributes are ranked based on the distance between its importance number V_h and L_{bb} in order to formulate the vector $L_B = (L_{b1}, L_{b2}, ...L_{bk})$.

Similarly, L_{ww} is ranked as 1, while the rest of the attributes are ranked based on the reverse distance between them and L_{ww} in order to generate the worst-to-others vector $L_W = (L_{1w}, L_{2w}, ..., L_{kw})$. Vectors L_B and L_W then undergo a fuzzification according to Table 4.2. For example, the vector $L_B = (1, 6, 2)$ will be converted to the triangular fuzzy vector $L_B^f = \Big((0.5, 1.0, 1.5), (5.5, 6.0, 6.5), (1.5, 2.0, 2.5)\Big)$.

Fuzzy preference vectors L_B^f and L_W^f generated from the preference generation model are utilized to find the optimal weight for each attribute h that satisfies the following constraints:

$$\frac{M_B^f}{M_h^f} \;=\; L_{bh}^f \;\;\wedge\;\; \frac{M_h^f}{M_W^f} \;=\; L_{hw}^f \;\; \forall\, h \in R, \tag{4.14}$$

where M_B^f and M_W^f are the weights of the highest and worst ranking attributes, respectively. The conditions in (4.14) can be met by finding the weights that minimize the maximum absolute difference of the terms as per the following BWM model:

$$\text{Min Max:} \;\; \left\{ \left| \frac{M_B^f}{M_h^f} - L_{Bh}^f \right|, \left| \frac{M_h^f}{M_W^f} - L_{hW}^f \right| \right\} \;\; \forall\, h \in R, \tag{4.15}$$

$$\sum_h M_h^f = 1, \;\; \forall\, h \in R, \tag{4.16}$$

$$M_h^f \geq 0, \;\; \forall\, h \in R. \tag{4.17}$$

The triangular fuzzy weight values obtained from (4.15)–(4.17) are defuzzified using the following equation [128]:

$$M_h = \frac{M_h^{f1} + 4.M_h^{f2} + M_h^{f3}}{6}, \;\; \forall\, h \in R. \tag{4.18}$$

4.3.2 Proposed QoS-based SCMP Matching Mechanism

The evaluation of the EC utility in problem (4.6) involves the assessment of EP offers in terms of all QoS characteristics in the design space. In this regard, multiple-attribute decision making (MADM) methods are suitable for problems with explicitly defined alternatives that have multiple attributes (i.e. discrete decision field) [127]. Therefore, an SCMP matching scheme based on a MADM technique is introduced to find the offer that maximizes EC utility. MADM is divided into non-compensatory and compensatory techniques. Non-compensatory techniques could exclude an offer based on one bad attribute, while compensatory ones allow “trade offs"; a decrease in one attribute could be compensated by another attribute. In the SCMP matching, the effects of all QoS attribute values must be considered in the best offer selection criteria. Therefore, a non-compensatory MADM method is utilized in this work [127]. Among different non-compensatory MADM methods, the Technique for Order of Preference by Similarity to Ideal Solution (TOPSIS) closely represents the selection rational of humans [129]. The basic principle of the TOPSIS method is to choose the alternative that stands closest to the positive ideal solution and farthest from the negative ideal solution. TOPSIS measures the Euclidean distance between each alternative and the ideal solution and then ranks them based on these measurements. In this context, the positive ideal solution is the alternative that realizes the best values for all attributes considered in the problem. Similarly, the worst attribute values represent the negative ideal solution. The proposed SCMP matching mechanism is therefore presented as follows:

Considering the decision matrix in (4.5), a weighted and normalized value is calculated

for each QoS as in (4.19):

$$v_{jh} = M_h \, . \, \frac{y_{jh}}{\sqrt{\sum y_{jh}^2}}, \; \forall \;\; j = 1, ..., m, \;\; h = 1, ..., k, \tag{4.19}$$

where M_h is the weight value of the j^{th} required QoS. Each QoS value is normalized using $\frac{y_{jh}}{\sqrt{\sum y_{jh}^2}}$. For each QoS requirement, the ideal offer A^+ and the negative-ideal A^- offer are determined as below:

$$A_h^+ = max_j \left(v_{jh}\right), \;\; A_h^- = min_j \left(v_{jh}\right), \; h = 1, ., k. \tag{4.20}$$

Subsequently, the euclidean distances between each offer and the ideal offer are calculated as follows:

$$ED_j^+ = \sqrt{\sum_j (v_{jh} \; - \; A_h^+)^2}, \; ED_j^- = \sqrt{\sum_j (v_{jh} \; - \; A_h^-)^2} \tag{4.21}$$

Finally, the relative closeness RC_j to the ideal solution for each offer is calculated as per the following equation:

$$RC_j \; = \; \frac{ED_j^-}{ED_j^- + ED_j^+}, \tag{4.22}$$

where a higher value of RC_j indicates a higher utility obtained from offer j in relative to other offers.

4.3.3 Proposed QoS-based MCMP Matching Mechanism

In this section, a QoS-based matching mechanism is proposed to allocate multiple EP offers to EC requests. The matching of multiple EP offers to multiple EC requests is a

combinatorial optimization problem that considers the objective of finding the optimal assignment of EPs to ECs that maximizes total social welfare as follows:

$$\max \sum_{i=1}^{n} \sum_{j=1}^{m} e_{i,j} \, . U_{i,j}, \tag{4.23}$$

where $e_{i,j}$ represents the linking between the i^{th} EC and j^{th} EP, whereas $U_{i,j}$ expresses the utility resulting from this linking. The problem in (4.23) is subject to:

$$\sum_{i=1}^{n} e_{i,j} = 1, \quad \forall \ \ j \in D, \tag{4.24}$$

$$\sum_{j=1}^{m} e_{i,j} = 1, \quad \forall \ \ i \in C, \tag{4.25}$$

$$e_{i,j} \in \{0,1\}^{nxm}, \quad \forall i \ \in C \quad \wedge \forall \ j \in D, \tag{4.26}$$

where (4.24) and (4.25) indicate that only one EP can be assigned to one EC. In this study, an MCMP matching mechanism with elements from matching theory and auction algorithm [130] is introduced to solve the integer optimization problem in (4.23)–(4.26).

The procedures of this mechanism are shown in Algorithm 4.2. In this mechanism, the matching of multiple ECs and EPs based on QoS attributes is modeled as a weighted bipartite graph [131]. Using the energy requests and offers received by the smart contract, an undirected bipartite graph model $G = (C, D, E)$ is constructed. In this model, C and D are two independent sets of vertices that represent n EC requests and m EP offers, respectively. E denotes the set of edges e that link requests to the offers that can satisfy their QoS as per (4.7). Each edge e_{ij} in G that links between the i^{th} request and j^{th} offer is assigned a value Uij that represents the utility of the i^{th} EC obtained from the

j^{th} EP offer. Similar to the SCMP mechanism, a special utility calculation method must be employed considering different attribute units and weights. However, the MCMP mechanism requires a method that finds the absolute utility for each EC in order to maximize the utilities of all ECs.

Therefore, the weighted sum model (WSM) [129] is employed to calculate U_{ij} as follows:

$$U_{ij} = \sum M_h \times \eta(O_h^j) \tag{4.27}$$

where M_h is the weight of the h^{th} QoS attribute, while $\eta(O_h^j)$ is the h^{th} normalized QoS attribute. The constructed weighted bipartite graph G is used to produce a maximum weighted matching $\mathcal{M}$. In the matching phase of the MCMP mechanism, ECs are considered as bidders, EPs as goods, and the utility that an EP j gives to EC i as the value of the matching. The matching could be initialized with any set of assignments and prices while each round of the mechanism has its own assignment and prices set. In this case, an empty assignment set $\mathbb{M}$ is considered, and all unassigned ECs are grouped in a queue set S, while the prices for EP offers in the set P_j are initialized to zero. The matching phase consists of two parts: bidding and assignment. In the bidding part, all unassigned bidders place their bids on the goods that provide them with the best utility. The bids are calculated as follows:

$$bid_{i,j} = p_j^* + v_i - u_i + \delta \tag{4.28}$$

where p_j^* is the previous round price for the good, v_i and u_i are the highest and second highest utilities of all objects, respectively, and δ is a positive real number value that prevents infinitive bidding rounds when two bidders get the same utility from one good [130].

Algorithm 4.2: Proposed MCMP Matching Mechanism

Input: C & D

Output: Maximum weighted matching $\mathcal{M}$

Graph Construction Phase:

$E \leftarrow \emptyset$

for *each* $j \in D$ *&* $i \in C$ **do**

  if $|O^j| \geq |R_i|$ **then**

    $U_{ij} = \sum M_h \times \eta(O_h^j))$

    $E \cup (j \leftrightarrow i, U_{ij})$

  end

end

Matching Phase:

$\mathcal{M} \leftarrow \emptyset$

$S = \{c_1, c_2, ...c_n\}$ //unassigned ECs

$p_j \leftarrow 0 \ \ \forall \ j \in D$

$NT = n + m$ //number of trading participants

$\delta = \frac{1}{1+(NT)}$

while $S \neq \emptyset$ **do**

  ***Bidding*:**

  for *each* $i \in S$ **do**

    $j_i^* = argmax_j \ \ (U_{ij} - p_j)$

    $v_i = max_j \ \ (U_{ij} - p_j)$

    $u_i = max_{j \neq j_i^*} \ \ (U_{ij} - p_j)$

    $bid_{i,j} = p_j + v_i - u_i + \delta$

    $P(j) \cup \ i$

  end

  ***Assignment*:**

  for *each* $j \in D$ **do**

    if $P(j) \neq \emptyset$ **then**

      $i^* = argmax_{i \in P(j)} \ \ (bid_{i,j}) \ \ \forall i \in P(j)$

      $p_j = max_{i \in P(j)} \ \ (bid_{i,j}) \ \ \forall i \in P(j)$

      $\mathcal{M} \cup \ \ (i^*, j)$

      $\mathcal{M} = \mathcal{M} \setminus (i, j)$

    end

  end

end

In the assignment part, each good j is assigned to the highest bidder i^* and its price is updated by the highest bid value. The matching phase terminates when a complete assignment is achieved.

4.3.4 Proposed Penalty Mechanism

A penalty mechanism is developed to discourage dishonest requests/offers and ensure that ECs and EPs stick to their contractual obligations. This means that both transaction parties must carry out the P2P energy transfer as per the agreed-upon QoS values. The penalty mechanism depends mainly on the total energy transferred, rate of transfer, and time of connection. These attributes are measured through the smart charger, which is connected to the blockchain network. Based on these measurements, the smart contract can monitor the QoS delivery and calculate the penalty value. The smart contract is authorized to use a reserved amount of trading participants' e-wallets in penalty payments. If a party fails to carry out the trade (i.e. does not connect to the smart charger as per agreed time and considering T_{EP}), then a penalty is levied as per the following term:

$$B_{pen,i} = \frac{100 - RD_{EC}}{100} \, . \, B_{EP} \tag{4.29}$$

$$B_{pen,j} = \frac{100 - RD_{EP}}{100} \, . \, B_{EP} \tag{4.30}$$

where (4.29) indicates the penalty for EC i considering the required risk RD_{EC}, while the penalty for EP j is given by (4.30) taking into account offered risk RD_{EP}. It is noted that the penalty increases as the requested/offered risk decreases in both equations.

In the case where the actual QoS delivered by an EP j is worse than offered, the

penalty affects the payment received as follows:

$$B_{pay,j} = \frac{E^N_{act} + P^N_{act} + T^N_{act}}{E^N_{EP} + P^N_{EP} + T^N_{EP}} \; . \; B_{EP} \tag{4.31}$$

where $(.^N)$ indicates a normalized parameter. If the reason for EP j failing to deliver full QoS lays on the EC, (e.g. disconnection by EC before energy transfer is complete), then EC i must compensate the EP for the lost opportunity in the form of penalty payment as follows:

$$B_{pay,i} = B_{EP} - \frac{E^N_{act} + P^N_{act} + T^N_{act}}{E^N_{EP} + P^N_{EP} + T^N_{EP}} \; . \; B_{EP} \tag{4.32}$$

4.4 Numerical Simulation

In this section, numerical studies are conducted in order to validate the superiority and effectiveness of the proposed QoS-based mechanisms.

4.4.1 QoS Attributes Weight Calculation and SCMP Matching Mechanisms Analysis

The first study examines optimal QoS attributes weight calculation and SCMP matching mechanisms. The QoS requirements and linguistic variables of a random request are listed in Table 4.3. The QoS values in Table 4.3 are selected from realistic values that can be requested by energy consumers. For example, the energy requested range is set to values (i.e. [20-30] kWh) that are not very high to drain the energy provider's battery and not very low to make it unprofitable/unreasonable to participate in the

trade [52]. Similarly, minimum discharging power is set a range of 70-100% to avoid long trading sessions while allowing flexibility in energy providers' offers [15]. Two EC

Table 4.3: QoS attributes simulation parameters

QoS Requirement	QoS Values	Linguistic Variables Set I	Linguistic Variables Set II
$[E_{EC}^{min},\ E_{EC}^{max}]$ (kWh)	[20,30]	VH	VH
$[P_{EC}^{min},\ P_{EC}^{max}]$ (%)	[70,100]	L	M
CR_{EC}^{min}	3.5/5	MH	MH
RD_{EC}^{max} (%)	40	EH	ML
T_{EC}^{max} (min)	30	ML	EH
B_{EC}^{max} (¢/kWh)	9.5	VH	H

linguistic variable sets are considered to demonstrate the effect of changing importance input on weight calculation and offer selection using the SCMP mechanism. Six offers are generated randomly in response to the request in Table 4.3. The decision matrix created from the received offers is:

$$Q = \begin{bmatrix} & E & P & CR & RD & T & B \\ O^1 & 20 & 70 & 3.8 & 40 & 15 & 8.2 \\ O^2 & 25 & 80 & 3.9 & 25 & 40 & 8.3 \\ O^3 & 30 & 80 & 3.1 & 10 & 25 & 8.1 \\ O^4 & 27 & 70 & 3.9 & 30 & 15 & 8.4 \\ O^5 & 25 & 80 & 4.0 & 10 & 15 & 8.0 \\ O^6 & 30 & 80 & 4.0 & 25 & 15 & 7.8 \end{bmatrix}$$

Based on set I in Table 4.3, the preference generation model in Algorithm 4.1 generates the following best-to-others and worst-to-others fuzzy pairwise comparison

vectors:

$$A_{Bfuzzy} = \begin{bmatrix} (1.5, 2.0, 2.5) \\ (6.5, 7.0, 7.5) \\ (3.5, 4.0, 4.5) \\ (0.5, 1.0, 1.5) \\ (5.5, 6.0, 6.5) \\ (1.5, 2.0, 2.5) \end{bmatrix} A_{Wfuzzy} = \begin{bmatrix} (6.5, 7.0, 7.5) \\ (0.5, 1.0, 1.5) \\ (4.5, 5.0, 5.5) \\ (7.5, 8.0, 8.5) \\ (2.5, 3.0, 3.5) \\ (6.5, 7.0, 7.5) \end{bmatrix}$$

It can be noticed from A_{Bfuzzy} that RD has been ranked as the most important attribute with a fuzzy preference base of 1, whereas other attributes have been given values that correspond to their preference position in relation to the RD preference value in Table 4.3. Similarly, T is ranked as the least important attribute in A_{Wfuzzy} taking the rank of 1 but with the other attributes ranking in reverse order. The optimal fuzzy weight distribution values for sets I and II are shown in Figs. 4.4 (a) and (b), respectively.

It can be noticed from both figures that the weight values are distributed based on their importance in Table 4.3. For example, Fig. 4.4 (a) shows that attributes RD and P have the highest and lowest weight values, respectively. This is a result of having respective EH and L input by EC in set I of linguistic importance variables. Further, Figs. 4.4 (a) and (b) clearly show that weight values distribution changes in response to linguistic importance terms change for each attribute. In particular, it can be noticed that attribute RD has been given the lowest weight distribution in Fig. 4.4 (b) after having the highest values in Fig. 4.4 (a). This change is a result of changing

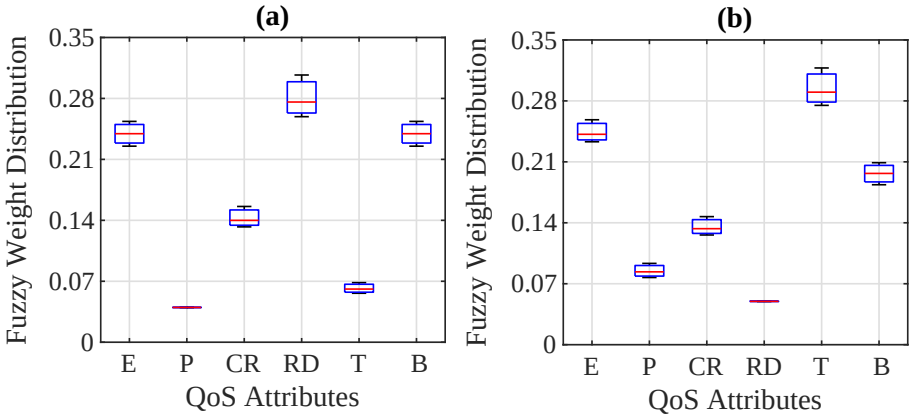

Fig. 4.4. Fuzzy weight distribution of QoS requirement for (a) Linguistic variables set I, and (b) Linguistic variables set II.

the importance from EH to ML as listed in Table 4.3. Another notable change occurs for T, which changes from having the lowest value in set I to the highest value in set II.

In the SCMP mechanism simulations, offers that is not within the QoS limits specified by the EC are discarded as given by the modified decision matrix Q_{mod}:

$$Q_{mod} = \begin{bmatrix} & E & P & CR & RD & T & B \\ O^1 & 20 & 70 & 3.8 & 40 & 15 & 8.2 \\ O^4 & 27 & 70 & 3.9 & 30 & 15 & 8.4 \\ O^5 & 25 & \mathbf{80} & \mathbf{4.0} & \mathbf{10} & 15 & 8.0 \\ O^6 & \mathbf{30} & \mathbf{80} & \mathbf{4.0} & 25 & 15 & \mathbf{7.8} \end{bmatrix}$$

where the bold numbers indicate the best QoS attribute value among different offers in Q_{mod}. As can be seen from the original Q and modified Q_{mod} decision matrices, O^2 and O^3 have been discarded due to violations of EC QoS requirements stated in Table 4.5. Particularly, the values of T in O^2 and CR in O^3 do not satisfy the stated requirements.

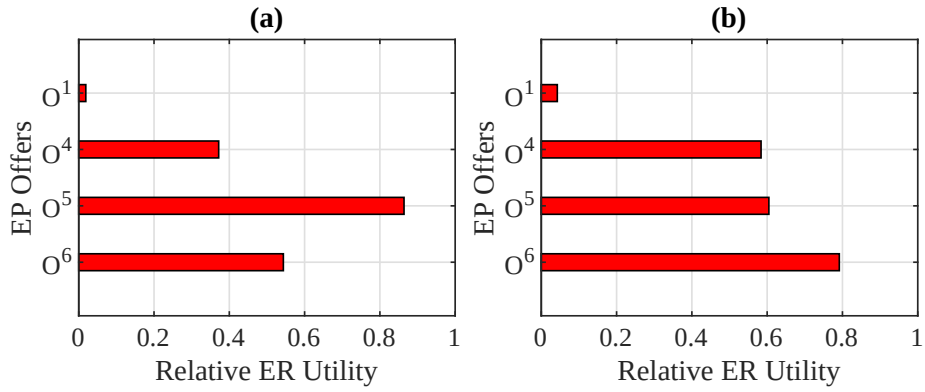

Fig. 4.5. Offers Ranking based on SCMP mechanism considering weights generated from (a) Linguistic variables set I, and (b) Linguistic variables set II.

The ranking of offers for the SCMP mechanism in Q_{mod} is demonstrated in Figs. 4.5 (a) and (b), which show the ranking of offers for set I and II of the linguistic variables, respectively. It can be noticed from Fig. 4.5 (a) that the mechanism matches the EC request with O^5 for set I despite offering slightly less E and requesting higher B than O^6. The reason is that O^5 offers a significantly lower RD, which has a high weight value in set I, resulting in higher utility for EC from this offer. When RD is assigned a low weight value in set II, O^6 is selected as the best offer by the SCMP mechanism as shown in Fig. 4.5 (b) due to offering relatively higher QoS values for multiple attributes.

4.4.2 MCMP Mechanism Analysis

In this study, randomly generated QoS-based energy requests and offers that follow a Gaussian distribution are utilized to validate the effectiveness of the proposed MCMP mechanism. QoS attributes in each request are assigned random weight values. The parameters of the distribution for the six QoS attributes specified in Section 4.2 are $((\mu_E = 12\ , \sigma_E = 1)$,$(\mu_P = 80\ , \sigma_P = 2)$,$(\mu_{CR} = 4\ , \sigma_{CR} = 0.1)$,$(\mu_{RD} = 18\ , \sigma_{RD} =$

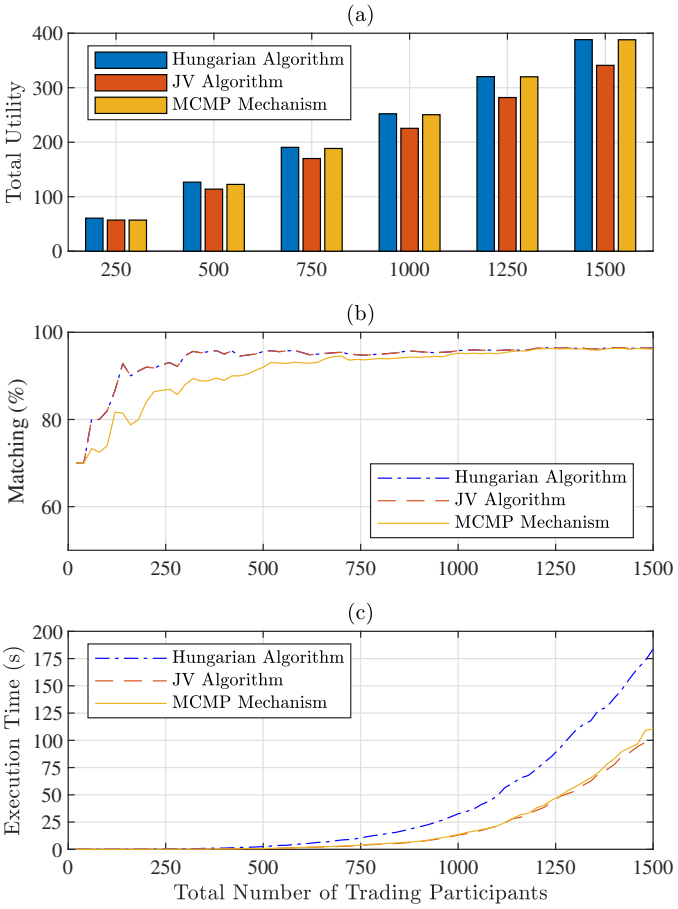

Fig. 4.6. Simulation results of the proposed MCMP mechanism compared to the Hungarian and JV algorithms for, (a) Total EC utility, (b) Percentage of matched participants, and (c) Matching algorithms execution time.

2),($\mu_T = 9$, $\sigma_T = 2$),($\mu_B = 9.5$, $\sigma_B = 1$)). The number of trading participants is varied from 20 to 1000 with a random distribution of ECs and EPs among these participants. The MCMP matching algorithm is compared with two well-known algorithms to test its performance. The first algorithm is the Hungarian algorithm, which is a primal-dual method that can solve linear assignment problems based on the principle of finding feasible augmenting paths [132]. The Hungarian algorithm enjoys a high reputation and popularity since it has been proven to always find the minimum weight-matching

Table 4.4: Simulation results for MCMP, Hungarian, and JV algorithms

Total Number of Trading Participants	Total Utility			Matching (%)			Execution Time (s)		
	Hungarian	JV	MCMP	Hungarian	JV	MCMP	Hungarian	JV	MCMP
250	60.9	57.1	57.1	92.5	92.5	86.1	0.3	0.05	0.1
500	126.7	113.9	122.6	95.0	95.0	91.2	2.1	0.6	0.6
750	190.6	170.1	188.5	95.0	95.0	93.6	9.0	2.9	3.2
1000	252.2	225.5	250.5	95.4	95.4	94.4	26.9	10.1	10.7
1250	320.3	282.0	320.0	96.3	96.3	96.1	73.4	35.7	37.9
1500	388.3	341.1	388.0	96.3	96.3	96.2	183.7	104.1	110.6

in assignment problems [133]. Therefore, it is widely used in the literature [134],[135] and industrial applications [136],[137]. In terms of efficiency, the Hungarian algorithm outperforms linear programming based methods, including different variants of simplex algorithms. The second algorithm to compare the proposed MCMP with is the shortest path algorithm, which is also known as the Jonker and Volgenant (JV) algorithm [138]. JV is a dual algorithm that is based on the principle of finding the shortest augmenting path. Compared to the Hungarian algorithm, JV can obtain optimal assignments within a shorter execution time [132].

The algorithms are coded and simulated in the MATLAB environment, which is run on a PC with the following specifications: Core i7-8700T, 2.4 GHz CPU, 16 GB RAM, and 64 bits system. Simulation results for the MCMP, Hungarian, and JV algorithms are demonstrated in Figs. 4.6 (a)–(c). A summary of the results shown in Figs. 4.6 (a)–(c) is also listed in Table 4.4. Fig. 4.6 (a) demonstrates the total utility for different numbers of trading participants. As shown in the figure, the proposed algorithm clearly outperforms the JV algorithm in terms of maximizing the total EC utility for different

numbers of participants. However, it has a slightly lower performance in comparison to the Hungarian algorithm when the number of participants is low. As the number of participants increases, MCMP provides similar performance to the Hungarian algorithm while still outperforming the JV. Besides, as depicted in Fig. 4.6 (b), the percentage of matched participants of the Hungarian and JV algorithms is slightly higher ($\simeq 4\%$) than MCMP when the number of participants is low and almost similar for a high number of participants. Fig. 4.6 (c) depicts the execution time of the three algorithms for different numbers of participants. It is noticed from the figure that the MCMP algorithm is marginally slower than JV and much faster than the Hungarian in terms of the computational time required to reach the assignment solution. On average, the proposed algorithm can solve the problem in less than 50% of the time required by the Hungarian algorithm and slightly higher time than JV (i.e. 7%). This shows that the proposed MCMP mechanism (i) can provide fast near-optimal solutions under different scales of data, and (ii) it is scalable, where its superiority increases with the increase of the number of participants.

The results reported in Fig. 4.6 and Table 4.4 can be explained by certain characteristics in the compared algorithms. The MCMP provides a slightly lower utility and matching percentage at low numbers of participants because it is based on approximate optimality represented by the $\delta - complementary\ \ slackness$ in the bidding equation (4.28) in algorithm 2. The δ parameter, which is set to $\frac{1}{1+NT}$ in algorithm 2 according to the minimum recommended value by [139], increases the aggressiveness of the algorithm to terminate faster but might slightly reduce the utility and matching percentage. Since δ is inversely proportional to the number of trading participants NT, the effect of δ on the optimality of the solution decreases as NT increases. This can be seen in Fig.

4.6 that shows that Hungarian and MCMP algorithms approach the same utility and matching values for high numbers of trading participants. Moreover, the reason that MCMP provides solutions with higher utility than the JV algorithm could be attributed to the original design of JV that assumes a balanced number on both sides of the assignment problem, as well as an integer edges' weights (i.e. utility) [138], [140]. In this context, the MCMP is a better fit for the problem formulated in (4.23) since it can accept an unbalanced number of ECs and EPs along with utilities that contain floating decimal points.

4.5 Discussion and Summary

This research proposes a novel decentralized scheme for P2P energy trading between EVs that takes into consideration QoS management and utilizes smart contracts to match and administer the energy trade. SCMP and MCMP mechanisms are proposed to match EC requests and EP offers based on QoS attributes. In these mechanisms, each attribute is assigned a weight value according to a fuzzy-based optimal weight calculation method. Further, a penalty mechanism is developed to discourage dishonest requests/offers and ensure that ECs and EPs stick to their contractual obligations. Numerical simulations are conducted to validate the effectiveness of the proposed mechanisms. The results show that the SCMP mechanism selects the EP offer that provides the best utility to EC with high awareness of EC preferences represented by weight values assigned to QoS attributes. The results also demonstrate that the MCMP mechanism is superior in finding fast near-optimal solutions when matching a high number of ECs and EPs.

Chapter 5 - Bidirectional Smart Charging of Electric Vehicles Considering User Preferences

The research on G2V, V2G, and V2V schemes mainly focuses on scheduling of EV charging and/or discharging from the perspective of system operators and aggregators. However, given that there is at least one human user per vehicle, it is expected that EV users will have various interactions based on their own preferences, and therefore, require different options to accommodate their preferences. It is also argued that EVs can be scheduled for joint applications concurrently including P2P energy trade and ancillary services to the grid. Thus, it is important to consider EV users' input into the scheduling process through new models that help each individual EV user determine the optimal charging and discharging schedule for their EV batteries. This research argues that the EV user's input can be taken into consideration for the scheduling process. The inputs considered in this research are utilized to provide a personalized user control over P2P transactions and ancillary services participation as well as battery SOC management and trips adjustment.

To that end, the present research contributes to the existing literature by:

- Presenting a new algorithm for bidirectional smart charging of EVs considering

P2P energy trade, provision of ancillary services to the grid and utilization of low electricity prices for battery charging.

- Incorporating user preferences into the scheduling process enabling the model to adapt to various conditions.
- Utilizing optimization slack variables for optimal management of EV battery SOC and energy allocation for multiple services.
- Introducing indices for quantification of EV participation in ancillary services and P2P transactions.

Without loss of generality, the following assumptions are made during development of this research:

- Due to the mobility nature of EVs and users' uncertain schedules, ancillary service signals are assumed to be an optional request sent by the aggregator on an ad hoc basis. EV users would decide whether they want to participate in ancillary services six hours ahead of the request time.
- While the EV user's behavior is stochastic in nature, the scheduling process is adaptive to various conditions based on the human input into the scheduling algorithm. The input from the human user is utilized to deal with the uncertainties of the scheduling parameters.
- Time–of–use electricity prices are considered in this research since trading is done at the distribution level. This would also reduce the uncertainties associated with the price data since they are predictable.

- Due to the dynamic nature of smart grids and uncertainties in renewable energy generation as well as the issues that can be caused by bidirectional power flow, P2P energy trading is carried out on the same feeder. This would also help alleviate power congestion, reduce power losses, and decrease the complexity of power flow management [141]. In addition, distribution system constraints and transaction fees are neglected.

Table 5.1: Chapter 5 Nomenclature

Indices

t	Index for time steps.

Sets

$\mathbb{T}$	Set time steps in optimization problem.

Constants

ΔT	Optimization problem time interval (h).
η^{Chg}	Charging efficiency.
η^{Dhg}	Discharging efficiency.
κ^{Dsp}	Battery dissipation factor (%).
F^{Con}	Rate of energy consumption per distance unit (kWh/km).
OC^{Chg}	Battery charging operating cost ($/kWh).
OC^{Dhg}	Battery discharging operating cost ($/kWh).
SOC_{min}	Physical minimum level of EV battery (kWh).

Parameters

$\beta_t^{P,P2P,Dhg}$	P2P Discharging penalty factor ($/kWh).
$\beta_t^{P,P2P,Chg}$	P2P Charging penalty factor ($/kWh).
$\beta_t^{P,Res}$	Penalty factor for management of reserve SOC ($/kWh^2).
$\beta_t^{P,Dod}$	Penalty factor for management of storage depth of discharge ($/kWh^2).
$\beta_t^{P,Tr2}$	Penalty factor for management of Tier 2 traveling distance ($/km·h).
$\beta_t^{P,Tr3}$	Penalty factor for management of Tier 3 traveling distance ($/km·h).
$\beta_t^{P,Anc}$	Ancillary service penalty factor ($/kWh).
B_t^{ToU}	Electricity time-of-use (ToU) prices ($/kWh).
B_t^{Anc}	Ancillary service price ($/kWh).
B_t^{P2P}	Peer-to-Peer energy exchange price ($/kWh).
D_t	EV traveling distance during time period t (km).
D_t^{Tr1}	EV Tier 1 traveling distance time period t (km).
D_t^{Tr2}	EV Tier 2 traveling distance during time period t (km).
D_t^{Tr3}	EV Tier 3 traveling distance during time period t (km).
P_t^{P2P}	P2P power trade quantity (kW).
S_t^{Anc}	Ancillary service signal (kW).
SOC_t^{Res}	Reserve SOC level (kWh).
SOC_t^{Dod}	SOC level for depth of discharge management (kWh).
SOC_{min}^{Usr}	SOC user adjustable minimum (kWh).
$SOC_{max,y}$	Maximum degraded SOC level (kWh).

Table 5.1: Chapter 5 Nomenclature ... continued.

Variables

C_t	EV charger plug–in status, $C = 1$ when plugged–in.
$D_t^{Sch,Tr2}$	Scheduled EV Tier 2 traveling distance during time period t (km).
$D_t^{Sch,Tr3}$	Scheduled EV Tier 3 traveling distance during time period t (km).
$D_t^{Tr2,S}$	Binary slack variable for management of Tier 2 traveling distance.
$D_t^{Tr3,S}$	Binary slack variable for management of Tier 3 traveling distance.
E_t^{Drv}	EV energy consumption during driving (kWh).
P_t^{Grd}	EV power charge from the grid (kW).
$P_t^{P2P,Chg}$	EV power charge from the peer (kW).
$P_t^{P2P,Dhg}$	EV power discharge to the peer (kW).
P_t^{Anc}	Ancillary service power (kW).
$P_t^{P2P,Chg,S}$	Slack variable for management of EV power charge from the peer (kW).
$P_t^{P2P,Dhg,S}$	Slack variable for management of EV power discharge from the peer (kW).
$S_t^{Anc',S}$	Slack variable for ancillary service contribution (kW).
$S_t^{Anc'',S}$	Slack variable for ancillary service contribution (kW).
$SOC_t^{Res,S}$	Reserve SOC level slack variable (kWh).
$SOC_t^{Dod,S}$	SOC level for depth of discharge management slack variable (kWh).

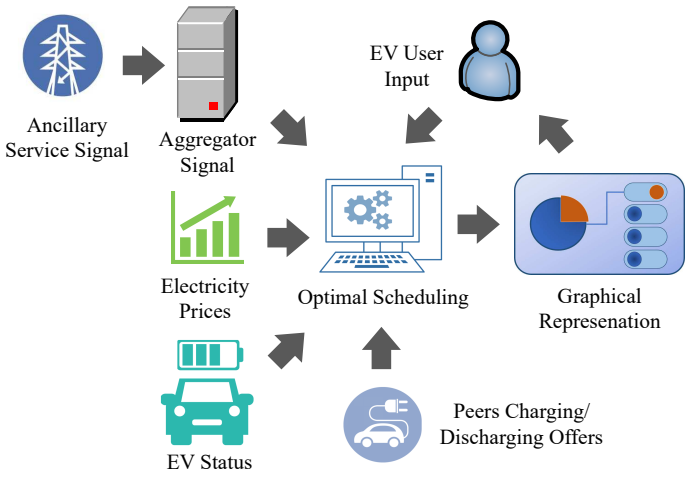

Fig. 5.1. Proposed smart charging mechanism of EVs considering user preferences.

5.1 Proposed Model

5.1.1 Optimal Scheduling Model

Fig. 5.1 presents the proposed smart charging model which takes into consideration user preferences in the optimal management of EV charging and discharging. As shown in the figure, an optimal model schedules the EV battery charging and discharging setpoints based on the following inputs: (i) EV status such as charging system physical limits and battery capacity, (ii) TOU electricity prices, (iii) reserve provision for participation in ancillary service market and P2P energy trade, and (iv) user input which includes EV expected location throughout scheduling time period as well as scheduling risk profile. In order to account for the time-varying nature of the energy demand, optimization results are updated by re-running the optimization calculations at every time step. In this case, the optimal scheduling algorithm would include six-time steps, each of which represents a one-hour time interval. As such, optimization variables would be

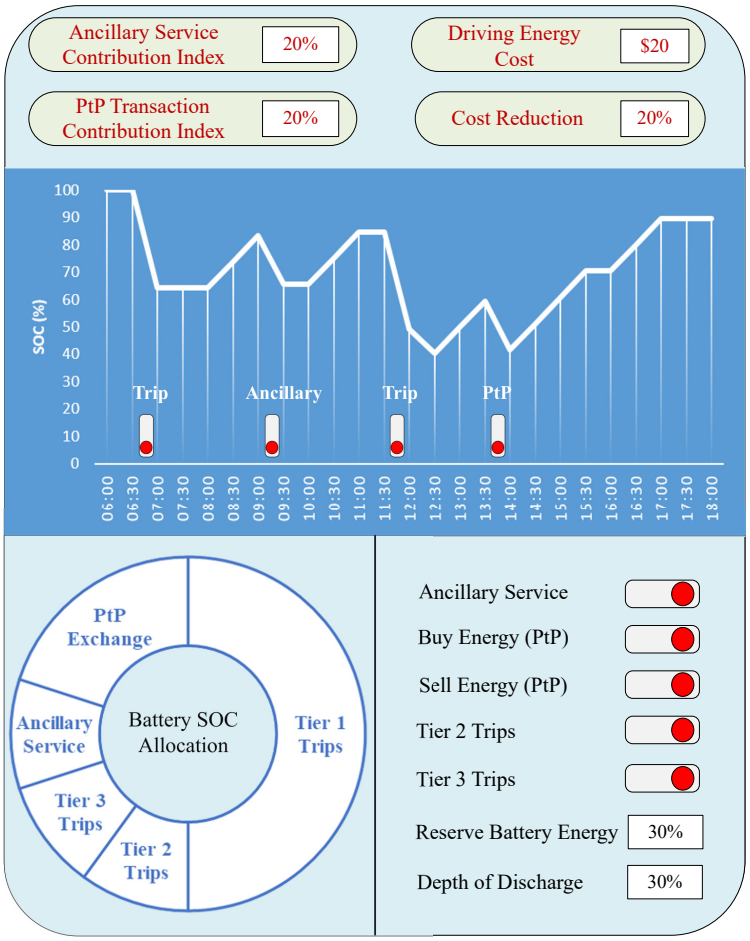

Fig. 5.2. Example of a GUI for user-based scheduling of EV battery.

1-dimension arrays with six elements determined at the end of each time interval. This method for scheduling is referred to as the rolling time horizon or model predictive control [109], [110]. The algorithm generates time-ahead charging scheduling profiles, conveyed to the EV user through an interactive graphical user interface (GUI) as shown in Fig 5.2.

The user can interact with the application to dynamically adjust certain inputs aiming to maximize/minimize the income/cost of EV operation. Using a GUI, the

EV user can check the total driving energy cost as per the electricity prices and learn how much it could be potentially reduced by their scheduling settings. The GUI also demonstrates the expected battery SOC throughout the scheduling time horizon. The user will then have the option of adjusting individual trips and choosing whether to participate in different charging/discharging events related to the ancillary services and P2P transactions. In the proposed model, users are given an option for optimally adjusting a trip based on the type of trips. Without loss of generality, trips are assumed to be of three types as follows: Tier 1, Tier 2, and Tier 3. Tier 1 represents critical trips that a user must take during the day at the pre-specified time such as commute to work or medical appointments, while Tiers 2 and 3 indicate non-critical trips that a user can afford to adjust or reschedule. Tier 2 trips come with a higher priority than Tier 3 trips (i.e., essential trips such as shopping or banking), while Tier 3 trips are non-essential trips such as recreational activities [112]. It should be noted that other types of trips can be added to the algorithm, and this trips classification is only intended to demonstrate how the algorithm can make adjustments for users depending on their inputs. After the user adjusts the inputs through the GUI, the application will apply these adjustments based on the input data and a new scheduling profile is generated.

Further, the algorithm incorporates EV user input with the aim of maximizing revenue and/or minimizing the cost of EV operation through ancillary service provision to the grid, P2P energy exchange, and electricity prices arbitrage exploitation. Thus, scheduling is carried out from the perspective and for the benefit of the EV owners. While the grid's ancillary services are considered in the scheduling, the model does not aim to minimize or discuss the cost of the grid operation. Fig. 5.3 demonstrates different user profiles and how they affect the scheduling algorithm. In this regard, three users'

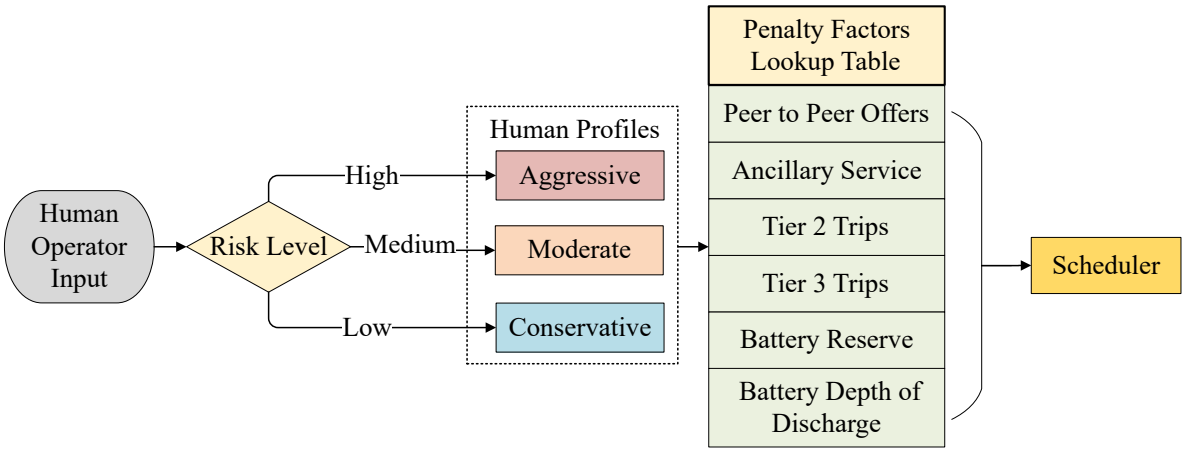

Fig. 5.3. Process flow for specification of the EV scheduling model.

profiles are defined in this research as follows: conservative, moderate, and aggressive. Without loss of generality, these profiles are adopted in this research to represent risk levels chosen by the user in pursuing their preferences for maximizing the income and/or minimizing the EV cost of operation. In such a case, the conservative profile represents the lowest risk level and the aggressive profile represents the highest risk level.

By choosing a profile through the GUI, the user changes the penalty values on the slack variables. These slack variables are related to various functionalities as depicted in the figure. Slack variables act as factitious quantities decided by the optimization problem in order to 1) maximize the profit, 2) satisfy the need of the user, and 3) create soft constraints to ensure the optimization converges in cases where deviation from the hard constraints is needed. As such, depending on the choices of the user, the parameters of the scheduling model, and thus, the scheduling results are adopted. As the risk level increases, the penalty values on the P2P and ancillary service slack variables will increase in order to force more participation in these transactions while the penalty factors on the battery SOC and trips adjustment slack variables decrease; giving the algorithm more flexibility to adjust the charge/discharge setpoints to increase

the income and/or minimize the cost. By looking at the value of the slack variable, EV users would learn whether a solution is obtained through the soft constraints and how such a solution impacts the results. If the slack variable is zero, then hard constraints have been used and results are not impacted by the slack variable. On the other hand, if it is non-zero for any time step, that means soft constraints are used, and the results are impacted. With operation at a higher risk level, the user's comfort could slightly be compromised, but this will be rewarded by a higher income and lower cost. The mathematical formulation of the model is given below.

Objective Function

The objective function of the optimization problem is stated in the following:

$$\text{Maximize}: \sum_{t\in\mathbb{T}} \left\{ \begin{array}{l} P_t^{Anc} \,.\, B_t^{Anc} + P_t^{P2P,Dhg} \,.\, B_t^{P2P} \\ -P_t^{Grd} \,.\, B_t^{ToU} - P_t^{P2P,Chg} \,.\, B_t^{P2P} \\ -OC^{Dhg} \,.\, (P_t^{Anc} + P_t^{P2P,Dhg}) \\ -OC^{Chg} \,.\, (P_t^{Grd} + P_t^{P2P,Chg}) \\ -\beta_t^{P,Anc} \,.\, (S_t^{Anc',S} + S_t^{Anc'',S}) \\ -\beta_t^{P,P2P,Chg} \,.\, P_t^{P2P,Chg,S} \\ -\beta_t^{P,P2P,Dhg} \,.\, P_t^{P2P,Dgh,S} \\ -\beta_t^{P,Res} \,.\, SOC_t^{Res,S} - \beta_t^{P,Dod} \,.\, SOC_t^{Dod,S} \\ -\beta_t^{P,Nct} \,.\, D_t^{Tr2,S} - \beta_t^{P,Opt} \,.\, D_t^{Tr3,S} \end{array} \right\} . \Delta T. \tag{5.1}$$

The objective function aims to maximize the profit and/or minimize the cost for EV users through the following:

- Contributing to ancillary services:

  $P_t^{Anc} \,.\, B_t^{Anc}$

- Exchanging energy with other EV peers:

  $B_t^{Anc} + P_t^{P2P,Dhg} \,.\, B_t^{P2P} - P_t^{Chg} \,.\, B_t^{ToU}$

- Exploiting low electricity prices for battery charging:

  $-P_t^{Chg} \,.\, B_t^{ToU}$

- Managing ancillary signals contribution:

  $-\ \beta_t^{P,Anc} \,.\, (S_t^{Anc',S} + S_t^{Anc'',S})$

- Managing P2P energy transactions:

  $-\ \beta_t^{P,P2P,Chg} \,.\, P_t^{P2P,Chg,S} - \beta_t^{P,P2P,Dhg} \,.\, P_t^{P2P,Dgh,S}$

- Controlling reserve and minimum battery level:

  $-\ \beta_t^{P,Res}.SOC_t^{Res,S} - \beta_t^{P,Dod}.SOC_t^{Dod,S}$

- Controlling user specified trips:

  $-\ \beta_t^{P,Nct}.D_t^{Tr2,S} - \beta_t^{P,Opt}.D_t^{Tr3,S}$

EV Driving Constraints

Energy consumed during driving is represented by [47]:

$$E_t^{Drv} = (1 - C_t) \,.\, D_t \,.\, F^{Con} \quad \forall t \in \mathbb{T}, \tag{5.2}$$

where the term $(1 - C_t)$ ensures that driving energy is only consumed when the vehicle is not plugged into the grid. EV trips driving distance D_t in (5.2) is constrained by the following:

$$D_t = D_t^{Tr1} + D_t^{Sch,Tr2} + D_t^{Sch,Tr3} \quad \forall t \in \mathbb{T}, \tag{5.3}$$

where (5.3) sets EV trips distance based on the different trips categories defined earlier, while ensuring that different types of trips do not occur concurrently. While Tier 1 trips are categorized as the critical ones and not adjusted by the algorithm, Tiers 2 and Tier 3 trips can be adjusted as the non-critical and low priority ones:

$$D_t^{Sch,Tr2} = D_t^{Tr2} - D_t^{Tr2,S} \,.\, D_t^{Tr2} \quad \forall t \in \mathbb{T}, \tag{5.4}$$

$$D_t^{Sch,Tr3} = D_t^{Tr3} - D_t^{Tr3,S} \,.\, D_t^{Tr3} \quad \forall t \in \mathbb{T}, \tag{5.5}$$

where trips adjustment in (5.4) and (5.5) depends on binary slack variables $D_t^{Tr2,S} \in \{0, 1\}$ and $D_t^{Tr3,S} \in \{0, 1\}$.

EV Charging/Discharging Constraints

The objective function (5.1) is subject to the following charging and discharging constraints:

$$C_t \,.P_{min}^{Chg} \leq P_t^{Chg} \leq C_t \,.P_{max}^{Chg} \qquad \forall t \in \mathbb{T}, \tag{5.6}$$

$$C_t \,.P_{min}^{Dgh} \leq P_t^{Dhg} \leq C_t \,.P_{max}^{Dhg} \qquad \forall t \in \mathbb{T}, \tag{5.7}$$

$$P_t^{Chg} = (P_t^{Grd} \vee P_t^{P2P,Chg}) \quad \forall\, P_t^{Dhg} = 0 \quad \wedge t \in \mathbb{T}, \tag{5.8}$$

$$P_t^{Dhg} = (P_t^{Anc} \vee P_t^{P2P,Dhg}) \quad \forall\, P_t^{Chg} = 0 \quad \wedge t \in \mathbb{T}, \tag{5.9}$$

where (5.6) and (5.7) state the operational constraints of the EV charging converter when connected to the grid. The variable C_t in (5.6)–(5.7) ensures that no energy is taken from or given to the grid without EV charger being plugged in. The constraints in (5.8) and (5.9) ensure that charging and discharging do not occur at the same time.

EV Battery Constraints

The EV battery is subject to the following operational and physical constraints:

$$SOC_t = SOC_{t-1} + \Big(C_t . P_t^{P2P,Chg} - C_t . P_t^{P2P,Dhg} + C_t . P_t^{Anc} + C_t . P_t^{Grd} - (1 - C_t) . D_t . F^{Con} - \kappa^{Dsp} . SOC_t \Big) . \Delta t \quad \forall t \in \mathbb{T}, \tag{5.10}$$

$$SOC_{t,min}^{Usr} \leq SOC_t \leq SOC_{max} \quad \forall t \in \mathbb{T}, \tag{5.11}$$

where (5.10) expresses the energy balance equation considering the charging, discharging, and dissipation of the EV battery, while (5.11) states the battery minimum and maximum SOC constraints. The lower bound SOC_{min}^{Usr} is expressed by:

$$SOC_{t,min}^{Usr} = SOC_{min} + SOC_t^{Dod} + SOC_t^{Res} - SOC_t^{Res,S} - SOC_t^{Dod,S} \quad \forall t \in \mathcal{T}, \tag{5.12}$$

$$0 \leq SOC_t^{Res,S} \leq SOC_t^{Res} \quad \forall t \in \mathcal{T}, \tag{5.13}$$

$$0 \leq SOC_t^{Dod,S} \leq SOC_t^{Dod} \quad \forall t \in \mathcal{T}, \tag{5.14}$$

where $SOC_{t,min}^{Usr}$ value in (5.12) depends on the physical lower limit of the battery along with user specified reserve and depth of discharge SOC levels. The slack variables $SOC_t^{Res,S}$ and $SOC_t^{Dod,S}$ relax the user-specified values to ensure the feasibility of the

optimization problem and maximize the profit when needed.

Ancillary Service Constraints

The EV receives an ancillary service request from the electricity market and contributes based on the following constraints:

$$P_t^{Anc} = C_t \,.\, S_t^{Anc} - S_t^{Anc',S} + S_t^{Anc'',S} \quad \forall t \in \mathbb{T}, \tag{5.15}$$

$$0 \leq S_t^{Anc',S} \leq S_t^{Anc} \quad \forall t \in \mathbb{T}, \tag{5.16}$$

$$0 \leq S_t^{Anc'',S} \leq S_t^{Anc} \quad \forall t \in \mathbb{T}, \tag{5.17}$$

where S_t^{Anc} in (5.15) can take both the negative and positive values depending on the type of the ancillary service required. The slack variables $S_t^{Anc',S}$ and $S_t^{Anc'',S}$ act as soft constraints allowing the algorithm to converge in case it is not feasible or profitable to contribute to the ancillary service market.

Applied Constraints for P2P

The P2P offers received by the EV user through the P2P network are managed through the following constraints:

$$P_t^{P2P,Chg} - P_t^{P2P,Dhg} = C_t \,.\, P_t^{P2P} - P_t^{P2P,Chg,S} + P_t^{P2P,Dgh,S} \quad \forall t \in \mathbb{T}, \tag{5.18}$$

$$0 \leq P_t^{P2P,Chg,S} \leq P_t^{P2P} \forall t \in \mathbb{T}, \tag{5.19}$$

$$0 \leq P_t^{P2P,Dgh,S} \leq P_t^{P2P} \forall t \in \mathbb{T}, \tag{5.20}$$

where P_t^{P2P} in (5.18) states the energy exchange value between the EV user and other peers.

5.1.2 Ancillary Services and P2P Participation Indices

In order to quantify the contribution of the EV user to ancillary services and P2P transactions, the following ancillary service participation index (ASPI) and P2P transactions involvement index (P2PTII) are proposed, respectively:

$$\text{ASPI}\,\% = \left(1 - \frac{\sum_{t\in\mathbb{T}}(S_t^{Anc',S} + S_t^{Anc'',S})}{\sum_{t\in\mathbb{T}} S_t^{Anc}}\right) \times 100 \tag{5.21}$$

$$\text{P2PTII}\,\% = \left(1 - \frac{\sum_{t\in\mathbb{T}}(P_t^{P2P,Chg,S} + P_t^{P2P,Dgh,S})}{\sum_{t\in\mathbb{T}} P_t^{P2P}}\right) \times 100. \tag{5.22}$$

5.2 Numerical Studies

The proposed model in Section 5.1 is numerically evaluated using the specification of a Tesla Model S AWD - P75D which is one of the most popular EV models available in the market [142]. The maximum battery capacity for this model is 75kWh with energy consumption F^{Con} of 22.2 kWh/100 km [143]. The onboard charger is rated at 11.5 kW [144]. Battery reserve $SOC^{Res,S}$ and battery depth of discharge $SOC^{Dod,S}$ are both set to 10%. ToU prices of Ontario, Canada are used in this work which are set at an off-peak rate of 6.5 cent/kWh from 7 p.m. to 7 a.m. and mid-peak rate of 9.4 cent/kWh from 7:00 a.m. to 11:00 a.m. and from 5:00 p.m. to 7:00 p.m. The on-peak rate is set

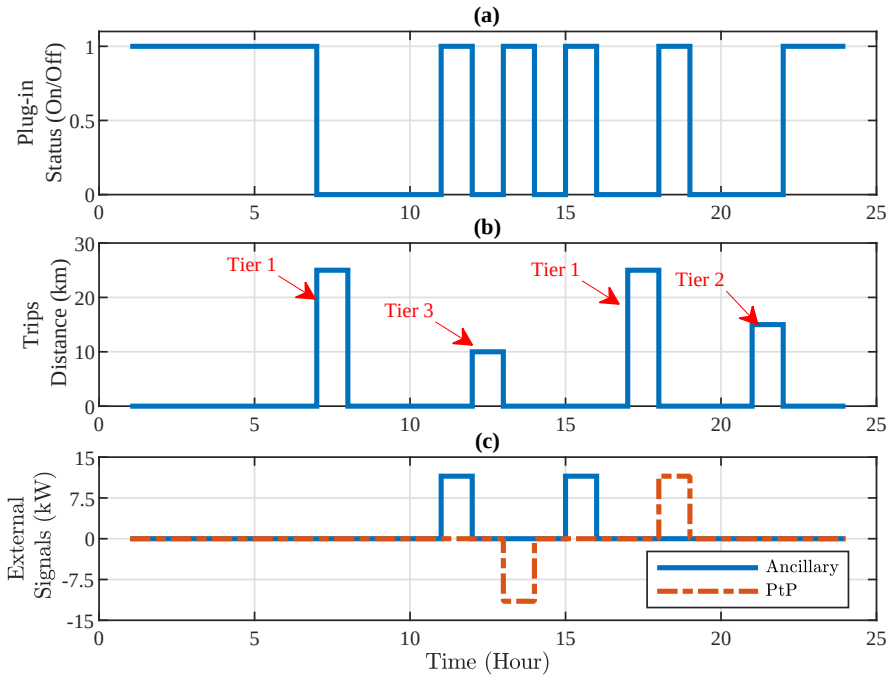

Fig. 5.4. (a) EV battery plug–in status, (b) User trip distances, (c) External signals compiled by the algorithm.

at 13.2 cent/kWh from 11:00 a.m. to 5:00 p.m. [145]. The P2P prices for mid-peak time and on-peak time are 7.95 and 11.3, respectively, while ancillary service prices are set at 13.2 cent/kWh. These prices are set at mid-point between different ToU levels presuming that an EV user is looking to sell energy at rates higher than utility prices and buy energy at rates lower than utility prices. However, the algorithm is designed to be generic, where different rates and specifications can be utilized with the aim of maximizing profit and/or minimizing cost for EV users. This case study is focused on the provision of operating reserve to the grid as an ancillary service. Operating reserve services are utilized during unexpected or contingency situations when regulation services are not enough to keep the balance between the generation and demand [146].

Survey data represented in [112] is used to construct a trip profile from a typical EV

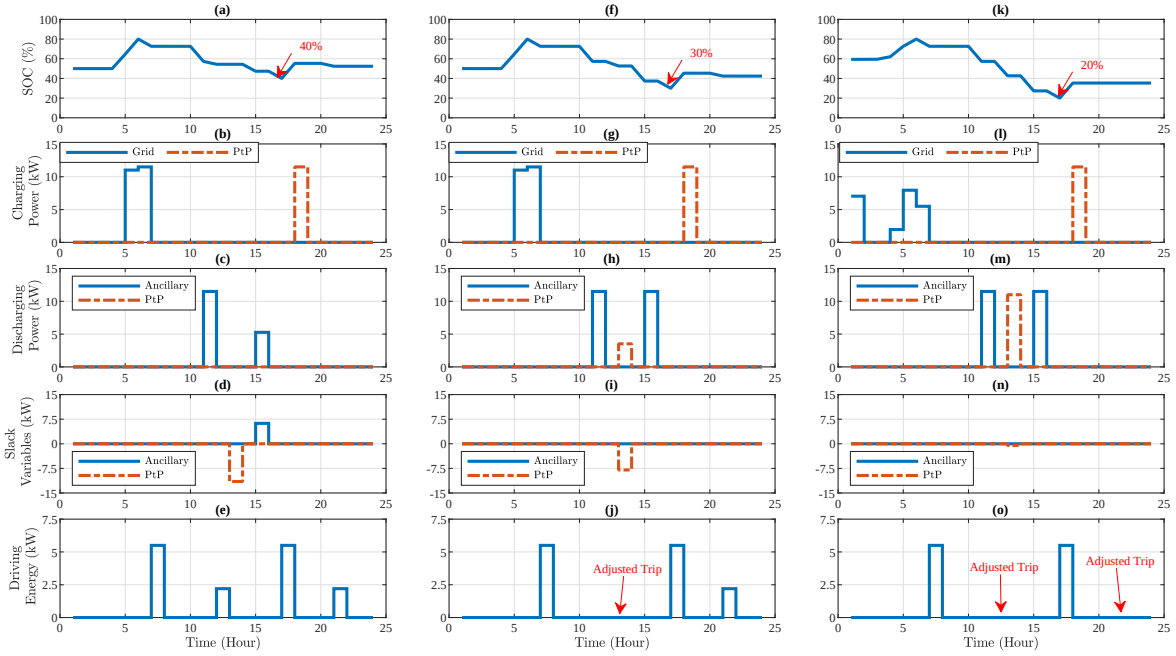

Fig. 5.5. EV scheduling setpoints based on, conservative profile (a)-(e), moderate profile (f)-(j), and aggressive profile (k)-(o).

user. Without loss of generality, this profile is considered for simulation studies in this section. The profile is based on EV users' responses in regard to the average daily trips. The survey results in [112] show that most respondents take 1 to 6 trips per weekdays on average; thus, four trips are considered for simulation studies. Moreover, the average traveling distance per each EV user in a weekday comes to 50 km which is considered as the essential trips' total distance in the numerical studies. The time of the day when charging typically takes place is used to create a profile for charger plug-in status. It is also assumed that EVs come with a bidirectional onboard charger allowing them to charge or discharge when connected to any outlet.

Figs. 5.4 (a)–(c) show the expected charger plug-in status, trips, and external signal profiles for a typical day, respectively. During the implementation of the model, it is

assumed that the location information given by the user is analyzed and compared with the data on online maps to generate the expected charger plug-in status profile and expected trip duration and distance as seen in Figs. 5.4 (a) and (b), respectively. The trip duration is considered as one hour, but changing the duration does not impact the validity of the model. The model is also assumed to obtain the importance of these locations for the user in order to classify the trips into Tier 1, Tier 2 or Tier 3. After generating the EV charger plug-in status, the model analyzes the time-ahead ancillary service requests and P2P transaction offers that coincide with the expected connected status throughout the scheduling time; this information is then used to generate a profile representing the ancillary and P2P signals as shown in Fig. 5.4 (c). In such a case, it is expected that multiple P2P offers will be available within the same hour but the model will only retrieve the ones with the lowest cost or highest profit. Using the data in Fig. 5.4, the algorithm is executed for a period of 24 hours using the three profiles described in Section 5.1. For illustration purposes, the minimum scheduling time for each variable is set to one hour. The initial SOC is set to 50% at the beginning of the simulation. The penalty factors are varied according to the profile risk level. Penalty factors that manage slack variables related to P2P charging/discharging participation and ancillary service responses are increased as the risk level in the profile increases. In the case of other slack variables, the penalty factors are decreased as the risk level in the profile increases. The penalty values utilized for different user profiles are categorized in Table 5.2. These values are in the range of near-zero level (i.e. 10^{-6}–1), low level (i.e. 1–10), medium level (i.e. 10–100), and high level (i.e. >100). These ranges are exclusive for this application and are obtained through numerical experimentation. A different application would require different penalty values to achieve its objectives.

Table 5.2: Penalty values for different user profiles.

Penalty Factor	Conservative Profile	Moderate Profile	Aggressive Profile
$\beta_t^{P,Anc}$	Near Zero	Low	Medium
$\beta_t^{P,P2P,Chg}$	Near Zero	Low	Medium
$\beta_t^{P,P2P,Dhg}$	Near Zero	Low	Medium
$\beta_t^{P,Res}$	High	Near Zero	Near Zero
$\beta_t^{P,Dod}$	High	Medium	Near Zero
$\beta_t^{P,Nct}$	High	High	Near Zero
$\beta_t^{P,Opt}$	High	Medium	Near Zero

5.2.1 Scheduling Results

Fig. 5.5 shows the scheduling setpoints based on the proposed three user profiles; where Figs. 5.5 (a)-(e) are based on the conservative profile, Figs. 5.5 (f)-(j) are based on the moderate profile, and Figs. 5.5 (k)-(o) are given for the aggressive one. Comparing the EV battery SOC in the three user profiles, it can be noticed that the SOC never goes below 40% under the conservative profile due to the high penalty factors on the slack variables that manage the battery depth of discharge and reserve levels. The reserve battery slack variable becomes more relaxed in the moderate setting, which allows the SOC to drop to 30% shown in Fig. 5.5 (f). Under the aggressive profile, the battery SOC-related penalty values are very low allowing the SOC to reach 20%, pertaining to the recommended minimum SOC level without causing serious degradation to the battery life. Figs. 5.5 (b) and (c) represent the conservative-based hourly scheduled charging and discharging power, respectively. As clearly depicted, involvement in P2P transactions and participation in ancillary services are kept at a low level, and half of the external requests are canceled by the algorithm through the slack variables as shown in Fig. 5.5 (d). Figs. 5.5 (g)-(i) and Figs. 5.5 (l)-(n) show the scheduled charging and

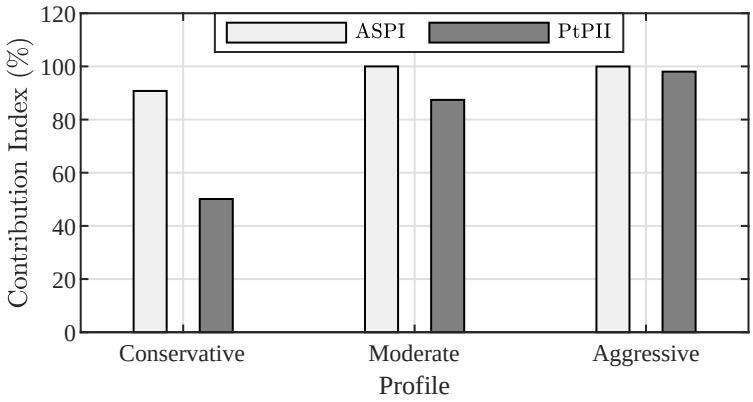

Fig. 5.6. Ancillary service participation index (ASPI) and P2P transactions involvement index (P2PII).

discharging power for moderate and aggressive profiles, respectively. It is noted that ancillary service participation is increased to its maximum as can be seen in Figs. 5.5 (h)-(i) and (m)-(n) while more involvement in P2P transactions takes place in Figs. 5.5 (l)-(m) than Figs. 5.5 (g)-(h). This shows that the aggressive setting has the highest contribution to the external energy exchanges. Figs. 5.5 (e), (j), and (o) represent driving energy under the conservative, moderate and aggressive settings, respectively. It is worth noting that due to the high penalty values on Tier 2 and Tier 3 trip slack variables under the conservative profile, all trips detailed in Fig. 5.4 are scheduled to take place without any adjustment, as shown in Fig. 5.5 (e). By contrast, Tier 2 and Tier 3 trips are adjusted under the aggressive setting as depicted in Fig. 5.5 (o). This expresses the aggressive behavior of the algorithm to minimize the cost and increase the income of the EV user. The extra available energy is clearly utilized to respond to the external energy requests as shown in Figs. 5.5 (l) and (m).

5.2.2 Ancillary Services and P2P Participation Indices

The algorithm is executed for a period of one year using a driving profile based on the survey results in [112]. Analysis and quantification under various user profiles are shown in Fig. 5.6 demonstrating the ASPI and P2PII values for each profile. It is clear that as the risk level in the profile rises, the index values increase where the ASPI increases from 90% under the conservative setting to 100% under the moderate and aggressive profiles; whereas the P2PII increases from 50% in the conservative setting to 98%. Table 5.3 lists the annual cost and revenue as well as the savings for different operating modes. The savings represent the cost reductions that the EV user achieves by utilizing the proposed model.

Table 5.3: Annual cost/revenue incurred under different operating modes.

Operating Mode	Cost ($)	Revenue ($)	Savings ($)
Unoptimized Charging	535	0	0
Optimized Charging Only	361	0	174
Conservative Profile	717	628	446
Moderate Profile	805	776	506
Aggressive Profile	792	845	588

In the unoptimized mode, the EV is charged as needed without any look-ahead optimization. Meanwhile, the second mode (i.e. optimized charging only) involves the exploitation of low electricity prices for charging without participation in any external transactions. The last three modes follow the profiles described in the previous sections. It can be observed from the values in Table 5.3 that the second mode reduces the annual cost of charging by $174. Further, participation in external transactions in the last three modes leads to an increase in charging costs. However, this increase in cost is partially

counterbalanced in the conservative and moderate profiles with an increase of revenues that leads to savings of $446 under the conservative profile and $506 under the moderate profile. Under the aggressive profile, the user starts to generate a small annual profit of $53 and a high saving of $588.

The simulation is executed for one year using light and heavy driving schedules (in extreme cases). The new results are compared with those related to the average driving profile as shown in Fig. 5.4. The light schedule represents one or two trips per weekday while the heavy schedule implies more than five trips in a weekday. The ASPI and P2PII values for the light and heavy trip schedules are indicated in Fig. 5.7 and 5.8, respectively.

Fig. 5.7 illustrates that with fewer trips per weekday, EV owner could fully follow the ancillary services signal, where it is also able to participate more in P2P transactions. Conversely, it can be seen from Fig. 5.8 that participation in external transactions is slightly decreased due to less battery energy available for peers and grid. For example, ASPI and P2PII values are decreased by 7% for the conservative profile in comparison with the results obtained under the average driving profile as shown in Fig. 5.6.

Table 5.4: Annual cost/revenue incurred under different operating modes for light trip plan.

Operating Mode	Cost ($)	Revenue ($)	Savings ($)
Unoptimized Charging	295	0	0
Optimized Charging Only	152	0	143
Conservative Profile	612	711	394
Moderate Profile	697	806	404
Aggressive Profile	710	854	439

Tables 5.4 and 5.5 list the annual cost and revenue values as well as savings for

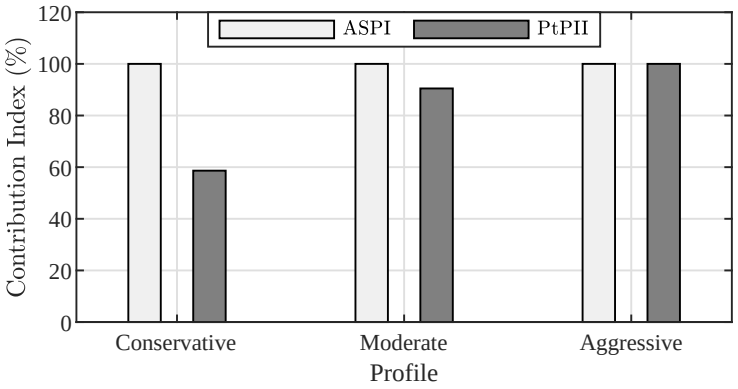

Fig. 5.7. Ancillary service participation index (ASPI) and P2P transactions involvement index (P2PII) for light trip plan.

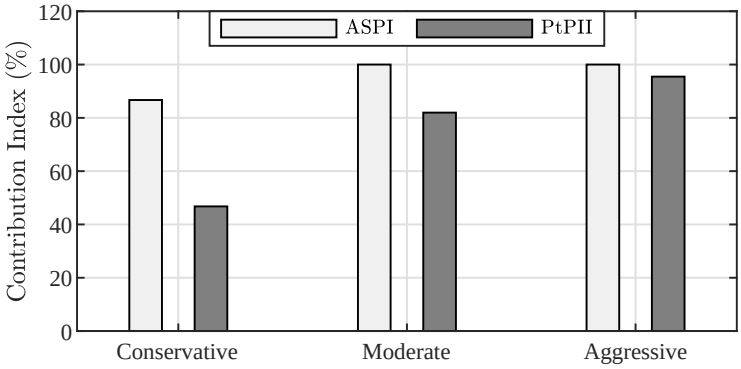

Fig. 5.8. Ancillary service participation index (ASPI) and P2P transactions involvement index (P2PII) for heavy trip plan.

Table 5.5: Annual cost/revenue incurred under different operating modes for heavy trip plan.

Operating Mode	Cost ($)	Revenue ($)	Savings ($)
Unoptimized Charging	621	0	0
Optimized Charging Only	393	0	228
Conservative Profile	771	528	378
Moderate Profile	860	734	495
Aggressive Profile	866	822	577

different operating modes in case of light and heavy trip schedules, respectively. Table 5.4 indicates that the EV owner with a light trip schedule could generate profit under any profile that allows participation in external transactions. With a heavy trip schedule, EV owners could reduce the cost of unoptimized charging by a maximum of 93% through the aggressive profile without generating any profit.

5.3 Discussion and Summary

This research argues that EV user's input can be taken into the scheduling process. It is also argued that EVs can be scheduled for joint applications concurrently including P2P energy trade and ancillary services to the grid. To that end, the research proposes a new bidirectional smart charging model of EVs for P2P energy trade and ancillary services provision to the grid. The user input is incorporated into the scheduling model using optimization variables and soft constraints. The EV user is able to adjust some of the settings of the scheduling model that would make the model adaptive to various conditions. Optimization slack variables are utilized for optimal management of the battery SOC and energy allocation for multiple service. Real-world data collected from EV owners pertaining to the usage of their EVs are utilized for numerical studies. Through numerical studies, the efficacy and feasibility of the proposed model are evaluated. The results demonstrate how the incorporation of user preferences into the scheduling process can enhance the aggregated revenue generated by the EV scheduling model.

Chapter 6 - Autonomous Control of EV Residential Charging

6.1 Introduction

Recently, research on EV charging control has focused on developing communication-based techniques for residential EV charging control [147–150]. However, direct charging control will necessitate significant expenditures to supply the extra communication infrastructure and control technologies required for each EV customer. Further, a failure in the communication network means that either the EVs will have to charge without control which could result in power quality issues and overloading of power system equipment, or that the EV chargers will have to be deactivated which will cause a significant inconvenience to EV users. As a result, autonomous charging control is required in the residential sector where it can control the charging power at the local level without requiring a communication network. Autonomous controllers can be utilized in stand-alone mode where they serve as the main control method of EV charging at homes, or they can be installed as a backup controllers that can be activated in case of failure in communication networks.

With respect to autonomous charging control, the existing research has the following shortcomings and gaps. First, the communication-less controllers proposed in the

literature are very conservative, causing unnecessarily slow charging without fully utilizing the capacity of the power system. In this regard, the frequency and voltage-based controllers proposed in previous studies reduce the EV charging load even when the system frequency and the bus voltage are above their respective nominal values. Second, the charging control logic implemented in previous studies can result in unfair allocation of power system capacity among EVs. In this context, social charging fairness is defined as the equal share of limited power system capacity among EVs when power resources are in short supply [151]. Multiple solutions have been proposed to solve the issue of charging fairness in communication-based EV energy management techniques, see [147–150]. In regards to communication-less techniques, the controller proposed in [87] considers equal charging rate for EVs in the system. Further, the study in [152] investigates the use of voltage sensitivity to achieve charging fairness among EVs in the system. However, both of the controllers in [87] and [152] allocate power system capacity among EVs based on "memory-less fairness", which is allocating resources fairly in the present moment without regard for historical allocations [153]. A memory-less fairness policy equates the EVs that are being charged for hours and the EVs that are just plugged-in into the system, which does not achieve charging fairness. Third, the voltage and frequency based controllers in [83]-[88] are set to regulate the EV charging load down to the minimum acceptable charging rate and then switch off the charger when the system frequency and/or bus voltages go below their respective acceptable limit. This creates a discontinuity in controllers that could lead to charging load oscillations around the cut-off point. In this regard, the EV chargers are switched off due to violation of the system operating conditions, i.e., frequency and/or bus voltages, and as a result, the system frequency and/or bus voltages rebound, which causes the chargers to activate

again and so forth.

Therefore, this research aims to develop a communication-less control strategy for EV charging via an adaptive Sigmoid-based controller. The strategy considers social charging fairness and can work in droop-controlled IMGs. The key contributions of this research are as follows:

1. An adaptive Sigmoid-based controller that manages the rate of charging based on the system frequency and bus voltages is proposed. Compared to previous works, the proposed controller provides more flexibility and better utilization of the power system capacity in EV charging without jeopardizing stability.

2. A social charging fairness system that assigns priority levels to EVs based on their past charging power allocation is developed. The priority level for each EV is autonomously lowered as its charging allocation in the historical time horizon increases. The priority level is utilized to adjust the Sigmoid-based controller to provide more system capacity to the EVs with higher priority levels.

3. The cut-off point in the controllers proposed in previous works has been replaced by a novel EV load shedding scheme that gets triggered when an under-voltage or under-frequency event occurs in the IMG when the generation does not meet the required demand. The proposed shedding scheme is coordinated with the priority level of EVs to ensure fair EVs shedding.

4. A system violations index (SVI) is proposed to quantify the effectiveness of the proposed strategy in reducing violations of system operating constraints that result from EV charging.

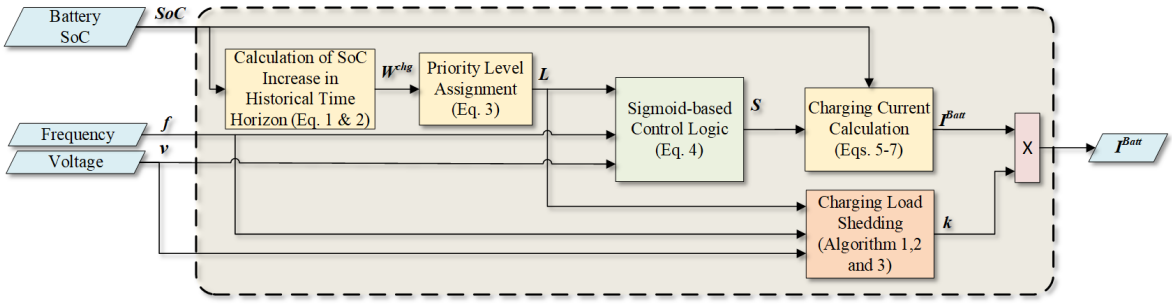

Fig. 6.1. The proposed communication-less EV charging control strategy

Without loss of generality, the following assumptions are made during development of this work:

- Similar to the works in [88] and [154], it is assumed that this strategy is programmed into all EV smart chargers connected to the microgrid, and cannot be modified by EV users.
- All chargers follow the constant current/constant voltage (CC/CV) charging profile, which is widely used in charging EV lithium-ion batteries [155].
- When compared to other residential loads, EVs have a greater degree of flexibility due to the energy stored in their batteries. As a result, during periods when the microgrid is not operating normally, the normal load is prioritized while EV charging load is reduced or interrupted before any other loads.

6.2 Proposed Communication-less EV Charging Load Control Strategy

This section describes the proposed communication-less EV charging load control strategy. The proposed strategy is applied locally by each EV charger in the system without any communication with the system operator or other EV chargers. The block diagram of the proposed strategy is shown in Fig. 6.1. As depicted in the figure, the proposed control strategy receives inputs which are, (i) local system measurements (i.e., bus voltage and system frequency) taken at PCC, and (ii) EV's battery SoC. The proposed control strategy calculates the battery SoC increase for each EV once it starts charging. An EV priority system then assigns a priority level to the EV based on how much SoC it gained in the past hours. The priority level of the EV will affect the logic of a Sigmoid-based controller that is responsible for regulating EV charging based on changes in the system's frequency and bus voltage. In this regard, a lower priority level for an EV indicates that a decrease in frequency or voltage will result in a higher reduction of charging speed in comparison to higher priority EVs. Moreover, in situations where system frequency or bus voltage go below their respective lower limit despite the reduction of EV charging current to the minimum by the other controllers, the proposed control strategy can deactivate the EV charger through its shedding scheme. The proposed strategy is explained in detail in the following subsections.

6.2.1 EV Priority System

The proposed control strategy continuously logs the charging process and calculates the increase in EV battery SoC in the past time horizon to determine the priority level

assigned to the EV. Let D be the set of historical time steps and d is the length of historical time horizon considered with $D = \{t-1, t-2, ..., t-d\}$. This means that if $d = 4$ hours for example, then the smart charger will continuously calculate the total SoC increase in the last four hours. Parameter d is programmed into all EV smart chargers and can be decided by the IMG operator depending on system requirements. In this regard, a higher SoC increase during the historical time horizon leads to a lower priority assignment in comparison to the EVs with less past charging. The priority level affects the degree to which the EV charging speed is reduced when the system frequency and/or bus voltage are below their nominal values. The SoC increase of the j^{th} EV at each time step is estimated by integrating the charging current and adding it to the previous state as follows [81]:

$$SOC_{t,j} = SOC_{t-1,j} + \frac{1}{C_{batt}} \int_{t-1}^{t} I_{t,j}^{Batt} dt, \tag{6.1}$$

where C_{batt} is the rated capacity of the j^{th} EV battery in Ampere-hour (Ah). The total SoC increase $W_{t,j}^{chg}$ during the historical time horizon for the j^{th} EV is calculated as follows:

$$W_{t,j}^{chg} = SOC_{t,j} - SOC_{t-d,j}. \tag{6.2}$$

The proposed control strategy assigns a priority level $L_{t,j}$ to the j^{th} EV at time t according to (6.3):

$$L_{t,j} = \begin{Bmatrix} 1, & W_{t,j}^{chg} < \phi \\ 2, & \phi \leq W_{t,j}^{chg} < 2 \cdot \phi \\ . & . \\ \lambda, & (\lambda - 1) \cdot \phi \leq W_{t,j}^{chg} < \lambda \cdot \phi \end{Bmatrix}, \tag{6.3}$$

where λ is the number of priority levels in the system that can be assigned to EVs, while ϕ is the total SoC increase that moves an EV from one priority level to another. In (6.3), $L = 1$ is a higher priority level than $L = 2$ because that latter has gained higher SoC in the past time horizon. In summary, the priority system embedded in each local charger uses the EV battery SoC increase in the historical time horizon to assign an EV a priority level without the need for communication with system operator or other chargers. The priority level will affect the charging power that an EV is allocated through the adaptive parameter in Sigmoid-based controller as explained in the next subsection.

6.2.2 Adaptive Sigmoid-based Controller

A Sigmoid controller is programmed on each EV charger. The voltage and frequency Sigmoid-based functions that control the rate of EV charging are given by (6.4):

$$S_{t,j} \;=\; \frac{1}{\left(1 + e^{-\rho(L_{t,j}) \cdot v_{t,j}}\right)} \cdot \frac{1}{\left(1 + e^{-\rho(L_{t,j}) \cdot f_{t,j}}\right)}, \tag{6.4}$$

where $v_{t,j}$ and $f_{t,j}$ are voltage and frequency measured by the charger at the PCC, respectively. $\rho(L_{t,j})$ is a parameter that is a function of the priority level $L_{t,j}$. Relation (6.4) consists of two Sigmoid functions multiplied by each other. The first function changes in response to changes in the bus voltage $v_{t,j}$ at time t, while the second function is changed according to the system frequency $f_{t,j}$. The parameter ρ in (6.4) changes according to the priority level $L_{t,j}$ of the EV. This parameter affects the rate of change of the Sigmoid functions (i.e. the shape and rise of the function). In this context, a lower priority level for an EV indicates that a decrease in frequency or voltage will result in a higher reduction of charging in comparison to higher priority EVs. The effect of the priority level on the level of charging derating in the frequency-based control function is demonstrated in Fig. 6.2. As shown in the figure, the decrease in the priority level from level 1 ($L = 1$) to level 6 ($L = 6$) increases the rate of decay of the function in response to the decrease of system frequency and, therefore, increases the charging derating level. The voltage-based control function has a similar behavior but with an input range corresponding to voltage measurements. In this work, it is proposed that the setting of parameter ρ is based on providing high derating in charging power for the lower priority levels and slight derating to higher priority levels in the event that system parameters (i.e., voltage and/or frequency) decrease from their nominal values. Once voltage and/or frequency are in the midpoint between their nominal value and lower limit, the function should start to steeply derate the charging power for EVs from all priority levels, albeit keeping the higher charging rate for high priority levels. When system parameters are close to their lower limits, then the derating are almost equal for all priority levels.

The Sigmoid controller is utilized in the proposed strategy because it provides a

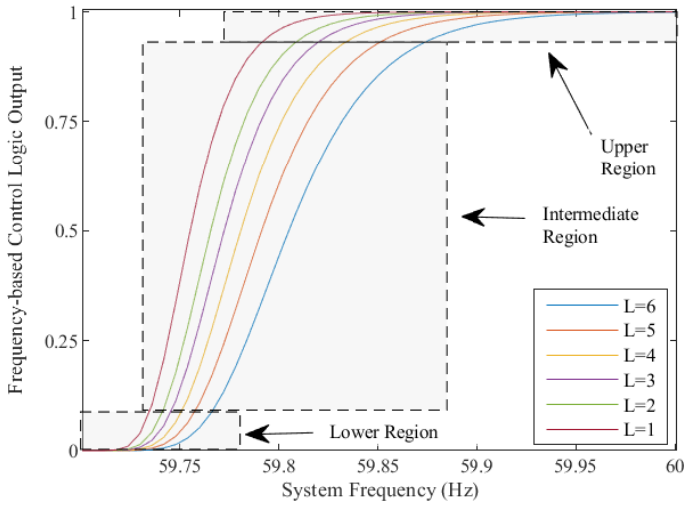

Fig. 6.2. Example of how the EV charging speed for the frequency-based control logic varies with priority level

flexible three regions of continuous EV charging control as illustrated in Fig 6.2. At nominal system operating condition (frequency and/or voltage is one per unit), the EV charging speed factor is set at unity i.e., EV charges at full speed. When the deviation for the system operation from the nominal values is small (upper region), the EV charging speed decreases slowly. This prevents unnecessary reduction of charging power when the system operating parameter is slightly deviating from its nominal value. The intermediate region provides a rapid reduction in the charging speed to slow the decrease in frequency and/or voltage. When the system parameter is near its lower acceptable limit in the lower control region, the charging speed is slowly changed to prevent any large power oscillation near this point in case of synchronized actions of controllers. For example, if the system parameter is increasing in the lower region, the charging speed factor is slowly increased to ensure that the power system can handle the extra load without putting its stability at risk.

6.2.3 Charging Current Calculation

The charging current of the j^{th} EV at each time step t is determined by the following equations:

$$I_{t,j}^{Batt} = I_j^{max}, \quad SoC_{t,j} < SoC_j^{min} \tag{6.5}$$

$$I_{t,j}^{Batt} = I_j^{min} + (I_j^{max} - I_j^{min}) \cdot S_{t,j}, \quad SoC_j^{min} \leq SoC_{t,j} < SoC_j^{max} \tag{6.6}$$

$$I_{t,j}^{Batt} = 0, \quad SoC_{t,j} \geq SoC_j^{max} \tag{6.7}$$

where I_j^{min} and I_j^{max} are the minimum and the maximum output current limits of the j^{th} EV charger, respectively. A minimum charging current is included based on the requirements of EV charging standards [156]. In summary, when the $SoC_{t,j}$ is below the pre-defined minimum level SoC_j^{min}, the EV charger provides the maximum charging current to the EV battery. When the $SoC_{t,j}$ is below the max level but above the minimum value, the proposed strategy adjusts the charger current based on the Sigmoid-based controller represented by the factor $S_{t,j}$ calculated in (6.4). If the $SoC_{t,j}$ is higher than the maximum level SoC_j^{max}, the strategy switches off the EV charger in order to extend the battery lifetime.

6.2.4 Communication-less EV Load Shedding Scheme

In the situations where the system frequency and/or bus voltage go below their respective lower limit despite the reduction of EV charging current to the minimum, the proposed control strategy can deactivate the EV charger through its shedding scheme. While the charger is plugged-in, a communication-less EV load shedding scheme continuously monitors the system frequency, bus voltage, and EV priority level at each time step

t as shown in Fig. 6.1 above. Based on these inputs, the scheme decides the charger status through the shedding control signal $K_{t,j}$, where $K_{t,j} = 0$ deactivates the charger. Algorithm 6.1 demonstrates the overall logic of this scheme. By default, $K_{t,j} = 1$ for

Algorithm 6.1: Proposed EV Load Shedding Scheme

Input : Priority level $L_{t,j}$, System frequency f_t and bus voltage $v_{t,j}$ measured at EV j PCC

Output : Shedding control signal $K_{t,j}$

$K_{t,j} \leftarrow 1; \forall t$

Function `Main`(f_t, $v_{t,j}$, $L_{t,j}$)**:**

```
while EV Plugged In do
    if f_t < f_r || v_t < v_r then
        if I_{t,j}^{Batt} == 0 then
            K_{t+1,j} ← 0;
        else
            if τ_j == 0 then
                τ_j = Time_Delay(L_{t,j});
                event ← t;
            else
                if τ_j == (t − event); then
                    K_{t+1,j} = Shedding_Cont(L_{t,j});
            end
        end
    else
        τ_j ← 0;
    end
end
```

return $K_{t,j}$

any time step unless it is changed by the scheme. When the frequency or the voltage goes below its respective acceptable limit f_r or v_r, the scheme checks whether the EV is being charged at the current time step t. If the EV is charging, then the EV is assigned a time delay based on the function $Time\_Delay$, which is detailed in Algorithm 6.2. The purpose of the time delay is to wait for the frequency and/or voltage to return

to their normal operating range and prevent nuisance load shedding. The time delay assigned by this function varies according to the priority level assigned to the EV at that particular time step. In this regard, EVs with lower priority levels are assigned shorter time delays to be shed. It is worth noting that the function *Time_Delay* assigns random time delays within a certain range for each priority level. This prevents the simultaneous shedding of EVs that belong to the same priority level, which could lead to large swings in the system load that affect its stability. In case the EV charger is not charging because it has been deactivated by a previous shedding control signal, the scheme will not make any changes and the shedding signal for the next time step is kept at zero. In a situation where a time delay is assigned, the scheme checks if the time delay has passed based on the recorded event time. In that case, function *Shedding_Cont* in Algorithm 6.3 deactivates the charger for a future time set Δ based on the priority level. The deactivation time (i.e., the total time in which the charger is switched off) increases as the priority level decreases.

Algorithm 6.2: Time Delay Function

Function `Time_Delay(`$L_{t,j}$`):`
- **switch** $L_{t,j}$ **do**
  - **case** λ **do**
    - $\tau_j = rand(\pi, 2\pi)$;
  - **case** $\lambda - 1$ **do**
    - $\tau_j = rand(2\pi, 3\pi)$;
    - .
    - .
  - **case** 1 **do**
    - $\tau_j = rand(\lambda.\pi, (\lambda + 1).\pi)$;

Algorithm 6.3: Shedding Control Function

Function `Shedding_Cont(`$L_{t,j}$`):`

- **switch** $L_{t,j}$ **do**
  - **case** λ **do**
    - $\Delta_1 = [t + x_1, t + x_2]$;
    - $K_{\Delta_1,j} = 0$;
  - **case** $\lambda - 1$ **do**
    - $\Delta_2 = [t + x_2, t + x_3]$;
    - $K_{\Delta_2,j} = 0$;
  - .
  - .
  - **case** 1 **do**
  - $\Delta_\lambda = [t + x_y, t + x_z]$;
  - $K_{\Delta_\lambda,j} = 0$;

6.2.5 Performance Index

The effectiveness of the proposed charging control strategy to reduce the violations of the system operating constraints that result from EV charging is quantified using the system violations index (SVI) as follows:

$$SVI = \sum_{t \in T} |\Omega_t^f| \cdot \Delta t + \sum_{j \in \mathbb{B}} \sum_{t \in T} |\Omega_{t,j}^v| \cdot \Delta t \quad \forall t \in T \wedge \forall j \in \mathbb{B}, \tag{6.8}$$

where:

$$\Omega_t^f = \begin{cases} f_t - f_{ru} & , \quad f_t > f_{ru} \\ f_{rl} - f_t & , \quad f_t < f_{rl} \\ 0 & , \quad \text{else} \end{cases} \tag{6.9}$$

$$\Omega^{v}_{t,j} = \begin{cases} v_{t,j} - v_{ru} & , \quad v_{t,j} > v_{ru} \\ v_{rl} - v_{t,j} & , \quad v_{t,j} < v_{rl} \\ 0 & , \quad \text{else} \end{cases} \tag{6.10}$$

Parameters f_{rl} and v_{rl} in (6.8) are the minimum operating limits for system frequency and bus voltage, while f_{ru} and v_{ru} represent the maximum limits for frequency and voltage, respectively. Also, $\mathbb{B}$ is the set of buses in the power system and T is set of time steps in the studied duration.

6.3 Droop-based Islanded Microgrid Test Model

In IMGs, DGs are the main components responsible for creating balanced power generation in the distribution systems [157]. Due to the absence of a slack bus, DGs are operated to follow the power demand by controlling the IMG system frequency and bus voltages. Therefore, the suitable operation mode for DGs is the droop control, where without loss of generality, the injected active power P_i^{Src} increases by drooping the frequency of the DG unit output voltage, and the reactive power Q_i^{Src} increases by drooping the magnitude of the DG unit output voltage as follows [86]:

$$P^{Src}_{i,t} = \Big(\frac{\omega^*_i - \omega_t}{m_{P_{i,t}}}\Big) \;\; \forall i \in \mathbb{G},\; \mathbb{G} \subseteq \mathbb{B}, \tag{6.11}$$

$$Q^{Src}_{i,t} = \Big(\frac{|V^*_i| - |V_{i,t}|}{n_{q_{i,t}}}\Big) \;\; \forall i \in \mathbb{G} \subseteq \mathbb{B}, \tag{6.12}$$

where, $m_{P_{i,t}}$ and $n_{q_{i,t}}$ are the droop control settings for DG i, ω^*_i is the frequency

setting for the DG at no load, $|V_i^*|$ is the voltage at no load for the DG, $|V_{i,t}|$ is the voltage of the bus connected to the DG, ω_t is the system operating frequency at time instant t, $\mathbb{G}$ is a subset of buses with DGs, and $\mathbb{B}$ is the set of all buses in the system. The drooped injected active and reactive power are balanced with the load demand $P_{i,t}^{Dmd}$ and $Q_{i,t}^{Dmd}$ through the power mismatch equations as follow:

$$P_{i,t}^{Src} - \sum_{l \in \mathbb{B}} \Big(|V_{i,t}| \cdot |V_{l,t}| \cdot Y_{il}.cos(\theta_{il} + \delta_{l,t} - \delta_{i,t}) \Big) = P_{i,t}^{Dmd} \quad \forall i, l \in \mathbb{B} \wedge i \neq l, \tag{6.13}$$

$$Q_{i,t}^{Src} + \sum_{l \in \mathbb{B}} \Big(|V_{i,t}| \cdot |V_{l,t}| \cdot Y_{il}.sin(\theta_{il} + \delta_{l,t} - \delta_{i,t}) \Big) = Q_{i,t}^{Dmd} \quad \forall i, l \in \mathbb{B} \wedge i \neq l. \tag{6.14}$$

where, Y_{ij} and θ_{ij} are the Y-bus admittance magnitude and angle, respectively, and δ_i is the voltage phase angle at any bus i.

6.4 Numerical Simulations

Numerical simulations are performed in a MATLAB environment to test the effectiveness of the proposed strategy. The modified IEEE benchmark distribution system shown in Fig. 6.3 (a) is selected as the test system [158]. The power distribution system operates as an IMG and consists of a 33-bus primary distribution network operating at a nominal voltage of 12.47kV. In order to capture the interaction of IMG with EV chargers installed in residential areas, seven secondary distribution networks operating at 220V are modeled and connected to the primary buses in the system. Each secondary network is modeled as per the CIGRE 14-node residential lateral benchmark shown in Fig. 6.3 (b) [159]. Non-EV residential load profiles with a resolution of one minute are

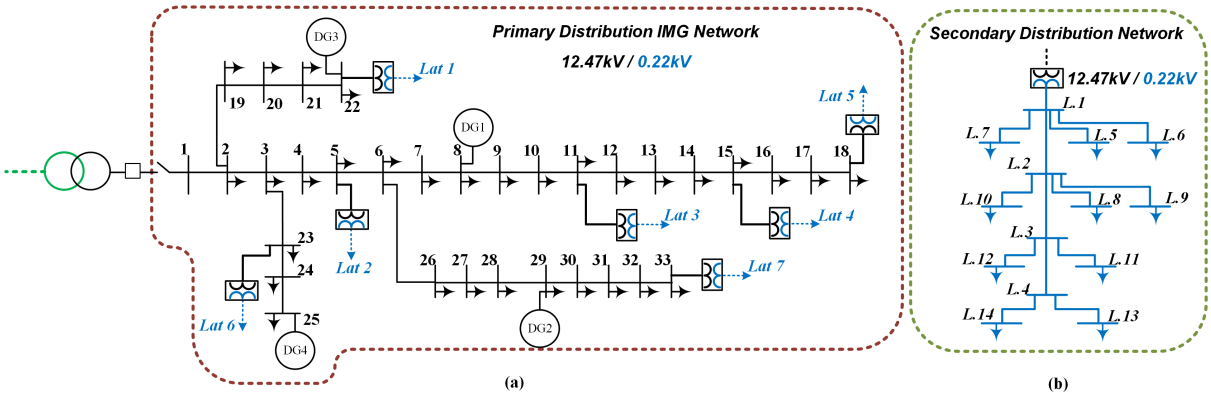

Fig. 6.3. Test IMG system, (a) IEEE 33-bus primary distribution network, and (b) CIGRE 14-node secondary network.

generated from real data of houses in Canada [160]. It is assumed that a total of four DGs are connected in the system, where all the DGs are dispatchable with the exception of DG2, which is wind-powered. The parameters of the DGs including ratings, droop, and nominal operating settings are listed in Table 6.1, while the wind power profile for DG2 is shown in Fig. 6.4 [161].

Table 6.1: DGs Parameters in 33-Bus Test IMG System

DG #	$\mathbf{m}_{\mathrm{p}}$ p.u.	$\mathbf{n}_{\mathrm{q}}$ p.u.	ω^* MVA	V^* p.u.	$\mathbf{S}_{\mathrm{gmax}}$ p.u.	PF
1	0.00208	0.0486	1	1.03	2.5	0.8
2	-	-	-	-	1.5	0.95
3	0.00505	0.101	1	1.02	1	0.8
4	0.00833	0.166	1	1.02	0.6	0.8

Level 2 chargers with a maximum charging power of 6.6 kW are considered in this study, and the minimum charging rate is set to 1.5 kW as per the IEC 61851 standard. A maximum of 200 EVs are assumed to be present in the IMG system, which sets the

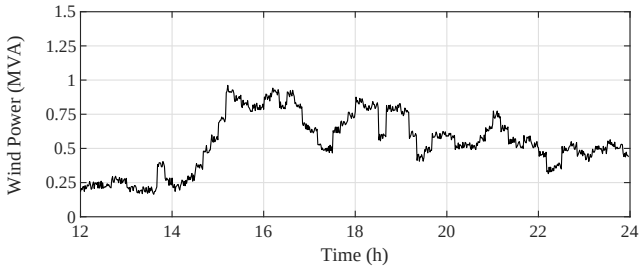

Fig. 6.4. DG2 wind-based power profile

rated EV charging load to be around 35% of the total rated system load. The battery capacities for all EVs are set at 62 kWh, which is similar to the Tesla 3 model, one of the most popular EVs in the market [162]. The parameters SoC^{min} and SoC^{max} are set at 25% and 85%, respectively. The EVs are assumed to be charged at homes while the arrival times follow a truncated Gaussian distribution [163], with a mean value μ equal to 5 p.m. and standard deviation σ set at 1.5h, while the initial battery SoCs of EVs distribution parameters are set at $\mu = 45\%$ and $\sigma = 10\%$. All case studies are run from 12 p.m to 12 a.m. Without loss of generality, six priority levels are chosen based on $d = 6$ hours and $\phi = 15\%$. The parameters of the adaptive Sigmoid-based controller are listed in Table 6.2. These parameters are chosen based on six priority levels to create a control that varies when voltage and frequency goes below 1 p.u and 60 Hz, respectively. It should be noted that Lx in Table 6.2 and following figures refers to priority level $L = x$ (e.g, $L6$ means $L = 6$).

Table 6.2: Sigmoid-based Controller Parameters

Parameter	L6	L5	L4	L3	L2	L1
ρ	2000	2300	2600	2900	3200	3500

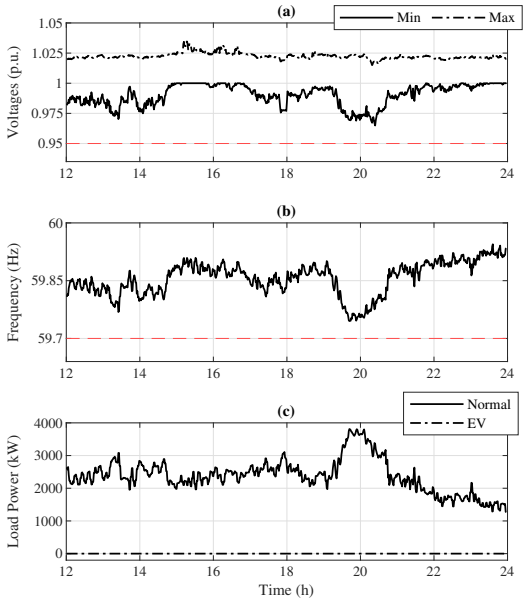

Fig. 6.5. Case 1 simulation results, (a) Minimum and maximum bus voltages, (b) System frequency, and (c) Normal load power.

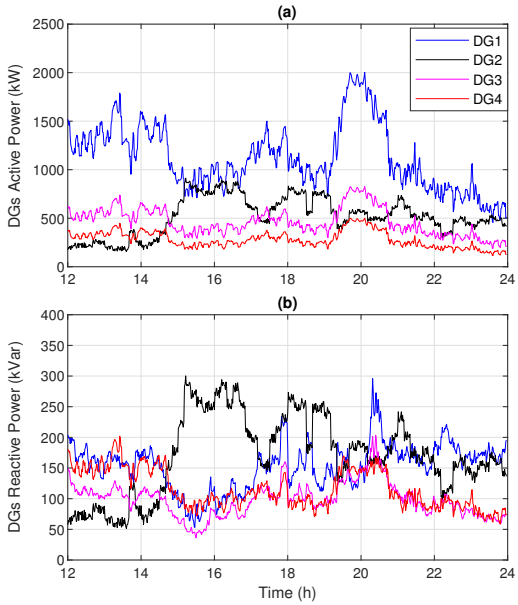

Fig. 6.6. Case 1 simulation results, (a) DGs active power, (b) DGs Reactive power.

6.4.1 System Operation Without EV

In the first case, the IMG is operated assuming that there are no EVs in the system. Figs. 6.5 (a) and (b) show the operating voltage and frequency parameters of the system, respectively, while the load power is shown in Fig. 6.5 (c). DGs active and reactive power outputs are shown in Figs 6.6 (a) and (b), respectively. It is noticed from Figs. 6.5 (a) and (b) that the system voltage and frequency are within the standard limits, which specify that the acceptable operating ranges for voltage and frequency are between 0.95 p.u and 1.05 p.u, and 0.995 p.u (59.7 Hz) to 1.005 p.u (60.3 Hz), respectively [164]. Both the bus voltages and system frequency reach their lowest operating points when

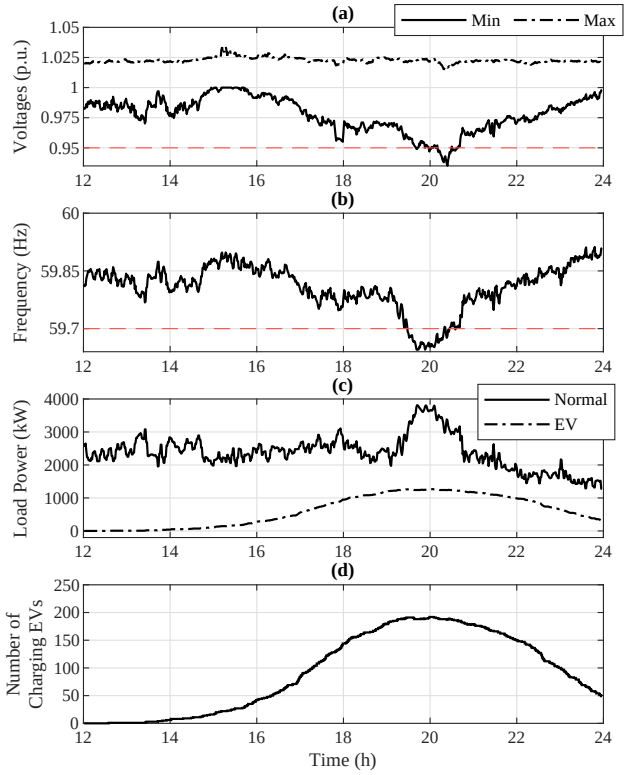

Fig. 6.7. Case 2 simulation results, (a) Minimum and maximum bus voltages, (b) System frequency, and (c) Normal and EV charging load power.

the normal load power peaks around 8 p.m as demonstrated in Fig. 6.5 (c).

6.4.2 Opportunistic Charging

In the second case, the IMG is simulated with the presence of EV load and the assumption that the EV chargers are operated without restrictions. Figs. 6.7 (a)-(d) demonstrate the operating parameters for this case. It is clear from Figs. 6.7 (a) and (b) that no violation is recorded in system parameters during light loading conditions. However, this type of uncontrolled EV charging results in an unacceptable violation of the respective limits of both the voltage and frequency during the peak loading time. The voltage

limit violations occur in laterals 4 and 5 because they are relatively farther from the nearest DGs than other laterals. It is noteworthy that these violations result from the coincidence of both normal and EV peak loads, which is clear from Fig. 6.7 (c). These conditions overload the DGs in the IMG and cause undesirable voltage drops across the distribution lines.

6.4.3 Controlled Charging

Proposed Strategy vs Voltage-based Controller

In this case, the control strategy proposed in Section 6.2 is simulated and compared with controllers from the state-of-the-art review. First, the proposed strategy is compared with the voltage-based charging controller proposed by the authors in [152]. The charging power controller proposed in [152] is given by the following equation:

$$EP_{t,j} = \begin{cases} P_j^{min} + \beta_j \cdot e^{-(u_{j,t})(v_{t,j}-v_r)} \cdot e^{(1-SoC_{t,j})}, & v_{t,j} \geq v_{rl} \\ 0, & v_{t,j} \leq v_{rl} \end{cases} \tag{6.15}$$

where β_j is a controller parameter for EV j while $v_{t,j}$ and $u_{t,j}$ are the voltage and sensitivity measured by EV charger j, respectively. The parameter v_{rl} in (6.15) is a reference voltage set to the lower acceptable limit, which is 0.95 p.u. The performance of the two controllers during peak load time from hour 19 to hour 21 are compared to test their effectiveness in controlling the EV charging load when system operating parameters approach their lower respective limits. Simulation results for the voltage-based controller are shown in Figs. 6.8 (a)-(c). Fig. 6.8 (a) shows that the voltage-based controller results in oscillations around the lower limit of bus voltage during the peak load period. These

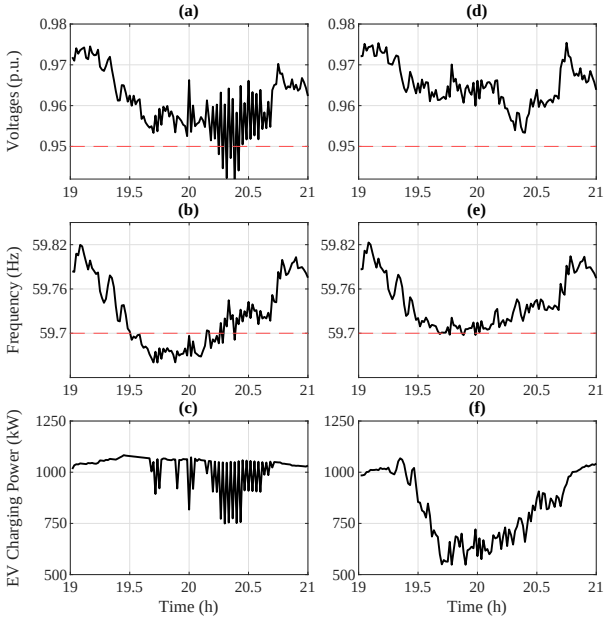

Fig. 6.8. Peak loading conditions, **voltage-based controller** simulation results, (a) Minimum bus voltages, (b) System frequency, and (c) EV charging power, and **proposed strategy** results (d) Minimum bus voltages, (e) System frequency, and (f) EV charging power.

oscillations occur because of the discontinuity in the controller that leads to charging load fluctuations as shown in Fig. 6.8 (c). It is worth to recall that this controller is designed to control EV charging based on voltage, and therefore, the frequency violation shown in Fig. 6.8 (b) is not corrected due to the absence of frequency in the input parameters of the controller. The results of the proposed strategy are demonstrated in Figs. 6.8 (d)-(f). Fig. 6.8 (d) and (e) show that the voltage and frequency of the system stay above their respective lower limits throughout the peak loading conditions. This is because each EV charger in the system modulates its power according to the measured voltage and frequency. This results in reduced total EV charging load as shown in Fig. 6.8 (f), which reliefs the DGs and reduce voltage drops across the system.

It is also important to note that in contrast to previous works, the charging fairness technique implemented in the proposed strategy does not degrade the performance of the EV charging control. This can be clearly observed from Figs. 6.8 (a)-(c) that show that the EV charging load for the voltage-based controller slightly changes in response to voltage changes due to the presence of sensitivity parameter that is used to achieve charging fairness. Meanwhile, the proposed strategy effectively controls the EV charging according to system conditions as shown in Figs. 6.8 (d)-(f).

The SVI index values for opportunistic charging, voltage-based controller, and proposed strategy are listed in Table 6.3. It can be observed that the proposed strategy provides a remarkable improvement in reducing system parameters violations.

Table 6.3: SVI for different charging techniques

Charging Control Technique	Opportunistic	Voltage-based	Proposed Strategy
SVI	0.0855	0.0196	0

As described in Section 6.2, the level at which chargers are reduced depends on the priority level of each EV. Fig. 6.9 demonstrates the power system capacity allocation for different priority level. It is clear from the figure that a higher priority level (less past charging allocation) will result in higher power allocation for the EV.

Proposed Strategy vs Frequency-based Controller

The proposed strategy is also compared with the frequency-based controller implemented by the authors in [87], which is represented by the following:

$$I_{t,j} = I_j^{min} + (I_j^{max} - I_j^{min}) * (f_t - f_{rl}) \; . \; \Psi \tag{6.16}$$

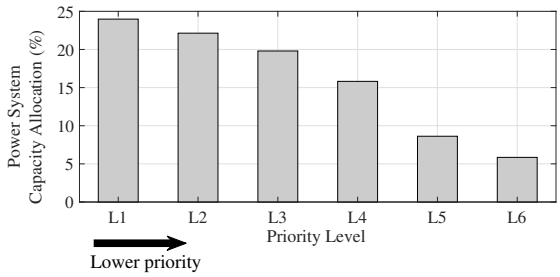

Fig. 6.9. EV priority level distribution during peak loading period for the proposed strategy

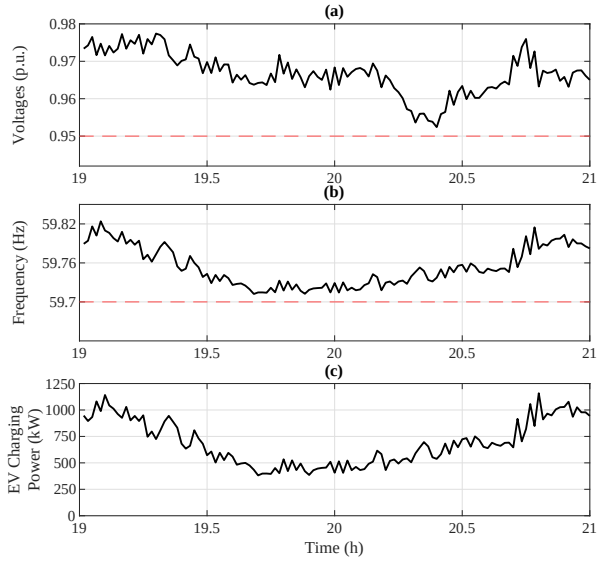

Fig. 6.10. Simulation results for frequency-based controller during peak loading conditions, (a) Minimum bus voltages, (b) System frequency, and (c) EV charging power

Parameter Ψ in (6.16) is the controller droop gain. Figs. 6.10 demonstrate system parameters during peak load time when the frequency-based controller is implemented in the IMG. As noticed from the figures, the controller helps to avoid violations in frequency and voltage during the peak time. Nonetheless, the controller applies equal charging reduction to all the EVs without the consideration of fairness as can be seen from Fig. 6.11, which shows that the charging power allocation during the peak load

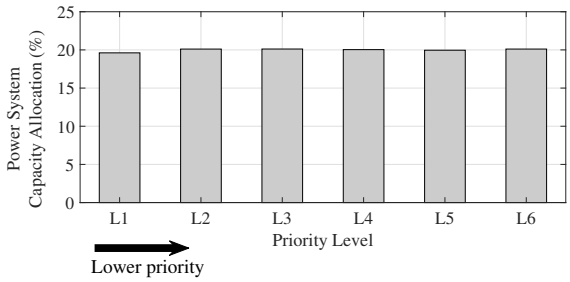

Fig. 6.11. EV priority level distribution during peak loading period for the frequency-based controller

time for frequency-based controller. The performances of the frequency-based controller and the proposed strategy are also compared during DG outages, which could cause a further drop in frequency during the peak loading conditions. A DG outage scenario is implemented where DG4 goes out of service at 18:30. Figs. 6.12 (a)-(c) illustrate the results for this scenario in the case of the frequency-based controller. It can be noticed from Figs. 6.12 (a)-(c) that oscillations in voltage, frequency, and EV charging load when the DG outage event occurs during the peak loading conditions. These oscillations occur despite the reduction of charging load to the minimum limit as shown in Fig. 6.12 (c), which indicates that further curtailment of EV load is required.

The simulation results of DG4 outage scenario are demonstrated in Figs. 6.12 (d)-(e) for the proposed strategy. It is worth noting that once the shedding scheme detects a violation of voltage and frequency in the system, it starts to curtail EV loads to prevent further violations and bring back the system parameters to the acceptable limits as shown in Fig. 6.12 (d) and (e). This results in shifting the peak EV charging load a bit further and reliefs the system during the abnormal condition of DG outage as demonstrated in Fig. 6.12 (f). The SVI index for this scenario is calculated for the frequency-based controller and the proposed strategy as shown in Table 6.4. The SVI

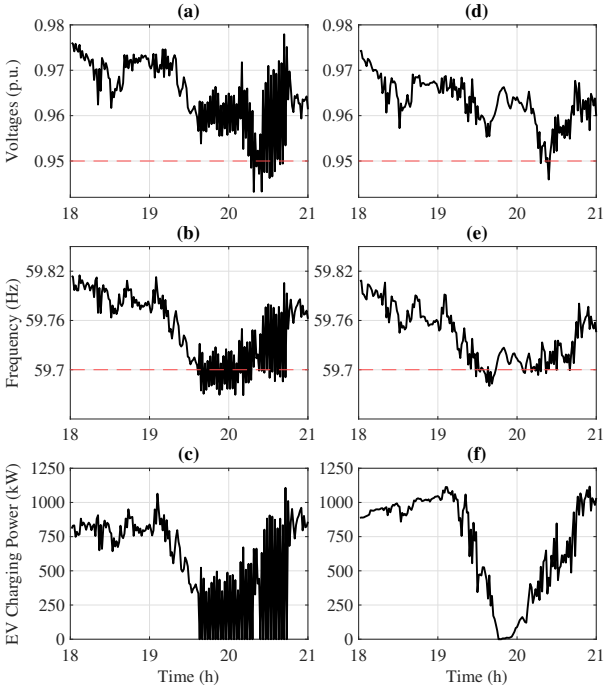

Fig. 6.12. DG outage scenario, simulation results for **frequency-based controller**; (a) Minimum bus voltages, (b) System frequency, and (c) EV charging power, and **proposed strategy** results, (d) Minimum bus voltages, (e) System frequency, and (f) EV charging power.

values indicate that the load shedding scheme incorporated in the proposed strategy greatly reduces the system parameter violations during the DG outage event.

Table 6.4: SVI for frequency-based Controller and Proposed strategy in a DG outage scenario

Charging Technique	Frequency-based	Proposed Strategy
SVI	0.0247	0.0039

6.5 Discussion and Summary

This research develops a communication-less control strategy for the EV charging load in droop-controlled IMGs. The proposed strategy controls the speed of EV charging based on both the system frequency and bus voltage, as well as the battery SoC and past charging power allocation. Further, a novel EV load shedding scheme is proposed that gets triggered when an under-voltage or under-frequency event occurs in the IMG. Moreover, a charging fairness system that assigns priority levels to EVs based on their past charging power allocation is developed. Numerical simulations are conducted to validate the effectiveness of the proposed strategy. The results demonstrate the superiority of the proposed control strategy to the state-of-the-art controllers in modulating the EV charging load. The results also show that the charging fairness system implemented in the proposed strategy does not degrade the performance of the EV charging control. During a DG outage scenario, the proposed control strategy successfully curtailed EV loads to prevent further violations and bring back the system operating parameters to the acceptable limits.

Chapter 7 - Optimal Design of Charging Facilities within Parking Lots

7.1 Introduction

The deployment of EV parking lots (EVPLs) with charging capability in commercial and workplace districts has been suggested as a solution that could serve the charging needs of EV owners in these areas [165]. However, the prior research on the topic of EVPL design and operation management are associated with shortcomings that need be addressed. First, the requirements, specifications, and limitations of electric DNs and/or transportation networks are the focal points in the EVPL design models proposed in the literature. Second, a common shortcoming in previous research that considers EVPL provision of V2G services to the grid is that they assume all chargers installed in the EVPL are of the BD type. However, such an assumption may not be practical due to (i) the cost of BD chargers being up to three times the cost of the UD type [166], and (ii) the lack of clear evidence that many EV users will participate in the provision of V2G programs due to fears about their EV batteries degradation [167]. Therefore, it is imperative to unveil a design model that can determine the optimal ratio of BD to UD chargers to be installed in the EVPLs according to the benefit to costs ratio and the projected EV owners' participation in V2G programs. Third, designed

financial models of EVPL in the literature follow a holistic approach that consolidates the financial aspects of different services (i.e., charging, V2G) into one model. However, it is imperative to have the ability to separately view each service contribution to the project's financial performance and optimize its related parameters. Such an approach allows efficient planning of the project through (i) effective utilization of investment capital on profitable services, (ii) re-evaluation of service operation and pricing strategy, (iii) reassessment of costs, and (iv) elimination of unprofitable services. Therefore, this research aims to develop a new approach for optimal design of an EVPL providing charging services to EV users and V2G support to the electrical power grid. In particular, the key contributions of this research are listed as follows:

1. A new multi-objective model is developed that allows for the maximization of EVPL owner profit and/or EVPL social responsibility using control parameters incorporated in the model.

2. The model provides the design of an EVPL with the optimal combination of UD and BD chargers, considering the financial aspects of V2G services as well as the incentive-participation scheme for EV users.

3. The model decouples the intertwined economic dynamics of EV charging and V2G services in the EVPL via revenue models targeting each service separately. This allows optimal pricing of services with respect to the invested capital.

Table 7.1 compares the proposed EVPL design model in this work with previous studies in the literature. The table indicates how the proposed model has contributed to the existing studies. As reported in the table, in the proposed model, various new features are included and integrated.

Table 7.1: Comparison of the Proposed EVPL Design Model with Prior Studies in Literature.

Model Features / Reference	[89]–[93]	[95]–[107]	Proposed
Provision of V2G services to the grid		✓	✓
Independent of DN and Transportation Requirements			✓
Optimal Ratio of BD to UD Chargers			✓
Decoupled Financial Models for Various Services			✓
Objective Customization			✓

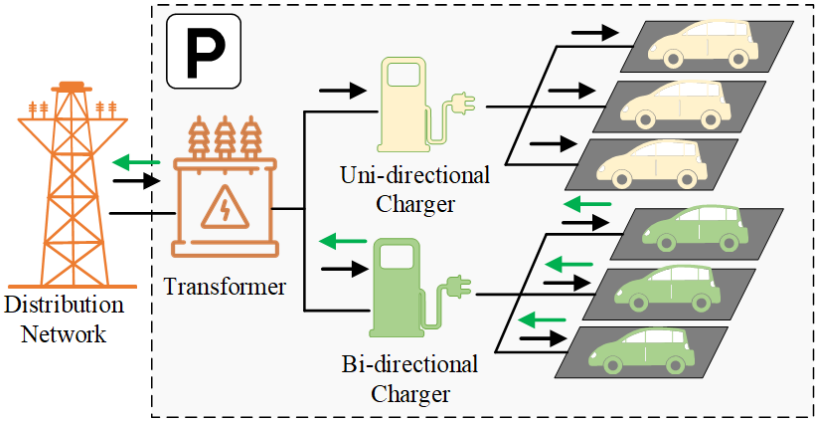

Fig. 7.1. Overview of Electric Vehicle Parking Lot Structure.

7.2 Problem Hypothesis and Specification

Fig. 7.1 depicts a schematic diagram of the proposed EVPL charging system. As shown in the figure, the EVPL is connected to the DN through a transformer. EVs in the EVPL can be charged by either UD or BD chargers. The installation of BD chargers increases the CAPEX incurred by the investors due to its relatively high costs. However, it can also provide an opportunity to reduce the OPEX of the EVPL or generate profit through the provision of V2G services. In this case, the EVPL owner would receive benefits from the

grid operator for the energy discharged by the EVs plugged in in the EVPL. Further, EVs discharging their power during peak times to charge other EVs at the EVPL could help reduce the transformer size, which in turn decreases the required CAPEX to construct the EVPL. Appropriate agreements between the EV users and EVPL owners are put in place for the purpose of vehicle registration, metering, utilization, and payments. EVPL owners have to offer an appropriate incentive model/mechanism to encourage EV users to participate in V2G provision while meeting the target benefits/costs ratio. In this work, the participation of EVs in the provision of V2G services depends mainly on the amount of incentive offered.

Without loss of generality, it is assumed in this work that two V2G programs are offered to EVPL owners:

1. *V2G Program:* this program encourages EV owners to discharge during peak times to reduce peak load. The EVPL owner receives benefits from the grid operator for any V2G discharging and uses a part of this proceeding to pay the EV users a V2G incentive.

2. *V2G Program + V2GAP:* DN operator introduces a V2G availability program (V2GAP) to defer/avoid assets upgrade at certain identified locations. DN operators offer an appropriate incentive model/mechanism to encourage EV users to participate in the V2GAP. The capacity availability of each EVPL depends on the capacity of installed BD chargers. EVPL owners will be incentivized for both the availability and V2G services utilization, and EV users receive specific payment from EVPL owners due to V2GAP service provision.

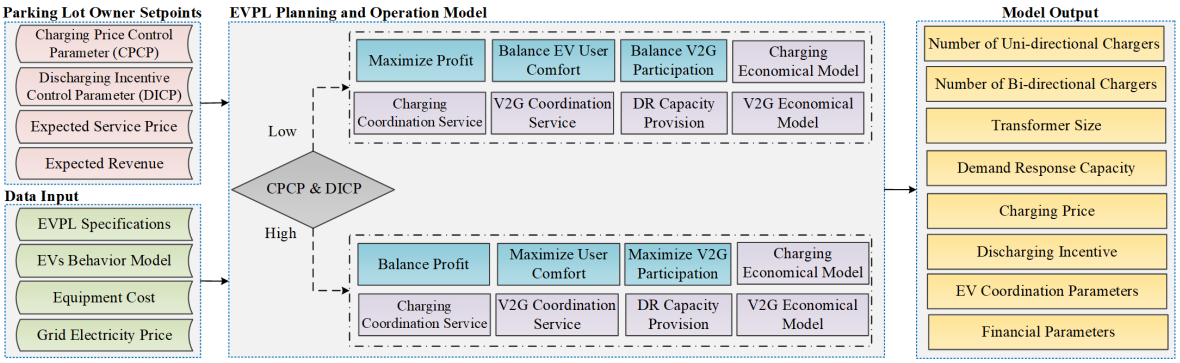

Fig. 7.2. Details of the EVPL design approach.

7.3 Proposed Model

Fig. 7.2 shows a detailed view of the proposed optimal EVPL design approach. As depicted in the figure, the model receives input data including: (i) owner setpoints that control the objective of the model, (ii) EVPL specifications, e.g., the number of parking spots, (iii) the EV charging behavior model including the expected time of arrival and departure, requested charging energy, and battery capacity, as well as how EV owners respond to charging price and V2G incentive, and (iv) grid electricity prices. The proposed model could run in two modes including:

- *Profit maximization*: maximizes the profit of the EVPL owner.
- *Social responsibility*: maximizes utilization of EV charging service and participation in V2G programs.

The model switches between the aforementioned modes depending on the value of charging price control parameter (CPCP) and V2G discharging incentive control parameter (DICP). These parameters are used to penalize the slack variables that control the charging price and V2G incentive paid to EV users to either maximize the benefits from

the EVPL services (i.e., prioritize generating the highest revenue), or allow them to change freely within the predefined limits (i.e., maximize utilization of EV charging services and participation in V2G programs). In this regard, the model assumes that when the charging price decreases, EV users increase their charging demand. Further, almost all EV users are willing to participate in V2G programs if sufficient financial incentives are provided, and their participation increases to a certain degree depending on the level of incentives provided. As shown in Fig. 7.2, in the profit maximization mode, the CPCP and DICP quantities are assigned low values, and thus, the revenue of the EVPL owner is maximized, while the user comfort and V2G participation are balanced. This means that the model will try to find the highest charging price and the lowest V2G incentive while minimizing the CAPEX and OPEX of the system. In the social responsibility mode, the operating profit is balanced, while the EV user comfort and V2G participation are maximized. This translates into finding the minimum charging price and highest V2G incentive that maximize the EV charging demand and V2G participation while satisfying the minimum target revenue of the owner. In this context, it is worth noting that the social responsibility mode could also be utilized by public EVPL and/or commercial entities that do not aim for a profit. In both modes, the technical and economical aspects of EV charging and discharging in the EVPL are coordinated through smart charging/discharging control and minimum target revenue constraints. Th objectives in these two modes are achieved through finding the optimal decision variables including: (i) sitting and sizing of UD chargers, (ii) sitting and sizing of BD chargers, (iii) transformer size, (iv) EV battery state of charge (SoC) and charging/discharging power of each EV in the EVPL for every time step in the planning horizon, (v) EV charging prices, (vi) V2G incentives, and (vii) the reserve power

capacity of the demand response (DR) service provision to the grid. The mathematical formulation of the above-described model is given hereunder.

7.3.1 Objective Function

Table 7.2 presents the nomenclature of the proposed approach.

Table 7.2: Chapter 7 Nomenclature

Indices

c	Indices for parking spots.
h, s	Indices for time steps and scenarios.

Sets

$\mathcal{C}, \mathcal{S}$	Sets of parking spots and scenarios.
$\boldsymbol{\mathcal{T}}$	Set of planning optimization time steps.

Parameters

α	Parking spot occupancy.
η^{Chg}	EV charging efficiency (%).
η^{Dhg}	EV discharging efficiency (%).
ρ^{CPCP}	Control parameter for EV charging price.
ρ^{DICP}	Control parameter for EV V2G incentive.
ϕ_s	Probability of scenario s .
B^{EV}	EV battery capacity (kWh).
C^{Tx}	Transformer cost ($/kVA).
C^{BD}	EV bi-directional (BD) charger cost ($).
C^{UD}	EV uni-directional (UD) charger cost ($).
C^{Ctl}	EV charging control system cost ($).
C^{Pli}	Parking lot instruction system cost ($).
E^{V2G}	V2G scheme payoff ($/kWh).
E^{Anc}	Demand response (DR) availability price ($/kWh).
E^{Grd}	Distribution network electricity price ($/kWh).
K^{DN}	Distribution network capacity limit (kVA).
LS	Equipment lifespan (years).
N^{PL}	Maximum number of parking spots.
$P^{Chg,max}$	Maximum EV charging power (kW).
$P^{Dhg,max}$	Maximum EV discharging power (kW).
r	Interest rate (%).
t^{Arr}	EVs arrival time.
t^{Dep}	EVs departure time.
SoC^{Arr}	EVs arrival state of charge (SoC) (%).
SoC^{Dep}	EVs departure SoC (%).

Variables

E^{PL}	Parking lot EV charging price ($/kWh).
$E^{Chg,S}$	Slack variable for EV charging price ($/kWh).
E^{Inc}	EV V2G incentive ($/kWh).
$E^{Inc,S}$	Slack variable for EV V2G incentive ($/kWh).
K^{Tx}	Transformer capacity (kVA).
L^{UD}	Placement variable for UD charger.
L^{BD}	Placement variable for BD charger.
$P^{DR,Cap}$	Parking lot DR capacity provision to the grid (kW).
$P^{Chg,EV}$	EV charging power (kW).
$P^{Dhg,EV}$	EV discharging power (kW).
SoC^{EV}	SoC of EV battery (%).

The optimal model is formulated with the following multi-objective function:

$$\text{Max: } \underbrace{\left(M^{Rev} - M^{Inv}\right)}_{\text{f}_1} \underbrace{- \left(\rho^{CPCP} \cdot E_s^{PL,S} + \rho^{DICP} \cdot E_s^{Inc,S}\right)}_{\text{f}_2} \tag{7.1}$$

The first objective in (7.1) is to maximize the difference between the operational revenue (M^{Rev}) and the annualized investment and operation and maintenance cost of the EVPL infrastructure (M^{Inv}). The second objective is to control charging prices and V2G incentives through control parameters (ρ^{CPCP}, ρ^{DICP}) and slack variables ($E^{PL,S}$, $E^{Inc,S}$), which are incorporated into the optimization problem. In the case where the EVPL owner sets the control parameters to high values, the slack variables are penalized to keep them at a minimum value for convergence of the algorithm. On the other hand, low control values allow the charging price and V2G incentive to change freely within the limits of the problem.

The operational revenue is obtained from selling energy to EVs and the grid, as well as providing DR capacity to the grid, while the operational cost, on the other hand, is calculated from the cost of energy bought from the grid and the EVs in the EVPL as:

$$M^{Rev} = \sum_{s\in\mathbb{S}} \sum_{h\in\mathbb{T}} \phi_s \Big(P_{s,h}^{Chg,PL} \cdot E_s^{PL} + P_{s,h}^{Dhg,PL} \cdot E^{V2G} + P_{s,h}^{DR,Cap} \cdot E_{s,h}^{Anc} - P_{s,h}^{Chg,PL} \cdot E_{s,h}^{Grd} - P_{s,h}^{Dhg,PL} \cdot E_s^{Inc} \Big). \tag{7.2}$$

It can be noted from the term $P_{s,h}^{Dhg,PL} \cdot E^{V2G}$ in (7.2) that EV users who participate in a V2G program are compensated with a “Pay As You Go" scheme. The value of ϕ_s represents the probability of the each scenario s according to the utilized probability distribution model . The total annualized investment along with the operation and

maintenance costs are represented by (7.3). This includes the costs related to the acquisition, installation, operation, and maintenance of the transformer as well as the BD and UD chargers.

$$M^{Inv} = (1 + C^{O\&M}) \cdot AF^{Chg} \cdot \sum_{c \in \mathbb{C}} \Big(L_c^{UD} \cdot C^{UD} + L_c^{BD} \cdot C^{BD} \Big) + (1 + C^{O\&M}) \cdot AF^{Tx} \cdot K^{Tx} \cdot C^{Tx}, \tag{7.3}$$

where the annuity factor AF is expressed by the following:

$$AF = \frac{r \cdot (1 + r)^{LS}}{(1 + r)^{LS} + 1}. \tag{7.4}$$

7.3.2 EVPL Charging and Discharging Power Constraints

The objective functions in (7.1) are subject to the following parking spots connection to chargers constraints:

$$0 \leq \Big(L_c^{UD} + L_c^{BD} \Big) \leq 1 \quad \forall c \in \mathbb{C}, \tag{7.5}$$

$$0 \leq \sum_{c \in \mathbb{C}} \Big(L_c^{UD} + L_c^{BD} \Big) \leq N^{PL}, \tag{7.6}$$

where (7.5) denotes that a parking spot can be connected to either a UD or BD charger, while (7.6) indicates that the total number of chargers is limited to the maximum number of spots in the EVPL. The charging and discharging power constraints of the parking spot connections to the chargers are represented by the following:

$$0 \leq P_{s,h,c}^{Chg,EV} \leq P^{Chg,max}, \ \ \forall s \in \mathbb{S} \wedge \ h \in \mathbb{T} \wedge c \in \mathbb{C}, \tag{7.7}$$

$$0 \leq P_{s,h,c}^{Dhg,EV} \leq P^{Dhg,max}, \ \ \forall s \in \mathbb{S} \wedge \ h \in \mathbb{T} \wedge c \in \mathbb{C}, \tag{7.8}$$

$$0 \leq \sum_{c}^{c+cm} P_{s,h,c}^{Chg,EV} \leq \sum_{c}^{c+cm} P^{Chg,max} \cdot (L_c^{UD} + L_c^{BD}), \ \ \forall s \in \mathbb{S} \wedge \ h \in \mathbb{T} \wedge c \in \mathbb{C}^*, \tag{7.9}$$

$$0 \leq \sum_{c}^{c+cm} P_{s,h,c}^{Dhg,EV} \leq \sum_{c}^{c+cm} P^{Dhg,max} \cdot L_c^{BD}, \ \ \forall s \in \mathbb{S} \wedge \ h \in \mathbb{T} \wedge c \in \mathbb{C}^*, \tag{7.10}$$

$$P_{s,h,c}^{Chg,EV} \cdot P_{s,h,c}^{Dhg,EV} = 0, \quad \forall s \in \mathbb{S} \wedge \ h \in \mathbb{T} \wedge c \in \mathbb{C}, \tag{7.11}$$

$$P_{s,h,c}^{Chg,EV} \cdot (1 - \alpha_{s,h,c}) = 0, \quad \forall s \in \mathbb{S} \wedge \ h \in \mathbb{T} \wedge c \in \mathbb{C}, \tag{7.12}$$

$$P_{s,h,c}^{Dhg,EV} \cdot (1 - \alpha_{s,h,c}) = 0, \quad \forall s \in \mathbb{S} \wedge \ h \in \mathbb{T} \wedge c \in \mathbb{C}, \tag{7.13}$$

where (7.7) and (7.8) represent the charging and discharging power limits of EV chargers in the EVPL, respectively. Equations (7.9) and (7.10) indicate that each charger can supply power to a maximum of cm EVs in the parking spots. The $\mathbb{C}^*$ in (7.9) and (7.10) represents a set of parking spots grouped based on the value of cm, with $\mathbb{C}^* = \{1, 1 + cm, 1 + 2 \cdot cm, ..., N^{PL}\}$. The constraint in (7.11) prevents simultaneous charging and discharging for the same parking spot, while (7.12) and (7.13) respectively force the charging and discharging power of the parking spot to zero if it is not occupied by an EV, where the parking spot occupancy parameter $\alpha_{s,h,c} = 1$ indicates that the spot is occupied.

The EVPL power demand P^{PL} at the PCC with the grid is formulated as follows:

$$P_{s,h}^{PL} = \sum_{c \in \mathbb{C}} P_{s,h,c}^{Chg,EV} - \sum_{c \in \mathbb{C}} P_{s,h,c}^{Dhg,EV}, \ \ \forall s \in \mathbb{S} \wedge \ h \in \mathbb{T} \wedge c \in \mathbb{C}, \tag{7.14}$$

$$0 \leq P_{s,h}^{PL} \leq K^{Tx} \quad \forall s \in \mathbb{S} \wedge \ h \in \mathbb{T}, \tag{7.15}$$

where (7.14) indicates that the EVPL power represents the total charging and discharging power of all parking spots, which is restricted to the rated capacity of the EVPL transformer as given by (7.15). It is worth noting that (7.15) also indicates that EV discharging in EVPL is limited to reducing the EVPL power consumption without discharging power into the grid.

The rated power of the transformer is a variable that is limited by the electric DN capacity at the node where the transformer is connected as follows:

$$0 \leq K^{Tx} \leq K^{DN} \tag{7.16}$$

7.3.3 EV Charging and Discharging Coordination

The EV battery charging and discharging powers are coordinated using the control mechanism represented by the following:

$$SoC^{EV}_{s,h,c} = SoC^{Arr}_{s,c}, \quad \forall s \in \mathbb{S} \ \wedge \ \ h = t^{Arr}_{s,c}, \tag{7.17}$$

$$SoC^{EV}_{s,h,c} = SoC^{End}_{s,c}, \forall s \in \mathbb{S} \wedge \quad h = t^{Dep}_{s,c}, \tag{7.18}$$

$$SoC^{EV}_{s,h,c} = \Big(\frac{\eta^{Chg} \cdot P^{Chg,EV}_{s,h,c}}{B_c} - \frac{P^{Dhg,EV}_{s,h,c}/\eta^{Dhg}}{B_c}\Big) \cdot \Delta t + \ SoC^{EV}_{s,h-1,c}, \quad \forall s \in \mathbb{S} \ \wedge \ \ t^{Arr}_{s,c} < h \leq t^{Dep}_{s,c}, \tag{7.19}$$

where (7.17) and (7.18) set the SoC of the battery to the arrival and requested departure SoC, respectively. It is noted that the requested departure SoC varies according to the charging price as indicated by (7.21). The battery SoC balance is represented by (7.19) taking into consideration the charging and discharging operations. The battery SoC

control mechanism in (7.17)-(7.19) shows that charging and discharging are coordinated to ensure that the target departure SoC is satisfied without any specific pattern. The charging/discharging patterns are dependent on the objective function. For instance, an objective function that tries to minimize the cost would shift the charging to lower grid price periods. The EVs battery is subject to the following constraints:

$$SoC^{EV}_{min,c} \leq SoC^{EV}_{s,h,c} \leq SoC^{EV}_{max,c} \;\; \forall s \in \mathbb{S} \;\; \wedge \;\; t^{Arr}_{s,c} < h \leq t^{Dep}_{s,c}, \wedge \forall c \in \mathbb{C}, \tag{7.20}$$

where (7.20) defines the operational limits of the battery SoC required to maintain its expected lifetime.

7.3.4 EVPL Charging and Discharging Economic Model

The economics of the EVPL depends mainly on two variables namely: (i) the charging price paid by the EV users to charge their batteries, and (ii) the V2G incentive given to EV users for providing V2G services. The charging price impacts the energy demand for EVs in the EVPL as follows:

$$SoC^{End}_{s,c} = SoC^{Dep}_{s,c} - \left(SoC^{Dep}_{s,c} - SoC^{Arr}_{s,c}\right) \cdot (1 - \frac{(E^{PL,max} - E^{PL}_{s})}{(E^{PL,max} - E^{PL,min}))}, \;\; \forall s \in \mathbb{S}. \tag{7.21}$$

As indicated by the linear price-demand model [168], [169], in (7.21), the lower the charging price is, the higher the charging demand by EV users would be. The EVPL

charging price is set by the following:

$$E_s^{PL} = E^{PL,min} + E_s^{PL,S}, \quad \forall s \in \mathbb{S}, \tag{7.22}$$

$$0 \leq E_s^{PL,S} \leq (E^{PL,max} - E^{PL,min}), \quad \forall s \in \mathbb{S}. \tag{7.23}$$

where (7.22) denotes that the charging price is controlled by the slack variable $E_s^{PL,S}$, which is penalized in the objective function through the CPCP parameter. A high control parameter value would force the charging price to a minimum, while a low control parameter value allows the price to change within the limit imposed on its slack variable as given by (7.23).

The changes in the charging price must satisfy the profitability constraint which sets a minimum target revenue as given by the following:

$$R^{Chg} \leq \sum_{s \in \mathbb{S}} \sum_{h \in \mathbb{T}} P_{s,h}^{Chg,PL} \cdot E_s^{PL} - P_{s,h}^{Chg,PL} \cdot E_{s,h}^{Grd}, \tag{7.24}$$

$$R^{Chg} = \beta_1 \cdot \sum_{c \in \mathbb{C}} \Big((L_c^{UD} + L_c^{BD}) \cdot C^{UD} \Big) + C^{Ctl} + C^{Pli} + K^{Tx} \cdot C^{Tx}. \tag{7.25}$$

The constraint in (7.24) adjusts the charging price to ensure that the revenue from charging operations in the EVPL meets a percentage β_1 of the minimum target revenue represented by (7.25). Depending on the project risk profile, an investor could set the target profitability of the charging operation, i.e., the return on investment considering the NPV of the CAPEX required to construct the charging infrastructure. This allows optimal pricing of charging service with respect to the invested capital. The charging infrastructure CAPEX includes the cost of EV chargers, charging control hardware and software, the EVPL instruction system required to route EVs to the designated parking

spot, and the transformer connected to the grid.

The V2G incentive is set as follows:

$$E_s^{Inc} = E^{Inc,max} - E_s^{Inc,S}, \quad \forall s \in \mathbb{S}, \tag{7.26}$$

$$0 \leq E_s^{Inc,S} \leq (E^{Inc,max} - E^{Inc,min}), \quad \forall s \in \mathbb{S}. \tag{7.27}$$

The slack variable $E_s^{Inc,S}$ controls the V2G incentive as expressed by (7.26) and (7.27). Therefore, a high control parameter value on the slack variable $E_s^{Inc,S}$ variable forces the incentive to higher values, which would increase the participation of EV users in the V2G programs as given by the following:

$$\sum_{c \in \mathbb{C}} (L_c^{BD}) \leq \lambda^{V2G}(E_s^{Inc}) \cdot N^{PL}, \tag{7.28}$$

where $\lambda^{V2G}(E_s^{Inc})$ represents the percentage of EV users willing to participate in V2G programs as a function of V2G incentive. The V2G participation restricts the number of BD chargers installed in the EVPL as expressed by (7.28). The minimum target revenue for V2G services is represented by the following:

$$R^{Dhg} \leq \sum_{s \in \mathbb{S}} \sum_{h \in \mathbb{T}} P_{s,h}^{DR,Cap} \cdot E_{s,h}^{Anc} + P_{s,h}^{Dhg,PL} \cdot E^{V2G} - P_{s,h}^{Dhg,PL} \cdot E_s^{Inc}, \tag{7.29}$$

$$R^{Dhg} = \beta_2 \cdot \sum_{c \in \mathbb{C}} L_c^{BD} \cdot (C^{BD} - C^{UD}), \tag{7.30}$$

where the EV V2G incentive is adjusted by the revenue model in (7.29) and (7.30). The parameter β_2 in (7.30) represents the percentage of the minimum target revenue from V2G operations that the EVPL must meet. It is noted from (7.25) and (7.30) that the

cost of a BD charger is divided into two parts. The first part is equal to the cost of a UD charger and it should be covered by the charging services revenue. The second part represents the marginal increase compared to a UD charger which is covered by V2G services revenue.

7.3.5 EVPL V2GAP Program Constraints

The EVPL provision of capacity-based DR services to the grid through the V2GAP program is determined by the design model as per the following:

$$0 \leq P^{DR,Cap} \leq \sum_{c \in \mathbb{C}} L_c^{BD} \cdot P_{max}^{Dhg,EV}, \tag{7.31}$$

where (7.31) restricts the DR capacity to the power capacity of BD chargers installed in the EVPL. In this regard, it is assumed that since a smart charging control scheme is applied by the EVPL as indicated by (7.17)-(7.19), the only way for EVPL to reduce its power consumption from the grid is to use the V2G services by the plugged-in EVs located in the EVPL.

7.3.6 EV Behavior Uncertainty Characterization

The uncertainty in the EV users charging demand stems mainly from five random parameters including: (i) time of arrival, (ii) time of departure, (iii) SoC at arrival, (iv) SoC at departure, and (v) EV battery capacities. According to [94], [100], and [170], the randomness in these parameters can be handled using a probabilistic approach with predetermined probability density functions (PDFs). In this work, truncated Gaussian

distribution functions are employed to estimate the charging behavior parameters of each EV user as follows:

$$SoC_{s,c}^{Arr} = f\left(x, \mu_{soc,arr}, \sigma_{soc,arr}^2, \left(\mathrm{soc}^{arr,\min}, \mathrm{soc}^{arr,\max}\right)\right) \tag{7.32}$$

$$SoC_{s,c}^{Dep} = f\left(x, \mu_{soc,dep}, \sigma_{soc,dep}^2, \left(\mathrm{soc}^{dep,\min}, \mathrm{soc}^{dep,\max}\right)\right) \tag{7.33}$$

$$t_{s,c}^{Arr} = f\left(x, \mu_{t,arr}, \sigma_{t,arr}^2, \left(t^{arr,\min}, t^{arr,\max}\right)\right) \tag{7.34}$$

$$t_{s,c}^{Dep} = f\left(x, \mu_{t,dep}, \sigma_{t,dep}^2, \left(\mathrm{Max}\left\{t^{dep,\min}, t^{arr}\right\}, t^{dep,\max}\right)\right) \tag{7.35}$$

$$B_{s,c} = f\left(x, \mu_B, \sigma_B^2, \left(\mathrm{B}^{\min}, \mathrm{B}^{\max}\right)\right) \tag{7.36}$$

In order to ensure that the requested energy by each EV is possible to be satisfied by the chargers in the parking lot, the following constraint is applied:

$$B_{s,c} \cdot \left(\frac{SoC_{s,c}^{Dep} - SoC_{s,c}^{Arr}}{t_{s,c}^{Dep} - t_{s,c}^{Arr}}\right) \leq P^{Chg,max} \tag{7.37}$$

7.4 Case Studies

7.4.1 Model Configuration

Case studies are conducted in this section to test the effectiveness of the proposed model. The case studies are carried out on an EVPL with a capacity of 250 EVs. The probability distribution of the EV behavior parameters is extracted from [94], [97]. Since the EVPL is assumed to be located in a workplace and/or commercial areas, the simulations are

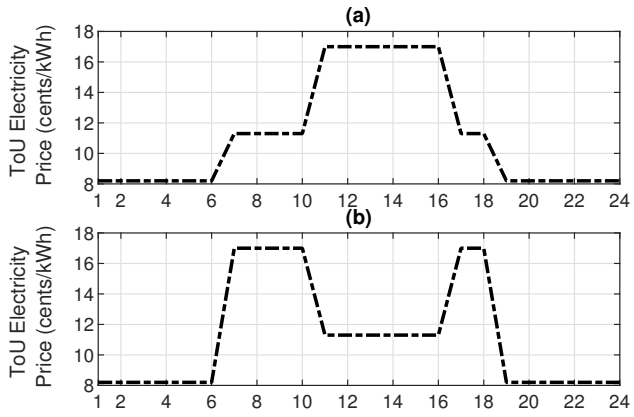

Fig. 7.3. ToU prices in Ontario; (a): summer rates and (b): winter rates.

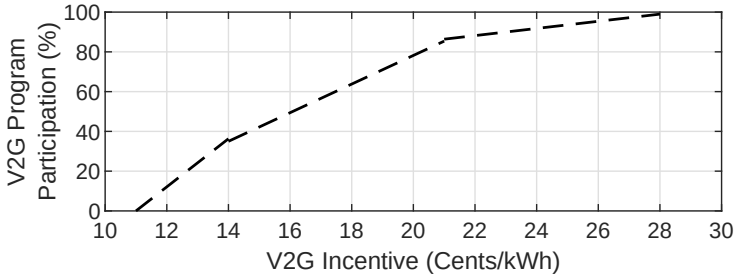

Fig. 7.4. V2G incentive-based participation model.

performed for weekdays only with one sample summer weekday and a sample winter weekday. The maximum number of EVs to be connected to a charger is set at $cm = 4$ [171].

The historical Ontario electricity market rates are used to construct the electricity rate profiles for case studies [118]. It is assumed that the EVPL purchases electricity from the grid at the hourly energy wholesale prices, and sells it to EVs at an average price that is lower than or equal to the average residential ToU rates. The Ontario time-of-use (ToU) rates for summer and winter seasons are shown in Fig. 7.3 [118]. Similarly, the V2G payments by the utility operator to the EVPL owner are set at 1.5 times the ToU peak rates to allow an effective V2G operation [94].

The percentage of EV users willing to participate in V2G programs is represented by the following:

$$\lambda^{V2G} = \begin{Bmatrix} \zeta_1 \left(E^{Inc} - \gamma_1\right), & \gamma_1 \leq E^{Inc} \leq \gamma_2 \\ \zeta_2 \left(E^{Inc} - \gamma_2\right) + \lambda_1, & \gamma_2 \leq E^{Inc} \leq \gamma_3 \\ \zeta_3 \left(E^{Inc} - \gamma_3\right) + \lambda_2, & \gamma_3 \leq E^{Inc} \leq \gamma_4 \end{Bmatrix}, \tag{7.38}$$

where (7.38) is a piecewise function that represents the V2G incentive-based participation assuming a contribution of 10 kWh per a working day. Through curve fitting analysis, the parameters in (7.38) are found to be as follows: $\gamma_1 = 0.11$, $\gamma_2 = 0.14$, $\gamma_3 = 0.21$, $\gamma_4 = 0.28$, $\zeta_1 = 12.1$, $\zeta_2 = 7.2$, $\zeta_3 = 1.8$, $\lambda_1 = 0.35$, $\lambda_1 = 0.88$. The V2G incentive-based participation model is plotted in Fig. 7.4. The remainder of the parameters are listed in Table 7.3.

Table 7.3: Modeling and Simulation Parameters.

$\beta_1 =$ 140%	$\beta_2 =$ 140%
$\eta^{Dhg} =$ 90%	$\eta^{Chg} =$ 90%
$SoC^{EV}_{min} = 20\%$	$SoC^{EV}_{max} = 90\%$
$\Delta t =$ 1 hour	$C^{Tx} = 10$ \$/kVA
$C^{UD} =$ \$3600	$C^{BD} =$ \$9000
$C^{O\&M} = 5\%$	$r = 2.5\%$
$LS^{Chg} = 12$ years	$LS^{Tx} = 25$ years
$E^{PL}_{min} =$ 0 ¢/kWh	$E^{PL}_{max} =$ 14.1 ¢/kWh
$E^{Inc}_{min} =$ 11 ¢/kWh	$E^{Inc}_{max} =$ 26 ¢/kWh
$E^{V2G} =$ 26 ¢/kWh	$E^{DR} =$ 0.03 ¢/kWh
$K^{Inc}_{DN} =$ 1500 kVA	$K^{Inc}_{DN} =$ 1500 kVA

The chargers' costs are obtained from [166] and [171], where they include the cost of acquisition, installation, smart meters, and wire connections to parking spots and the transformer. Based on [95] and [100], Level 2 chargers with a rated power of 11.5 kW are considered. The model is built in the MATLAB environment and solved using the

Gurobi Optimization Toolbox. The proposed model is simulated for six cases as listed in Table 7.4.

Table 7.4: Case Studies Specifications

Cases	Case 1	Case 2	Case 3	Case 4	Case 5	Case 6
Charging Service	Yes	Yes	Yes	Yes	Yes	Yes
V2G Program	No	No	Yes	Yes	Yes	Yes
V2GAP Program	No	No	No	No	Yes	Yes
Profit Maximization Mode	Yes	No	Yes	No	Yes	No
Social Responsibility Mode	No	Yes	No	Yes	No	Yes

7.4.2 Results

Fig. 7.5 shows the simulation results for EVPL charging and discharging power profile considering a typical summer weekday. Fig. 7.5 (a) illustrates the grid hourly electricity price profile for a summer weekday, while Figs. 7.5 (b) and (c) show the EVPL charging and discharging power profiles, respectively. It is noted from Fig. 7.5 (a) that peak demand occurs between Hours 12 and 20 with a peak at Hour 19 and a second peak at Hour 13. Therefore, the proposed model coordinates the EV charging power for all cases to be reduced during these projected peak rates and shifted to lower price periods as can be noted from 7.5 (b). Because of this shift in the EVPL charging power, the discharging by EVs for cases 3 to 6 are coordinated to be mainly during the periods when there is a peak in charging power as shown in Fig. 7.5. This can help reduce the total EVPL power at the PCC, which reduces the operating costs and the transformer size. It is also worth noting from Figs. 7.5 (b) and (c) that in cases where the EVPL design model is simulated for the social responsibility maximization (i.e., Cases 2, 4,

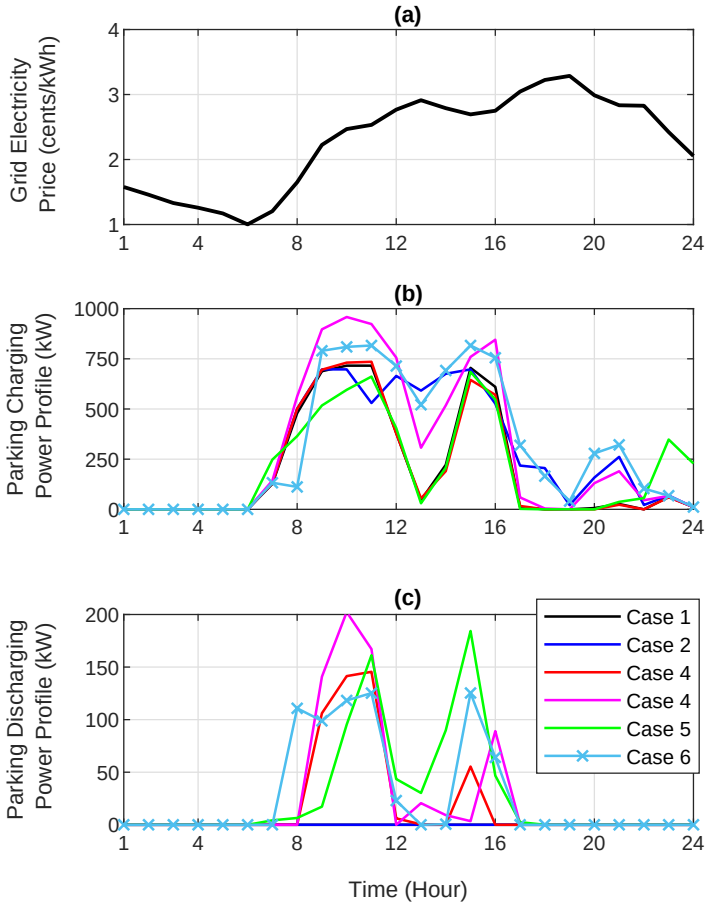

Fig. 7.5. Simulation results for Cases 1-6 considering EVPL charging and discharging power in a typical *summer* weekday, (a) Grid electricity price, (b) Parking *charging* power profile, and (c) Parking *discharging* power profile.

and 6) the EV charging demand and V2G discharging are increased in comparison to the profit maximization mode. Similar trends can be seen in the results for the EVPL charging and discharging power considering a typical winter weekday. For example, the EVPL is operated to shift the charging power from peak price periods (Hours 9 to 11 and 19 to 21), towards lower price rates (Hours 12 to 18) as can be seen in Fig. 7.6 (b).

Table 7.5 lists the output parameters of the optimization model for the case studies considered. It can be observed that charging prices are higher and V2G incentives

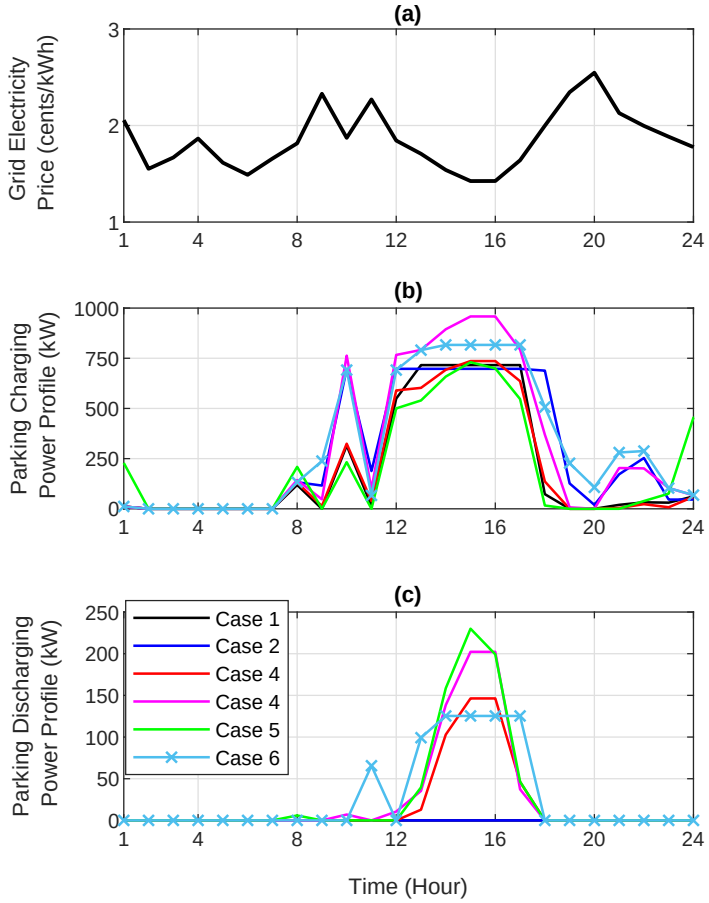

Fig. 7.6. Simulation results for Cases 1-6 considering EVPL charging and discharging power in a typical *winter* weekday, (a) Grid electricity price, (b) Parking *charging* power profile, and (c) Parking *discharging* power profile.

provided to EV users are lower for cases that operate in the profit maximization mode. This, would in turn, result in a lower charging demand and V2G participation, which is reflected in the lower number of UD and BD chargers installed in the EVPL. On the other hand, when the EVPL is operated for social responsibility maximization, the EV charging prices are lowered and the V2G incentives are increased, which results in higher charging demand and V2G participation. Therefore, the model suggests increasing the number of UD and BD chargers. It is also noted that the number of BD chargers for

Table 7.5: EVPL Parameters under Various Case Studies.

Cases	Case 1	Case 2	Case 3	Case 4	Case 5	Case 6
Charging Price (Cents/kWh)	10.26	5.69	11.66	6.19	11.66	5.57
V2G Incentive (Cents/kWh)	N/A	N/A	14.35	16.24	16.78	16.78
Number of UD Chargers	63	66	51	65	41	50
Number of BD Chargers	N/A	N/A	13	19	22	21
Demand Response Capacity (kW)	N/A	N/A	N/A	N/A	253	242
Transformer Capacity (kW)	900	900	750	950	750	900

Cases 5 and 6 is the highest because of the provision of DR capacity to the grid. Table 7.5 also indicates that the provision of V2G services reduces the size of the transformer when operated for profit maximization.

7.4.3 Financial Analysis

Table 7.6 lists the annualized revenue and costs for investment and charging and V2G services for Cases 1-6. It can be noted from Table 7.6 that the V2G service significantly increases the net revenue of the EVPL for both modes of operations. It can also be observed that Case 5 has the highest annual net revenue due to participation in the V2G service with the provision of DR service to the grid. It is worth noting that the net revenue represents the EVPL profit after taking into consideration all costs, including CAPEX and OPEX.

To further analyze the economic viability of the EVPL project, several financial parameters are calculated and shown in Fig. 7.7. The figure includes the following quantities:

1. NPV in Fig. 7.7 (a) which is the difference between the present and future

Table 7.6: Annualized Revenue and Cost Parameters in Thousands $ for Different Cases

Cases	Charging Services		V2G Services		Investment		
	Cost	Revenue	Cost	Revenue	CAPEX	O&M	Net Revenue
Case 1	22.98	126.70	0.00	0.00	28.00	12.60	61.03
Case 2	38.22	95.31	0.00	0.00	31.63	14.05	17.08
Case 3	26.28	143.60	18.06	34.46	34.70	15.28	82.49
Case 4	42.20	101.30	19.81	33.38	40.53	17.61	26.22
Case 5	27.16	148.07	24.79	45.30	36.97	16.19	87.69
Case 6	44.48	103.58	34.51	56.06	45.09	19.44	23.77

discounted cash inflows throughout the years,

2. the internal rate of return (IRR) in Fig. 7.7 (b) which is the percentage of profit from the EVPL throughout its lifetime,

3. the payback time in Fig. 7.7 (c) which is the time required for the discounted cash inflow to match the initial capital costs,

4. the profitability in Fig. 7.7 (d) which represents the EVPL profitability considering an expected return of investment set to 8% for the results in this figure. The profitability is calculated as follows:

$$\text{Profitability} = \frac{\text{Annualized Present Value of Future Cash Flows}}{\text{Initial Investment} \cdot \text{Profit Target} + \dfrac{\text{Initial Investment}}{\text{Project Lifetime}}} \times 100 \tag{7.39}$$

From Fig. 7.7, it can be concluded that while the profit maximization mode results

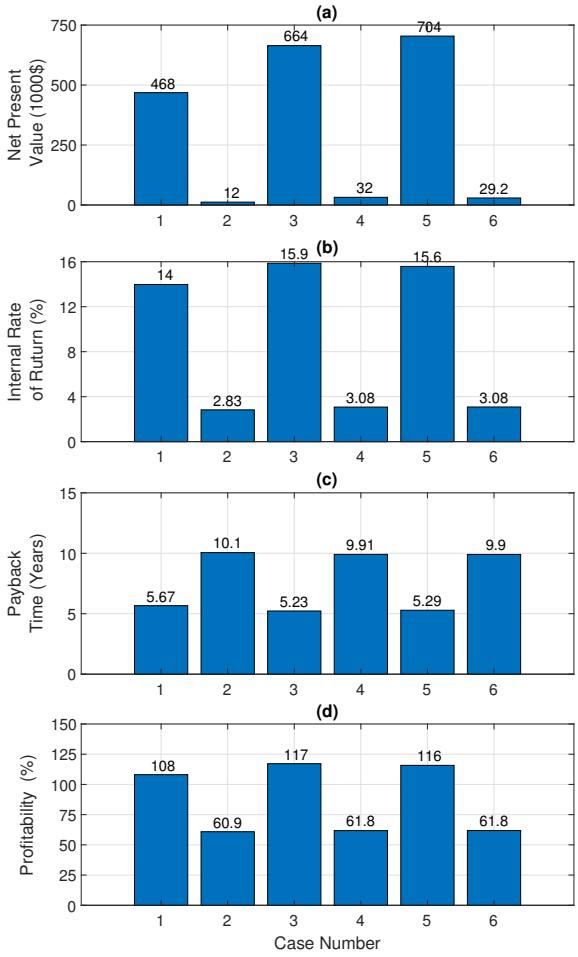

Fig. 7.7. Annual financial parameters of EVPL project for different case studies

in very promising financial parameters, the social responsibility mode is very modest economically.For instance, the NPV for Case 4 is only $32,000, while the payback time is 9.91 years which is very close to the EVPL lifetime set at 12 years. This observation is more clear through the obtained profitability parameters for Cases 2, 4, and 6 which averages around 60%. It is worth noting that the average of profitability values for the presented cases is used for illustration purposes. Taking the average of profitability for the profit maximization and social responsibility maximization modes results in a value

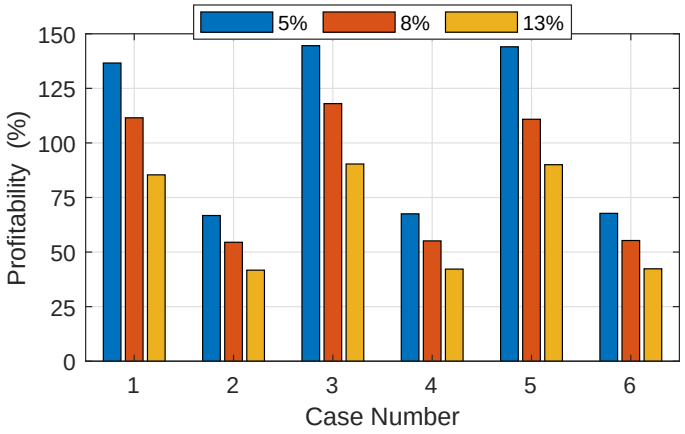

Fig. 7.8. Profitability of the EVPL project considering different targeted profit.

of around 90%. This means that for a profitability target of 8%, the EVPL project might not be profitable unless all the technical and financial projections of the project are assumed to be accurate. This is further confirmed by the results in Fig 7.8, which shows the profitability of the EVPL project considering different target values. From the figure, it is clear that only a 5% target results in a profitable project; however, this target is very low for such a risky project. Therefore, the profitability of such a project would remain below the target value without incentives from the government, different electricity rates, or other sources of revenue. Further investigation and proposals for incentivizing the EVPLs are needed which is considered by the authors as future research.

7.4.4 Discussion and Summary

This research proposes an optimal design model for an EVPL that can provide charging services to EVs and V2G services to the grid. The model realizes a multi-objective design scheme for the maximization of the EVPL owner profit or EV user comfort using a settable parameter and allows the design of an EVPL with the optimal combination of UD

and BD chargers. Historical operating quantities are utilized to verify the feasibility and efficacy of the model, and the results are analyzed. The results show that the proposed model is effective in achieving the design targets as well as the charging/discharging management requirements for the two modes of operations set by the EVPL operator. The V2G services, particularly with the provision of DR services to the grid, significantly add to the net revenue of the EVPL for both modes of operations. Advanced financial analysis shows that the best profitability target that can be achieved for the EVPL project is 5%. It is, therefore, concluded from the numerical studies that the EVPL project profitability can be enhanced through incentives from the government, use of higher electricity rates, or other sources of revenue due to higher CAPEX. Further, as new technology materializes, it is expected that the equipment degradation decreases, thereby enhancing the financial metrics of such EVPL projects. Further studies on the topic would include investigation and development of new models for incentivizing the EVPLs to further promote deployment of such EV charging stations.

Chapter 8 - Conclusions and Future Work

8.1 Summary and Conclusions

The research in this thesis presents a number of approaches that aim to enhance the adoption of EVs and their integration into the power grid. In particular, the thesis focuses on the development of adaptive systems that enhance the management of EV energy (Chapter 3, 4, and 5), and the development of charging strategies and design models that help to expand the proliferation of EV charging infrastructure (Chapter 6 and 7).

Chapter 3 develops a model for a central controller in a fleet system that allows adaptive utilization of EV batteries distributed energy for concurrent services to the transportation sector and ancillary services market. The optimization model incorporates various slack variables and control parameters for managing real–time fare prices, adaptive energy and reserve margin allocation, spotting EV locations, interaction with the grid operator, and meeting the fleet target revenue. The model allows EV drivers to flexibly manage their battery capacities based on their availability and assessment of the transportation services demand when needed. The numerical results for various cases including no contribution, low contribution, and high contribution levels to the ancillary services market are presented. The results demonstrate how distributed energy stored in several EV batteries within the fleet can be used as a whole to support the

grid without negative impacts on the regular trip schedule. The effectiveness of the proposed algorithm in Chapter 3 for creating the reserve margin is evident from the results. The reserve margin is optimally utilized to meet the grid's demand when needed. The success of the proposed dynamic pricing mechanism for real–time calculation of fare rates for achieving daily revenue target in a competitive market is indicated. The results demonstrate that the extra revenue stream from contribution to the ancillary services market on top of the one from regular passenger transport enhances the system profit. It is indicated that the more the EV fleet participates in the ancillary services, the lower the trip prices become, and the more the system profit is enhanced. As such, the proposed model can increase the profitability of an EV fleet management system, thereby promoting investment and success in this area in the near future.

Chapter 4 proposes a novel decentralized system for P2P energy trading between EVs that takes into consideration QoS management and utilizes smart contracts to match and administer the energy trade. SCMP and MCMP mechanisms are proposed to match EC requests and EP offers based on QoS attributes. In these mechanisms, each attribute is assigned a weight value according to a fuzzy-based optimal weight calculation method. Further, a penalty mechanism is developed to discourage dishonest requests/offers and ensure that ECs and EPs stick to their contractual obligations. Numerical simulations are conducted to validate the effectiveness of the proposed mechanisms. The results show that the SCMP mechanism selects the EP offer that provides the best utility to EC with high awareness of EC preferences represented by weight values assigned to QoS attributes. The results also demonstrate that the MCMP mechanism is superior in finding fast near-optimal solutions when matching a high number of ECs and EPs.

Chapter 5 proposes a new bidirectional smart charging algorithm of EVs for P2P

energy trade and ancillary services provision to the grid. The user input is incorporated into the scheduling model using optimization variables and soft constraints. The EV user is able to adjust some of the settings of the scheduling model that would make the model adaptive to various conditions. Optimization slack variables are utilized for optimal management of the battery SOC and energy allocation for multiple service. Real-world data collected from EV owners pertaining to the usage of their EVs are utilized for numerical studies. Through numerical studies, the efficacy and feasibility of the proposed model are evaluated. The results demonstrate how the incorporation of user preferences into the scheduling process can enhance the aggregated revenue generated by the EV scheduling model.

Chapter 6 develops a communication-less control strategy for the EV charging load in droop-controlled IMGs. The proposed strategy controls the rate of EV charging based on both the system frequency and bus voltage, as well as the battery SoC and past charging power allocation. Further, a novel EV load shedding scheme is proposed that gets triggered when an under-voltage or under-frequency event occurs in the IMG. Moreover, a charging fairness system that assigns priority levels to EVs based on their past charging power allocation is developed. Numerical simulations are conducted to validate the effectiveness of the proposed strategy. The results demonstrate the superiority of the proposed control strategy to the state-of-the-art controllers in modulating the EV charging load. The results also show that the charging fairness system implemented in the proposed strategy does not degrade the performance of the EV charging control. During a DG outage scenario, the proposed control strategy successfully curtailed EV loads to prevent further violations and bring back the system operating parameters to the acceptable limits.

Chapter 7 proposes an optimal design and operation model for an EVPL that can provide charging services to EVs and V2G services to the grid. The model realizes a multi-objective design scheme for the maximization of the EVPL owner profit or user comfort using a settable parameter and allows the design of an EVPL with the optimal combination of UD and BD chargers. Historical operating quantities are utilized to verify the feasibility and efficacy of the model, and the results are analyzed. The results show that the proposed model is effective in achieving the design targets as well as the charging/discharging management requirements for the two modes of operations set by the EVPL operator. The V2G services, particularly with the provision of DR services to the grid, significantly add to the net revenue of the EVPL for both modes of operations. Advanced financial analysis shows that the best profitability target that can be achieved for the EVPL project is 5%. It is, therefore, concluded from the numerical studies that the EVPL project profitability can be enhanced through incentives from the government, use of higher electricity rates, or other sources of revenue due to higher CAPEX. Further, as new technology materializes, it is expected that the equipment degradation decreases, thereby enhancing the financial metrics of such EVPL projects. Further studies on the topic would include investigation and development of new models for incentivizing the EVPLs to further promote deployment of such EV charging stations.

8.2 Future Work

The following list outlines some of the research points that can be pursued in the future, based on the proposed algorithms and the findings of this thesis:

- Development of an EV user-based scheduling algorithm that can link up with other EV users profiles to coordinate charging/discharging operation.

- Investigate the co-scheduling of EV fleet charging and trips considering traffic conditions.
- Development of a communication-free and artificial intelligence (AI) based scheme for the control of the EV charging load in islanded/isolated microgrids.
- Development of new economic models for electricity markets that can incentivize investment in EVPLs.

Bibliography

[1] S. M. Bagher Sadati, J. Moshtagh, M. Shafie-khah, A. Rastgou, and J. P. Catalão, "Operational scheduling of a smart distribution system considering electric vehicles parking lot: A bi-level approach," *International Journal of Electrical Power and Energy Systems*, vol. 105, pp. 159–178, 2019, ISSN: 0142-0615.

[2] *Environmental Sustainability Indicators: Greenhouse gas emissions.* English. Environment and Climate Change Canada, 2022. [Online]. Available: www.canada.ca/en/environment-climate-change/services/environmental-indicators/greenhouse-gas-emissions.html..

[3] X. Li and A. Jenn, "An integrated optimization platform for spatial-temporal modeling of electric vehicle charging infrastructure," *Transportation Research Part D: Transport and Environment*, vol. 104, p. 103 177, 2022, ISSN: 1361-9209.

[4] M. Klippenstein, *Subsidy's swansong: Canadian plug-in sales take a dip*, Oct. 2018. [Online]. Available: https://www.greencarreports.com/news/1119269_subsidys-swansong-canadian-plug-in-sales-take-a-dip.

[5] B. Schmidt, *There are now 5.6 million electric cars on the road, up 64 percent from last year*, Feb. 2019. [Online]. Available: https://thedriven.io/2019/02/13/there-are-now-5-6-million-electric-cars-on-the-road-up-64-from-last-year/.

[6] J. Y. Yong, V. K. Ramachandaramurthy, K. M. Tan, and N. Mithulananthan, "A review on the state-of-the-art technologies of electric vehicle, its impacts and prospects," *Renewable and Sustainable Energy Reviews*, vol. 49, pp. 365–385, 2015, ISSN: 1364-0321.

[7] H. A. U. Khan, S. Price, C. Avraam, and Y. Dvorkin, "Inequitable access to ev charging infrastructure," *The Electricity Journal*, vol. 35, no. 3, p. 107 096, 2022, ISSN: 1040-6190.

[8] L. Pieltain Fernández, T. Gomez San Roman, R. Cossent, C. Mateo Domingo, and P. Frías, "Assessment of the impact of plug-in electric vehicles on distribution networks," *IEEE Transactions on Power Systems*, vol. 26, no. 1, pp. 206–213, 2011.

[9] K. Qian, C. Zhou, and Y. Yuan, "Impacts of high penetration level of fully electric vehicles charging loads on the thermal ageing of power transformers," *International Journal of Electrical Power and Energy Systems*, vol. 65, pp. 102–112, 2015, ISSN: 0142-0615.

[10] Z. Moghaddam, I. Ahmad, D. Habibi, and Q. V. Phung, "Smart charging strategy for electric vehicle charging stations," *IEEE Transactions on Transportation Electrification*, vol. 4, no. 1, pp. 76–88, 2018.

[11] J. C. Mukherjee and A. Gupta, "Distributed charge scheduling of plug-in electric vehicles using inter-aggregator collaboration," *IEEE Transactions on Smart Grid*, vol. 8, no. 1, pp. 331–341, Jan. 2017.

[12] A. A. Al-Obaidi and H. E. Z. Farag, "Electric vehicles optimal scheduling for peer-to-peer energy trade and ancillary services provision to the grid," in *2020 IEEE Power & Energy Society General Meeting (PESGM)*, 2020, pp. 1–5.

[13] G. S. Bauer, A. Phadke, J. B. Greenblatt, and D. Rajagopal, "Electrifying urban ridesourcing fleets at no added cost through efficient use of charging infrastructure," *Transp. Res. Part C Emerg. Technol.*, vol. 105, pp. 385–404, 2019, ISSN: 0968-090X.

[14] C. M. Martinez, X. Hu, D. Cao, E. Velenis, B. Gao, and M. Wellers, "Energy management in plug-in hybrid electric vehicles: Recent progress and a connected vehicles perspective," *IEEE Transactions on Vehicular Technology*, vol. 66, no. 6, pp. 4534–4549, 2017.

[15] M. Zeng, S. Leng, Y. Zhang, and J. He, "Qoe-aware power management in vehicle-to-grid networks: A matching-theoretic approach," *IEEE Transactions on Smart Grid*, vol. 9, no. 4, pp. 2468–2477, 2018.

[16] J. Kang, R. Yu, X. Huang, S. Maharjan, Y. Zhang, and E. Hossain, "Enabling localized peer-to-peer electricity trading among plug-in hybrid electric vehicles using consortium blockchains," *IEEE Transactions on Industrial Informatics*, vol. 13, no. 6, pp. 3154–3164, 2017.

[17] M. Fakhari Moghaddam Arani and Y. A.-R. I. Mohamed, "Cooperative control of wind power generator and electric vehicles for microgrid primary frequency regulation," *IEEE Transactions on Smart Grid*, vol. 9, no. 6, pp. 5677–5686, 2018.

[18] P. Kou, D. Liang, R. Gao, Y. Liu, and L. Gao, "Decentralized model predictive control of hybrid distribution transformers for voltage regulation in active distribution networks," *IEEE Transactions on Sustainable Energy*, vol. 11, no. 4, pp. 2189–2200, 2020.

[19] A. Zahedmanesh, D. Sutanto, and K. M. Muttaqi, "Analyzing the impacts of charging plug-in electric vehicles in low voltage distribution networks: A case study of utilization of droop charging control system based on the sae j1772 standard," in *2017 AUPEC*, 2017, pp. 1–6.

[20] Lu Xia, I. Mareels, T. Alpcan, M. Brazil, J. de Hoog, and D. A. Thomas, "A distributed electric vehicle charging management algorithm using only local measurements," in *ISGT 2014*, 2014, pp. 1–5.

[21] R. R. Kumar, A. Chakraborty, and P. Mandal, "Promoting electric vehicle adoption: Who should invest in charging infrastructure?" *Transportation Research Part E: Logistics and Transportation Review*, vol. 149, p. 102 295, 2021, ISSN: 1366-5545.

[22] L. Zhang, Z. Zhao, and Z. Kan, "Private-sector partner selection for public-private partnership projects of electric vehicle charging infrastructure," *Energy Science & Engineering*, vol. 7, no. 5, pp. 1469–1484, 2019. eprint: https://onlinelibrary.wiley.com/doi/pdf/10.1002/ese3.367.

[23] W. Jiang and Y. Zhen, "A real-time ev charging scheduling for parking lots with pv system and energy store system," *IEEE Access*, vol. 7, pp. 86 184–86 193, 2019.

[24] M. Shafie-khah *et al.*, "Optimal behavior of electric vehicle parking lots as demand response aggregation agents," *IEEE Transactions on Smart Grid*, vol. 7, no. 6, pp. 2654–2665, 2016.

[25] R. Rana, S. Prakash, and S. Mishra, "Energy management of electric vehicle integrated home in a time-of-day regime," *IEEE Transactions on Transportation Electrification*, vol. 4, no. 3, pp. 804–816, 2018.

[26] M. Esmaili and A. Goldoust, "Multi-objective optimal charging of plug-in electric vehicles in unbalanced distribution networks," *International Journal of Electrical Power and Energy Systems*, vol. 73, pp. 644–652, 2015, ISSN: 0142-0615.

[27] S. Xu, Z. Yan, D. Feng, and X. Zhao, "Decentralized charging control strategy of the electric vehicle aggregator based on augmented lagrangian method," *International Journal of Electrical Power and Energy Systems*, vol. 104, pp. 673–679, 2019, ISSN: 0142-0615.

[28] Z. Yi *et al.*, "A highly efficient control framework for centralized residential charging coordination of large electric vehicle populations," *International Journal of Electrical Power and Energy Systems*, vol. 117, p. 105 661, 2020, ISSN: 0142-0615. [Online]. Available: https://www.sciencedirect.com/science/article/pii/S0142061519321775.

[29] V. Lakshminarayanan, V. G. S. Chemudupati, S. K. Pramanick, and K. Rajashekara, "Real-time optimal energy management controller for electric vehicle integration in workplace microgrid," *IEEE Transactions on Transportation Electrification*, vol. 5, no. 1, pp. 174–185, 2019.

[30] V. Gupta, S. R. Konda, R. Kumar, and B. K. Panigrahi, "Multiaggregator collaborative electric vehicle charge scheduling under variable energy purchase and ev cancelation events," *IEEE Transactions on Industrial Informatics.*, vol. 14, no. 7, pp. 2894–2902, 2018.

[31] A. Alsabbagh, H. Yin, and C. Ma, "Distributed electric vehicles charging management with social contribution concept," *IEEE Transactions on Industrial Informatics*, vol. 16, no. 5, pp. 3483–3492, 2020.

[32] C. D. Korkas, S. Baldi, S. Yuan, and E. B. Kosmatopoulos, "An adaptive learning-based approach for nearly optimal dynamic charging of electric vehicle fleets," *IEEE Transactions on Intelligent Transportation Systems*, vol. 19, no. 7, pp. 2066–2075, 2018.

[33] S. Limmer and T. Rodemann, "Peak load reduction through dynamic pricing for electric vehicle charging," *International Journal of Electrical Power and Energy Systems*, vol. 113, pp. 117–128, 2019, ISSN: 0142-0615.

[34] Z. Liu, Q. Wu, S. Huang, L. Wang, M. Shahidehpour, and Y. Xue, "Optimal day-ahead charging scheduling of electric vehicles through an aggregative game model," *IEEE Transactions on Smart Grid*, vol. 9, no. 5, pp. 5173–5184, 2018.

[35] Y. Cao, L. Huang, Y. Li, K. Jermsittiparsert, H. Ahmadi-Nezamabad, and S. Nojavan, "Optimal scheduling of electric vehicles aggregator under market price uncertainty using robust optimization technique," *International Journal of Electrical Power and Energy Systems*, vol. 117, p. 105 628, 2020, ISSN: 0142-0615.

[36] J. Hu, C. Si, M. Lind, and R. Yu, "Preventing distribution grid congestion by integrating indirect control in a hierarchical electric vehicles' management system,"

IEEE Transactions on Transportation Electrification, vol. 2, no. 3, pp. 290–299, 2016.

[37] L. Yao, W. H. Lim, and T. S. Tsai, "A real-time charging scheme for demand response in electric vehicle parking station," *IEEE Transactions on Smart Grid*, vol. 8, no. 1, pp. 52–62, 2017.

[38] J. Hernández, F. Sanchez-Sutil, P. Vidal, and C. Rus-Casas, "Primary frequency control and dynamic grid support for vehicle-to-grid in transmission systems," *International Journal of Electrical Power and Energy Systems*, vol. 100, pp. 152–166, 2018, ISSN: 0142-0615.

[39] H. Liu, Y. Yang, J. Qi, J. Li, H. Wei, and P. Li, "Frequency droop control with scheduled charging of electric vehicles," *IET Generation, Transmission and Distribution*, vol. 11, no. 3, pp. 649–656,

[40] X. Chen, K.-C. Leung, A. Y. S. Lam, and D. J. Hill, "Online scheduling for hierarchical vehicle-to-grid system: Design, formulation, and algorithm," *IEEE Transactions on Vehicular Technology*, vol. 68, no. 2, pp. 1302–1317, 2019.

[41] S. Paudyal, O. Ceylan, B. P. Bhattarai, and K. S. Myers, "Optimal coordinated ev charging with reactive power support in constrained distribution grids," in *2017 IEEE Power Energy Society General Meeting*, 2017, pp. 1–5.

[42] H. Zhang, Z. Hu, Z. Xu, and Y. Song, "Evaluation of achievable vehicle-to-grid capacity using aggregate pev model," *IEEE Transactions on Power Systems*, vol. 32, no. 1, pp. 784–794, 2017.

[43] W. Zhong, R. Yu, S. Xie, Y. Zhang, and D. K. Y. Yau, "On stability and robustness of demand response in mobile energy networks," *IEEE Transactions on Smart Grid*, vol. 9, no. 4, pp. 3203–3212, 2018.

[44] M. J. E. Alam, K. M. Muttaqi, and D. Sutanto, "Effective utilization of available pev battery capacity for mitigation of solar pv impact and grid support with integrated v2g functionality," *IEEE Transactions on Smart Grid*, vol. 7, no. 3, pp. 1562–1571, 2016.

[45] S. Pal and R. Kumar, "Electric vehicle scheduling strategy in residential demand response programs with neighbor connection," *IEEE Transactions on Industrial Informatics*, vol. 14, no. 3, pp. 980–988, 2018.

[46] A. Koufakis, E. S. Rigas, N. Bassiliades, and S. D. Ramchurn, "Offline and online electric vehicle charging scheduling with v2v energy transfer," *IEEE Transactions on Intelligent Transportation Systems Syst.*, vol. 21, no. 5, pp. 2128–2138, 2020.

[47] R. Alvaro-Hermana, J. Fraile-Ardanuy, P. J. Zufiria, L. Knapen, and D. Janssens, "Peer to peer energy trading with electric vehicles," *IEEE Intelligent Transportation Systems Magazine*, vol. 8, no. 3, pp. 33–44, 2016, ISSN: 1941-1197.

[48] X. Huang, Y. Zhang, D. Li, and L. Han, "An optimal scheduling algorithm for hybrid ev charging scenario using consortium blockchains," *FUTURE GENER COMP SY*, vol. 91, pp. 555–562, 2019, ISSN: 0167-739X.

[49] G. Sun, F. Zhang, D. Liao, H. Yu, X. Du, and M. Guizani, "Optimal energy trading for plug-in hybrid electric vehicles based on fog computing," *IEEE Internet Things J.*, vol. 6, no. 2, pp. 2309–2324, 2019.

[50] J. Kim, J. Lee, S. Park, and J. K. Choi, "Battery-wear-model-based energy trading in electric vehicles: A naive auction model and a market analysis," *IEEE Transactions on Industrial Informatics*, vol. 15, no. 7, pp. 4140–4151, 2019.

[51] D. Li, Q. Yang, D. An, W. Yu, X. Yang, and X. Fu, "On location privacy-preserving online double auction for electric vehicles in microgrids," *IEEE Internet Things J.*, vol. 6, no. 4, pp. 5902–5915, 2019.

[52] R. Zhang, X. Cheng, and L. Yang, "Flexible energy management protocol for cooperative ev-to-ev charging," *IEEE Transactions on Intelligent Transportation Systems Syst.*, vol. 20, no. 1, pp. 172–184, 2019.

[53] M. E. Kabir, I. Sorkhoh, B. Moussa, and C. Assi, "Joint routing and scheduling of mobile charging infrastructure for v2v energy transfer," *IEEE Transactions on Intelligent Vehicles*, vol. 6, no. 4, pp. 736–746, 2021.

[54] K. Christidis and M. Devetsikiotis, "Blockchains and smart contracts for the internet of things," *IEEE Access*, vol. 4, pp. 2292–2303, 2016.

[55] S. Ølnes, J. Ubacht, and M. Janssen, "Blockchain in government: Benefits and implications of distributed ledger technology for information sharing," *Gov. Inf. Q.*, vol. 34, no. 3, pp. 355–364, 2017, ISSN: 0740-624X.

[56] T. Aste, P. Tasca, and T. Di Matteo, "Blockchain technologies: The foreseeable impact on society and industry," *Computer*, vol. 50, no. 9, pp. 18–28, 2017.

[57] C. Liu, K. K. Chai, X. Zhang, E. T. Lau, and Y. Chen, "Adaptive blockchain-based electric vehicle participation scheme in smart grid platform," *IEEE Access*, vol. 6, pp. 25 657–25 665, 2018.

[58] J. Kang, R. Yu, X. Huang, S. Maharjan, Y. Zhang, and E. Hossain, "Enabling localized peer-to-peer electricity trading among plug-in hybrid electric vehicles using consortium blockchains," *IEEE Transactions on Industrial Informatics*, vol. 13, no. 6, pp. 3154–3164, 2017.

[59] Z. Zhou, B. Wang, Y. Guo, and Y. Zhang, "Blockchain and computational intelligence inspired incentive-compatible demand response in internet of electric vehicles," *IEEE Transactions on Emerging Topics in Computing*, vol. 3, no. 3, pp. 205–216, 2019.

[60] W. TU *et al.*, "Real-time route recommendations for e-taxies leveraging gps trajectories," *IEEE Transactions on Industrial Informatics*, pp. 1–1, 2020.

[61] A. Pan, T. Zhao, H. Yu, and Y. Zhang, "Deploying public charging stations for electric taxis: A charging demand simulation embedded approach," *IEEE Access*, vol. 7, pp. 17 412–17 424, 2019.

[62] C. Jiang, Z. Jing, T. Ji, and Q. Wu, "Optimal location of pevcss using mas and er approach," *IET Generation, Transmission and Distribution*, vol. 12, no. 20, pp. 4377–4387, 2018.

[63] S. Zhang, H. Wang, Y.-f. Zhang, and Y.-Z. Li, "A novel two-stage location model of charging station considering dynamic distribution of electric taxis," *Sustain. Cities Soc.*, vol. 51, p. 101 752, 2019, ISSN: 2210-6707.

[64] Z. Tian *et al.*, "Real-time charging station recommendation system for electric-vehicle taxis," *IEEE Transactions on Intelligent Transportation Systems*, vol. 17, no. 11, pp. 3098–3109, 2016.

[65] J. Yang, Y. Xu, and Z. Yang, "Regulating the collective charging load of electric taxi fleet via real-time pricing," *IEEE Transactions on Power Systems*, vol. 32, no. 5, pp. 3694–3703, 2017.

[66] Z. Yang, T. Guo, P. You, Y. Hou, and S. J. Qin, "Distributed approach for temporal–spatial charging coordination of plug-in electric taxi fleet," *IEEE Transactions on Industrial Informatics*, vol. 15, no. 6, pp. 3185–3195, 2019.

[67] C. Jiang, Z. Jing, X. Cui, T. Ji, and Q. Wu, "Multiple agents and reinforcement learning for modelling charging loads of electric taxis," *Appl. Energy*, vol. 222, pp. 158–168, 2018, ISSN: 0306-2619.

[68] C. Tseng, S. C. Chau, and X. Liu, "Improving viability of electric taxis by taxi service strategy optimization: A big data study of new york city," *IEEE Transactions on Intelligent Transportation Systems*, vol. 20, no. 3, pp. 817–829, 2019.

[69] C. Li, C. Liu, K. Deng, X. Yu, and T. Huang, "Data-driven charging strategy of pevs under transformer aging risk," *IEEE Transactions on Control Systems Technology*, vol. 26, no. 4, pp. 1386–1399, 2018.

[70] Z. Yang, L. Sun, M. Ke, Z. Shi, and J. Chen, "Optimal charging strategy for plug-in electric taxi with time-varying profits," *IEEE Transactions on Smart Grid*, vol. 5, no. 6, pp. 2787–2797, 2014.

[71] J. Shen, L. Wang, and J. Zhang, "Integrated scheduling strategy for private electric vehicles and electric taxis," *IEEE Transactions on Industrial Informatics*, vol. 17, no. 3, pp. 1637–1647, 2021.

[72] G. R. Chandra Mouli, M. Kefayati, R. Baldick, and P. Bauer, "Integrated pv charging of ev fleet based on energy prices, v2g, and offer of reserves," *IEEE Transactions on Smart Grid*, vol. 10, no. 2, pp. 1313–1325, 2019.

[73] N. Mehboob, M. Restrepo, C. A. Cañizares, C. Rosenberg, and M. Kazerani, "Smart operation of electric vehicles with four-quadrant chargers considering uncertainties," *IEEE Transaction on Smart Grid*, vol. 10, no. 3, pp. 2999–3009, 2019.

[74] Z. Ma, D. S. Callaway, and I. A. Hiskens, "Decentralized charging control of large populations of plug-in electric vehicles," *IEEE Transactions on Control Systems Technology*, vol. 21, no. 1, pp. 67–78, 2013.

[75] A. Ovalle, A. Hably, S. Bacha, G. Ramos, and J. M. Hossain, "Escort evolutionary game dynamics approach for integral load management of electric vehicle fleets," *IEEE Transactions on Industrial Electronics*, vol. 64, no. 2, pp. 1358–1369, 2017.

[76] L. Gan, U. Topcu, and S. H. Low, "Optimal decentralized protocol for electric vehicle charging," *IEEE Transactions on Power Systems*, vol. 28, no. 2, pp. 940–951, 2013.

[77] A. Ghavami, K. Kar, and A. Gupta, "Decentralized charging of plug-in electric vehicles with distribution feeder overload control," *IEEE Transactions on Automatic Control*, vol. 61, no. 11, pp. 3527–3532, 2016.

[78] S. Zhang and K.-C. Leung, "Joint optimal power flow routing and vehicle-to-grid scheduling: Theory and algorithms," *IEEE Transactions on Intelligent Transportation Systems Syst.*, pp. 1–14, 2020.

[79] J. Hu, H. Morais, T. Sousa, and M. Lind, "Electric vehicle fleet management in smart grids: A review of services, optimization and control aspects," *Renewable Sustainable Energy Rev.*, vol. 56, pp. 1207–1226, 2016, ISSN: 1364-0321.

[80] A. C. Melhorn, K. McKenna, A. Keane, D. Flynn, and A. Dimitrovski, "Autonomous plug and play electric vehicle charging scenarios including reactive power provision: A probabilistic load flow analysis," *IET Generation, Transmission and Distribution*, vol. 11, no. 3, pp. 768–775, 2017.

[81] M. H. Mobarak and J. Bauman, "Vehicle-directed smart charging strategies to mitigate the effect of long-range ev charging on distribution transformer aging," *IEEE Transactions on Transportation Electrification*, vol. 5, no. 4, pp. 1097–1111, 2019.

[82] J. E. Cardona, J. C. López, and M. J. Rider, "Decentralized electric vehicles charging coordination using only local voltage magnitude measurements," *Electric Power Systems Research*, vol. 161, pp. 139–151, 2018, ISSN: 0378-7796.

[83] P. Richardson, D. Flynn, and A. Keane, "Local versus centralized charging strategies for electric vehicles in low voltage distribution systems," *IEEE Transactions on Smart Grid*, vol. 3, no. 2, pp. 1020–1028, 2012.

[84] A. T. Al-Awami, E. Sortomme, G. M. Asim Akhtar, and S. Faddel, "A voltage-based controller for an electric-vehicle charger," *IEEE Transactions on Vehicular Technology*, vol. 65, no. 6, pp. 4185–4196, 2016.

[85] M. Singh, P. Kumar, and I. Kar, "Implementation of vehicle to grid infrastructure using fuzzy logic controller," *IEEE Transactions on Smart Grid*, vol. 3, no. 1, pp. 565–577, 2012.

[86] M. M. A. Abdelaziz, H. E. Farag, E. F. El-Saadany, and Y. A. I. Mohamed, "A novel and generalized three-phase power flow algorithm for islanded microgrids using a newton trust region method," *IEEE Transactions on Power Systems*, vol. 28, no. 1, pp. 190–201, 2013.

[87] Y. Ota, H. Taniguchi, J. Baba, and A. Yokoyama, "Implementation of autonomous distributed v2g to electric vehicle and dc charging system," *Electric Power Systems Research*, vol. 120, pp. 177–183, 2015, ISSN: 0378-7796.

[88] M. Tokudome, K. Tanaka, T. Senjyu, A. Yona, T. Funabashi, and C. Kim, "Frequency and voltage control of small power systems by decentralized controllable loads," in *2009 International Conference on Power Electronics and Drive Systems (PEDS)*, 2009, pp. 666–671.

[89] X. Huang, J. Chen, H. Yang, Y. Cao, W. Guan, and B. Huang, "Economic planning approach for electric vehicle charging stations integrating traffic and power grid constraints," *IET Generation, Transmission and Distribution*, vol. 12, no. 17, pp. 3925–3934, 2018.

[90] M. Rahmani-Andebili, H. Shen, and M. Fotuhi-Firuzabad, "Planning and operation of parking lots considering system, traffic, and drivers behavioral model," *IEEE Transactions on Systems, Man, and Cybernetics: Systems*, vol. 49, no. 9, pp. 1879–1892, 2019.

[91] L. Luo *et al.*, "Optimal planning of electric vehicle charging stations comprising multi-types of charging facilities," *Applied Energy*, vol. 226, pp. 1087–1099, 2018, ISSN: 0306-2619.

[92] U. B. Irshad, M. S. H. Nizami, S. Rafique, M. J. Hossain, and S. C. Mukhopadhyay, "A battery energy storage sizing method for parking lot equipped with ev chargers," *IEEE Systems Journal*, vol. 15, no. 3, pp. 4459–4469, 2021.

[93] H. Zhang, Z. Hu, Z. Xu, and Y. Song, "An integrated planning framework for different types of pev charging facilities in urban area," *IEEE Transactions on Smart Grid*, vol. 7, no. 5, pp. 2273–2284, 2016.

[94] B. Zeng, J. Feng, N. Liu, and Y. Liu, "Co–optimized parking lot placement and incentive design for promoting pev integration considering decision-dependent uncertainties," *IEEE Transactions on Industrial Informatics*, vol. 17, no. 3, pp. 1863–1872, 2021.

[95] N. Neyestani, M. Y. Damavandi, M. Shafie-Khah, J. Contreras, and J. P. S. Catalão, "Allocation of plug-in vehicles' parking lots in distribution systems considering network-constrained objectives," *IEEE Transactions on Power Systems*, vol. 30, no. 5, pp. 2643–2656, 2015.

[96] M. A. Kazemi, M. Sedighizadeh, M. J. Mirzaei, and O. Homaee, "Optimal siting and sizing of distribution system operator owned ev parking lots," *Applied Energy*, vol. 179, pp. 1176–1184, 2016, ISSN: 0306-2619.

[97] M. J. Mirzaei, A. Kazemi, and O. Homaee, "A probabilistic approach to determine optimal capacity and location of electric vehicles parking lots in distribution networks," *IEEE Transactions on Industrial Informatics*, vol. 12, no. 5, pp. 1963–1972, 2016.

[98] M. Moradijoz, M. Parsa Moghaddam, and M.-R. Haghifam, "A flexible distribution system expansion planning model: A dynamic bi-level approach," *IEEE Transactions on Smart Grid*, vol. 9, no. 6, pp. 5867–5877, 2018.

[99] M. Moradijoz, J. Heidari, M. P. Moghaddam, and M. R. Haghifam, "Electric vehicle parking lots as a capacity expansion option in distribution systems: A mixed-integer linear programing-based model," *IET Electrical Systems in Transportation*, vol. 10, no. 1, pp. 13–22, 2020.

[100] S. Karimi-Arpanahi, M. Jooshaki, M. Fotuhi-Firuzabad, and M. Lehtonen, "Flexibility-oriented collaborative planning model for distribution network and ev parking lots considering uncertain behaviour of evs," in *2020 International Conference on Probabilistic Methods Applied to Power Systems (PMAPS)*, 2020, pp. 1–6.

[101] M. Mozaffari, H. Askarian Abyaneh, M. Jooshaki, and M. Moeini-Aghtaie, "Joint expansion planning studies of ev parking lots placement and distribution network," *IEEE Transactions on Industrial Informatics*, vol. 16, no. 10, pp. 6455–6465, 2020.

[102] M. Moradijoz, M. Parsa Moghaddam, M. Haghifam, and E. Alishahi, "A multi-objective optimization problem for allocating parking lots in a distribution network," *International Journal of Electrical Power and Energy Systems*, vol. 46, pp. 115–122, 2013, ISSN: 0142-0615.

[103] M. Mohammadi-Landi, M. Rastegar, M. Mohammadi, and S. Afrasiabi, "Stochastic optimal sizing of plug-in electric vehicle parking lots in reconfigurable power

distribution systems," *IEEE Transactions on Intelligent Transportation Systems*, pp. 1–12, 2022.

[104] M. J. Mirzaei and A. Kazemi, "A dynamic approach to optimal planning of electric vehicle parking lots," *Sustainable Energy, Grids and Networks*, vol. 24, p. 100 404, 2020, ISSN: 2352-4677.

[105] O. M. Abdelwahab, A. A. Shalaby, and M. F. Shaaban, "An optimal resource allocation for future parking lots with charger assignment considering uncertainties," *Electric Power Systems Research*, vol. 200, p. 107 455, 2021, ISSN: 0378-7796.

[106] B. Zeng, Z. Zhu, H. Xu, and H. Dong, "Optimal public parking lot allocation and management for efficient pev accommodation in distribution systems," *IEEE Transactions on Industry Applications*, vol. 56, no. 5, pp. 5984–5994, 2020.

[107] S. M. Mohammadi-Hosseininejad, A. Fereidunian, A. Shahsavari, and H. Lesani, "A healer reinforcement approach to self-healing in smart grid by phevs parking lot allocation," *IEEE Transactions on Industrial Informatics*, vol. 12, no. 6, pp. 2020–2030, 2016.

[108] A. A. Al-obaidi and H. E. Z. Farag, "Adaptive optimal management of ev battery distributed energy for concurrent services to transportation and power grid in a fleet system under dynamic service pricing," *IEEE Transactions on Industrial Informatics*, vol. 18, no. 3, pp. 1618–1628, 2022.

[109] E. Camacho and C. Bordons, "Model predictive control," *Advanced Textbooks in Control and Signal Processing*, no. 9781852336943, pp. 1–401, 2007, cited By 536.

[110] L. Xie and M. D. Ilic, "Model predictive dispatch in electric energy systems with intermittent resources," in *2008 IEEE International Conference on Systems, Man and Cybernetics*, 2008, pp. 42–47.

[111] Y. Liang, Z. Ding, T. Ding, and W.-J. Lee, "Mobility-aware charging scheduling for shared on-demand electric vehicle fleet using deep reinforcement learning," *IEEE Transactions on Smart Grid*, vol. 12, no. 2, pp. 1380–1393, 2021.

[112] A. Al-Obaidi, H. Khani, H. E. Farag, and M. Mohamed, "Bidirectional smart charging of electric vehicles considering user preferences, peer to peer energy trade, and provision of grid ancillary services," *International Journal of Electrical Power and Energy Systems.*, vol. 124, p. 106 353, 2021, ISSN: 0142-0615.

[113] O. Frendo, J. Graf, N. Gaertner, and H. Stuckenschmidt, "Data-driven smart charging for heterogeneous electric vehicle fleets," *Energy and AI*, vol. 1, p. 100 007, 2020, ISSN: 2666-5468.

[114] G.-w. You, S. Park, and D. Oh, "Real-time state-of-health estimation for electric vehicle batteries: A data-driven approach," *Appl. Energy*, vol. 176, pp. 92–103, 2016, ISSN: 0306-2619.

[115] *What is a fleet vehicle? | a guide for business owners*. [Online]. Available: https://coastpay.com/blog/fleet-vehicle/.

[116] [Online]. Available: https://www.fueleconomy.gov/feg/Find.do?action=sbs.

[117] *Onboard charger*, Jun. 2020. [Online]. Available: https://www.tesla.com/support/home-charging-installation/onboard-charger.

[118] *Ontario hydro rates*. [Online]. Available: http://www.ontario-hydro.com/current-rates.

[119] D. L. Whitman, *Fundamentals of engineering economics and decision analysis* (Synthesis lectures on engineering, 18), eng. San Rafael, Calif. (1537 Fourth Street, San Rafael, CA 94901 USA): Morgan and Claypool, 2012, ISBN: 1-60845-865-2.

[120] H. E. Farag, A. Al-Obaidi, H. Khani, N. El-Taweel, E. El-Saadany, and H. Zeineldin, "Optimal operation management of distributed and centralized electrolysis-based hydrogen generation and storage systems," *Electric Power Systems Research*, vol. 187, p. 106 476, 2020, ISSN: 0378-7796. [Online]. Available: https://www.sciencedirect.com/science/article/pii/S0378779620302790.

[121] M. Banciu, "Dual simplex," in *Wiley Encyclopedia of Operations Research and Management Science*. American Cancer Society, 2011, ISBN: 9780470400531. eprint: https://onlinelibrary.wiley.com/doi/pdf/10.1002/9780470400531.eorms0269.

[122] L. Gurobi Optimization, *Gurobi optimizer reference manual*, 2021. [Online]. Available: http://www.gurobi.com.

[123] A. A. Al-Obaidi and H. E. Z. Farag, "Decentralized quality of service based system for energy trading among electric vehicles," *IEEE Transactions on Intelligent Transportation Systems*, pp. 1–10, 2021.

[124] W.-J. Deng and W. Pei, "Fuzzy neural based importance-performance analysis for determining critical service attributes," *Expert Syst. Appl.*, vol. 36, no. 2, Part 2, pp. 3774–3784, 2009, ISSN: 0957-4174.

[125] J. Rezaei, "Best-worst multi-criteria decision-making method," *Omega*, vol. 53, pp. 49–57, 2015, ISSN: 0305-0483.

[126] S. Guo and H. Zhao, "Fuzzy best-worst multi-criteria decision-making method and its applications," *Knowledge-Based Systems*, vol. 121, pp. 23–31, 2017, ISSN: 0950-7051.

[127] E. Triantaphyllou, *Multi-criteria decision making methods: a comparative study*. Springer, 2011.

[128] C. Carlsson and R. Fullér, "On possibilistic mean value and variance of fuzzy numbers," *Fuzzy Sets and Systems*, vol. 122, no. 2, pp. 315–326, 2001, ISSN: 0165-0114.

[129] J. M. Lafleur, "Probabilistic ahp and topsis for multi-attribute decision-making under uncertainty," in *2011 Aerospace Conference*, 2011, pp. 1–18.

[130] C. A. Floudas and P. M. Pardalos, *Encyclopedia of optimization*. Springer, 2009.

[131] T. Koshy, "Chapter 8 - graphs," in *Discrete Mathematics with Applications*, T. Koshy, Ed., Burlington: Academic Press, 2004, pp. 515–608, ISBN: 978-0-12-421180-3.

[132] K. Date and R. Nagi, "Gpu-accelerated hungarian algorithms for the linear assignment problem," *Parallel Computing*, vol. 57, pp. 52–72, 2016, ISSN: 0167-8191.

[133] F. Sun, V. O. K. Li, and Z. Diao, "Modified bipartite matching for multiobjective optimization: Application to antenna assignments in mimo systems," *IEEE Transactions on Wireless Communications*, vol. 8, no. 3, pp. 1349–1355, 2009.

[134] L. Wang and H. Wu, "Fast pairing of device-to-device link underlay for spectrum sharing with cellular users," *IEEE Communications Letters*, vol. 18, no. 10, pp. 1803–1806, 2014.

[135] A. J. Roumeliotis, C. I. Kourogiorgas, and A. D. Panagopoulos, "An optimized simple strategy for capacity allocation in satellite systems with smart gateway diversity," *IEEE Systems Journal*, pp. 1–7, 2020.

[136] H. Zhu, M. Zhou, and R. Alkins, "Group role assignment via a kuhn–munkres algorithm-based solution," *IEEE Transactions on Systems, Man, and Cybernetics - Part A: Systems and Humans*, vol. 42, no. 3, pp. 739–750, 2012.

[137] K. Riesen and H. Bunke, "Approximate graph edit distance computation by means of bipartite graph matching," *Image and Vision Computing*, vol. 27, no. 7, pp. 950–959, 2009, 7th IAPR-TC15 Workshop on Graph-based Representations (GbR 2007), ISSN: 0262-8856.

[138] R. Jonker and A. Volgenant, "A shortest augmenting path algorithm for dense and sparse linear assignment problems," *Computing*, vol. 38, pp. 325–340, 2005.

[139] D. Bertsekas, "A new algorithm for the assignment problem," *Mathematical Programming*, vol. 21, pp. 152–171, 1981.

[140] S. Hamzehi, K. Bogenberger, P. Franeck, and B. Kaltenhäuser, "Combinatorial reinforcement learning of linear assignment problems," in *2019 IEEE Intelligent Transportation Systems Conference (ITSC)*, 2019, pp. 3314–3321.

[141] J. Abdella and K. Shuaib, "Peer to peer distributed energy trading in smart grids: A survey," *Energies*, vol. 11, no. 6, 2018, ISSN: 1996-1073.

[142] S. Loveday, *Monthly plug-in ev sales scorecard: June 2019*, Jul. 2019. [Online]. Available: https://insideevs.com/news/357565/ev-sales-scorecard-june-2019/.

[143] *2018 tesla model s awd - p75d. - the official government source for fuel economy information.* [Online]. Available: https://www.fueleconomy.gov/feg/Find.do?action=sbs&id=39837.

[144] *Onboard charger*, Feb. 2022. [Online]. Available: https://www.tesla.com/support/home-charging-installation/onboard-charger.

[145] *Ontario hydro rates.* [Online]. Available: http://www.ontario-hydro.com/current-rates.

[146] M. Matos, R. Bessa, A. Botterud, and Z. Zhou, "11 - forecasting and setting power system operating reserves," in *Renewable Energy Forecasting*, ser. Woodhead Publishing Series in Energy, G. Kariniotakis, Ed., Woodhead Publishing, 2017, pp. 279–308, ISBN: 978-0-08-100504-0.

[147] Z. Fan, "A distributed demand response algorithm and its application to phev charging in smart grids," *IEEE Transactions on Smart Grid*, vol. 3, no. 3, pp. 1280–1290, 2012.

[148] N. Rahbari-Asr and M. Chow, "Cooperative distributed demand management for community charging of phev/pevs based on kkt conditions and consensus networks," *IEEE Transactions on Industrial Informatics*, vol. 10, no. 3, pp. 1907–1916, 2014.

[149] G. Binetti, A. Davoudi, D. Naso, B. Turchiano, and F. L. Lewis, "Scalable real-time electric vehicles charging with discrete charging rates," *IEEE Transactions on Smart Grid*, vol. 6, no. 5, pp. 2211–2220, 2015.

[150] N. I. Nimalsiri, C. P. Mediwaththe, E. L. Ratnam, M. Shaw, D. B. Smith, and S. K. Halgamuge, "A survey of algorithms for distributed charging control of electric vehicles in smart grid," *IEEE Transactions on Intelligent Transportation Systems*, vol. 21, no. 11, pp. 4497–4515, 2020.

[151] M. Zeballos, A. Ferragut, and F. Paganini, "Proportional fairness for ev charging in overload," *IEEE Transactions on Smart Grid*, vol. 10, no. 6, pp. 6792–6801, 2019.

[152] S. Shafiq and A. T. Al-Awami, "An autonomous charge controller for electric vehicles using online sensitivity estimation," *IEEE Transactions on Industry Applications*, vol. 56, no. 1, pp. 22–33, 2020.

[153] S. Tang, Z. Niu, B. He, B.-S. Lee, and C. Yu, "Long-term multi-resource fairness for pay-as-you use computing systems," *IEEE Transactions on Parallel and Distributed Systems*, vol. 29, no. 5, pp. 1147–1160, 2018.

[154] S. Faddel, T. Youssef, A. T. Elsayed, and O. A. Mohammed, "An automated charger for large-scale adoption of electric vehicles," *IEEE Transactions on Transportation Electrification*, vol. 4, no. 4, pp. 971–984, 2018.

[155] E. Inoa and J. Wang, "Phev charging strategies for maximized energy saving," *IEEE Transactions on Vehicular Technology*, vol. 60, no. 7, pp. 2978–2986, 2011.

[156] *Electric vehicle conductive charging system - part 1: General requirements*, International Electrotechnical Commission, 2017.

[157] M. Fatin Ishraque, S. A. Shezan, M. Ali, and M. Rashid, "Optimization of load dispatch strategies for an islanded microgrid connected with renewable energy sources," *Appl. Energy*, vol. 292, p. 116 879, 2021.

[158] M. E. Baran and F. F. Wu, "Network reconfiguration in distribution systems for loss reduction and load balancing," *IEEE Transactions on Power Delivery*, vol. 4, no. 2, pp. 1401–1407, 1989.

[159] K. Strunz, R. H. Fletcher, R. Campbell, and F. Gao, "Developing benchmark models for low-voltage distribution feeders," in *2009 IEEE PES General Meeting*, 2009, pp. 1–3.

[160] G. Johnson and I. Beausoleil-Morrison, "Electrical-end-use data from 23 houses sampled each minute for simulating micro-generation systems," *Applied Thermal Engineering*, vol. 114, pp. 1449–1456, 2017, ISSN: 1359-4311.

[161] S. Ramos, J. Soares, T. Pinto, and Z. A. Vale, "Short-term wind forecasting to support virtual power player operation," 2013.

[162] *Tesla model 3 mid range specs, price, photos, offers and incentives.* [Online]. Available: https://evcompare.io/cars/tesla/tesla-model-3-mid-range-rwd/.

[163] J. Antoun, M. E. Kabir, B. Moussa, R. Atallah, and C. Assi, "Impact analysis of level 2 ev chargers on residential power distribution grids," in *2020 IEEE 14th International Conference on Compatibility, Power Electronics and Power Engineering (CPE-POWERENG)*, vol. 1, 2020, pp. 523–529.

[164] "Ieee standard for interconnection and interoperability of distributed energy resources with associated electric power systems interfaces," *IEEE Std 1547-2018 (Revision of IEEE Std 1547-2003)*, pp. 1–138, 2018.

[165] D. Wu, H. Zeng, C. Lu, and B. Boulet, "Two-stage energy management for office buildings with workplace ev charging and renewable energy," *IEEE Transactions on Transportation Electrification*, vol. 3, no. 1, pp. 225–237, 2017.

[166] D. M. Steward, "Critical elements of vehicle-to-grid (v2g) economics," Sep. 2017. [Online]. Available: https://www.osti.gov/biblio/1390043.

[167] B. Bibak and H. Tekiner-Moğulkoç, "A comprehensive analysis of vehicle to grid (v2g) systems and scholarly literature on the application of such systems," *Renewable Energy Focus*, vol. 36, pp. 1–20, 2021, ISSN: 1755-0084.

[168] C. Luo, Y.-F. Huang, and V. Gupta, "Stochastic dynamic pricing for ev charging stations with renewable integration and energy storage," *IEEE Transactions on Smart Grid*, vol. 9, no. 2, pp. 1494–1505, 2018.

[169] A. S. Bin Humayd and K. Bhattacharya, "Design of optimal incentives for smart charging considering utility-customer interactions and distribution systems impact," *IEEE Transactions on Smart Grid*, vol. 10, no. 2, pp. 1521–1531, 2019.

[170] W. Yao, C. Y. Chung, F. Wen, M. Qin, and Y. Xue, "Scenario-based comprehensive expansion planning for distribution systems considering integration of plug-in electric vehicles," *IEEE Transactions on Power Systems*, vol. 31, no. 1, pp. 317–328, 2016.

[171] H. Chen, Z. Hu, H. Luo, J. Qin, R. Rajagopal, and H. Zhang, "Design and planning of a multiple-charger multiple-port charging system for pev charging station," *IEEE Transactions on Smart Grid*, vol. 10, no. 1, pp. 173–183, 2019.